

**SIMULACIÓN DEL SISTEMA DE CONTROL PARA UN VEHÍCULO
SUBACUÁTICO OPERADO REMOTAMENTE
(SIMULATION OF THE CONTROL SYSTEM FOR A REMOTELY
OPERATED UNDERWATER VEHICLE)**

SANTIAGO RÚA PÉREZ

**UNIVERSIDAD PONTIFICIA BOLIVARIANA
ESCUELA DE INGENIERÍAS
MAESTRÍA EN INGENIERÍA
MEDELLÍN
2015**

**SIMULACIÓN DEL SISTEMA DE CONTROL PARA UN VEHÍCULO
SUBACUÁTICO OPERADO REMOTAMENTE
(SIMULATION OF THE CONTROL SYSTEM FOR A REMOTELY
OPERATED UNDERWATER VEHICLE)**

SANTIAGO RÚA PÉREZ

Trabajo de grado para optar al título de Magíster en Ingeniería

**Director
Rafael Esteban Vásquez Moncayo
Ph.D. en Ingeniería Mecánica**

**UNIVERSIDAD PONTIFICIA BOLIVARIANA
ESCUELA DE INGENIERÍAS
MAESTRÍA EN INGENIERÍA
MEDELLÍN
2015**

Nota de aceptación

Firma
Nombre:
Presidente del jurado

Firma
Nombre:
Jurado

Firma
Nombre:
Jurado

DECLARACIÓN DE ORIGINALIDAD

“Declaro que esta tesis (o trabajo de grado) no ha sido presentada para optar a un título, ya sea en igual forma o con variaciones, en esta o cualquier otra universidad”.
Art. 82 Régimen Discente de Formación Avanzada, Universidad Pontificia Bolivariana.

FIRMA AUTOR

Santiago Rúa P.

I dedicate this work to my love (MGC), my family and my friends.

ACKNOWLEDGEMENT

I express my gratitude to my advisor Rafael E. Vásquez for his encouragement to continue my studies in the control area, and the time expended to solve my doubts about any topic on this matter. Also to Carlos A. Zuluaga for allowing me to participate in the project of the Visor3 electronic improvements. At last but not least, to my love (MGC) for her support and encouragement during this phase of my life; and my parents to believe in this formation process.

This thesis has been developed with the funding of the Fondo Nacional de Financiamiento para la Ciencia, la Tecnología y la Innovación, Francisco José de Caldas; the Colombian petroleum company, ECOPETROL; the Universidad Pontificia Bolivariana – Medellín, UPB; the Universidad Nacional de Colombia – Sede Medellín, UNALMED; through the Strategic Program for the Development of Robotic Technology for Offshore Exploration of the Colombian Sea Bottoms, project 1210-531-30550, contract 0265 – 2013.

TABLE OF CONTENTS

| | Pág. |
|--|------|
| 1. INTRODUCTION | 17 |
| 1.1. Mathematical Model | 19 |
| 1.2. Navigation System | 20 |
| 1.3. Control System | 21 |
| 2. 6-DOF MATHEMATICAL MODEL | 23 |
| 2.1. Kinematics | 23 |
| 2.1.1. Coordinate frames | 24 |
| 2.1.2. Transformations | 25 |
| 2.2. Rigid Body Dynamics | 27 |
| 2.3. Hydrodynamic Forces and Moments | 30 |
| 2.3.1. Added mass | 30 |
| 2.3.2. Hydrodynamic damping | 32 |
| 2.3.3. Restoring forces and moments | 33 |
| 2.4. Thruster Model | 35 |
| 2.5. Ocean Current | 37 |
| 3. NONLINEAR MODEL BASED OBSERVER | 39 |
| 3.1. Statistics and Stochastic systems | 39 |
| 3.1.1. Gaussian probability distribution | 40 |

| | | |
|--------|---|----|
| 3.1.2. | Some statistics definitions | 40 |
| 3.2. | Kalman Filter | 42 |
| 3.3. | Extended Kalman Filter | 47 |
| 3.4. | EKF for the ROV | 48 |
| 4. | CONTROL ALGORITHMS | 52 |
| 4.1. | Thruster Allocation problem | 54 |
| 4.2. | Multivariable PID-control | 56 |
| 4.3. | Linear Quadratic Regulator (LQR) | 57 |
| 5. | SIMULATION AND RESULTS | 61 |
| 5.1. | Description of the vehicle | 61 |
| 5.2. | Dynamic simulation | 61 |
| 5.3. | Thruster simulation | 63 |
| 5.4. | Navigation system | 66 |
| 5.5. | Controllers | 67 |
| 5.5.1. | PID and PID with gravity compensation | 67 |
| 5.5.2. | LQR controller | 70 |
| | CONCLUSIONS | 81 |
| | REFERENCES | 83 |
| | APPENDIX | 89 |
| A. | Papers | 90 |
| B. | Master Thesis Proposal | 98 |

C. Intellectual Property 139

LIST OF FIGURES

| | Pág. |
|---|------|
| 1 Underwater vehicles categories | 17 |
| 2 Control structure for an underwater vehicle. | 18 |
| 3 Coordinate frames | 24 |
| 4 Center of gravity and center of buoyancy | 34 |
| 5 Propulsion system scheme | 35 |
| 6 Propulsion system configuration for Visor3 | 36 |
| 7 Gaussian probability distribution | 41 |
| 8 Kalman filter structure with the dynamic system and the observation model | 47 |
| 9 Extended Kalman filter structure with the dynamic system and the obser- vation model | 49 |
| 10 Open-loop control system implemented in Visor3 | 52 |
| 11 Thrusters positions in Visor3 | 53 |
| 12 Closed-loop control system to be implemented in Visor3 | 54 |
| 13 Change of voltage according to u_i in the thruster allocation problem | 56 |
| 14 Closed-loop control system implemented in Visor3 | 58 |
| 15 State feedback control | 59 |
| 16 State feedback control with integral action and open loop gain | 60 |
| 17 Dynamic vehicle simulation | 63 |

| | | |
|----|---|----|
| 18 | Velocity transformation | 63 |
| 19 | Time response for a MAXON DC motor | 64 |
| 20 | Motor driver block. | 65 |
| 21 | Measure of the thruster position. | 65 |
| 22 | EKF Simulink® implementation. | 67 |
| 23 | Position estimation in Earth-fixed frame. | 68 |
| 24 | Velocity estimation in body-fixed frame. | 69 |
| 25 | Error in position estimation. | 70 |
| 26 | Error in velocity estimation. | 71 |
| 27 | PID controllers with and without compensation, for planar motion control | 73 |
| 28 | Control signal for each thruster, for planar motion control | 74 |
| 29 | PID controllers with and without compensation, for depth control | 75 |
| 30 | Control signal for each thruster, for depth control | 76 |
| 31 | PID controllers with and without compensation, for planar motion control with perturbation | 77 |
| 32 | Control signal for each thruster, for planar motion control with perturbation | 78 |
| 33 | LQR controller performance | 79 |
| 34 | Control signal for each thruster in LQR controller. | 80 |

LIST OF TABLES

| | Pág. |
|---|------|
| 1 SNAME notation | 23 |
| 2 MAXON Parameters | 36 |
| 3 ROV Visor3 parameters for simulation | 62 |
| 4 Thruster Visor3 parameters for simulation | 65 |
| 5 Thruster allocation | 66 |

GLOSSARY

AUV: an Autonomous Underwater Vehicle is a robotic device that is driven through the water by a propulsion system, controlled and piloted by an on-board computer, and maneuverable in three dimensions. This type of vehicle works under most environmental conditions, and they use to follow precise preprogrammed trajectories wherever and whenever required [1].

EKF: an Extended Kalman Filter implements a Kalman filter for a system dynamics that results from the linearization of the original non-linear filter dynamics around the previous state estimates [2].

GNC: Guidance, Navigation and Control.

KF: Kalman Filter is an estimator for the linear quadratic problem. The problem of estimating the instantaneous “state” of a linear dynamic system perturbed with white noise, by using measurements linearly related to the state but corrupted by white noise [3].

PID: it is a control algorithm, based on a proportional, integral and derivative actions. It is the most commonly used controller in industry.

ROV: Remotely Operated Vehicle. The motion of the vehicle can be controlled via autonomous logic direction or remote operator control depending on the vehicle’s capability and the operator’s ability [4].

UKF: the Unscented Kalman Filter belongs to a bigger class of filters called Sigma-Point Kalman Filters or Linear Regression Kalman Filters, which use the statistical linearization technique. This technique is used to linearize a nonlinear function of a random variable through a linear regression between n points drawn from the prior distribution of the random variable. The technique tends to be more accurate than the Taylor series linearization [5].

UUV: Unmanned Underwater Vehicle is defined as a self-propelled submersible whose operation is done fully autonomous (preprogrammed or real-time adaptive mission con-

trol) or under minimal supervisory control and is untethered except, possibly, for data links such as a fiber-optic cable [\[4\]](#).

ABSTRACT

This work addresses the development of the simulation of the control system for the underwater remotely operated vehicle Visor3 using a nonlinear model of the vehicle. The 6-DOF (degrees of freedom) mathematical model of Visor3 is presented using two coordinated systems: Earth-fixed and body-fixed frames, and takes into account the inertia forces, centripetal and Coriolis forces and gravitational forces, and was implemented in Simulink®. Visor3 parameters were obtained using CAD models (Solid-Edge® software) and CFD simulation (ANSYS® software), within a work that was developed by a person in the Jóvenes Investigadores program.

The guidance, navigation and control structure (GNC) is divided into three layers: the high level or the mission planner; the mid level or the path planner; and the low level formed by the control, navigation system and sensors. This thesis addresses only the problem of the simulation of the low level control. A nonlinear model based observer is proposed for the navigation system. This observer was developed using the extended Kalman filter (EKF) which uses the linearization of the model to estimate the current state. The behavior of the observer is verified through simulation using Simulink®. The navigation system is a fundamental part of the closed-loop control system that will allow Visor3's operators to take advantage of more advanced vehicle's capabilities during inspection tasks of port facilities, hydroelectric dams, and oceanographic research.

The main objective of the control algorithm is to execute the commands given by the operator in the surface station. These commands can be, for instance, a set-point for the vehicle's velocity or a trajectory that is to be tracked with a fixed attitude. Two operation modes were defined: planar motion control, which consist in depth regulation while the ROV is moving within the horizontal plane; and depth control in which the control system must maintain the same position in x-y while the vehicle is going up and down. To accomplish these tasks, three control algorithms were proposed: a multi-loop PID, PID with gravity compensation and LQR controller. These controllers and the nonlinear observer were tested using the 6-DOF mathematical model of Visor3; four of these DOF are controllable in Visor3: surge, sway, heave, and yaw. Finally, in order to accomplish the force commanded by the control algorithm, it is necessary to determine the commands for each thruster through the thruster allocation matrix.

KEYWORDS:

Robot navigation, Navigation systems, Kalman filters, PID multi-loop control, LQR control, Thruster allocation.

1. INTRODUCTION

Due to the growing interest around the world to explore the sea bottom, several researchers have focused their efforts on the construction of underwater vehicles that allow one to explore the ocean from a surface station. Underwater vehicles are divided into two categories: manned underwater vehicles and unmanned underwater vehicles (UUVs). The UUVs are all kinds of underwater vehicles that are able to operate without a human inside of them. UUVs are designed to accomplish different tasks such as observation, exploration and mapping of the sea bottom [6]; sampling; object manipulation [7]; monitoring and maintenance of structures and pipelines; and other underwater engineering operations [8].

There are two kinds of UUVs (see Figure 1.): remotely operated underwater vehicles (ROVs), which are remotely controlled from a surface vessel and by a human operator; therefore, there is a physical connection (data and power) between the vehicle and the surface [4]; and the autonomous underwater vehicles (AUVs), which are self-propelled vehicles that are typically deployed from a surface vessel, and can operate independently for periods that vary from a few hours to several days [8].

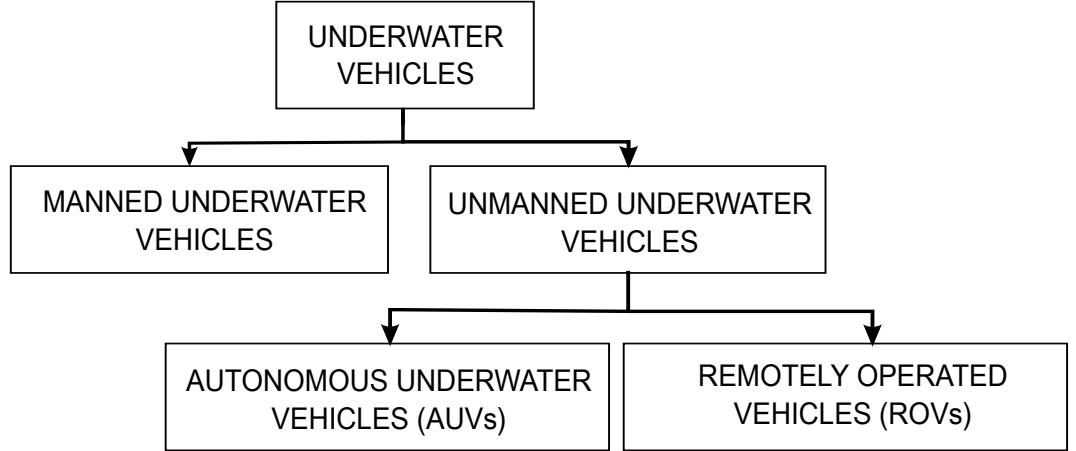


Figure 1. Underwater vehicles categories

Regardless, if they are operated by cable (ROVs) or autonomous (AUVs), it is necessary to develop control strategies to achieve the desired movements [9, 10]. When precise control is needed to follow a certain path, commands provided by a human operator

are not enough. When a vehicle is moving under the water, it is affected by viscous hydrodynamics and inertial forces [11, 12].

The guidance, navigation, and control (GNC) system for an underwater vehicle can have different degrees of sophistication, depending on the type of operation that is to be performed, and the autonomy levels that need to be achieved [10, 9]. One of the important vehicle design parameters is the number of degrees of freedom needed to perform the planned operations, because they represent the number of independent movements that the vehicle can achieve in the three-dimensional space. Additionally, the tasks that are to be performed determine the instrumentation (sensors, actuators, complementary systems, among others) required to control the vehicle. The desired level of autonomy, will determine what kind of algorithms are necessary to control the variables of interest, which are normally given by the position, attitude (orientation) and vehicle speed with respect to an inertial reference system located at the surface [13]. Figure 2 shows a three-level hierarchical GNC structure for a underwater vehicle; this kind of structure is useful to control and stabilize the vehicle [14].

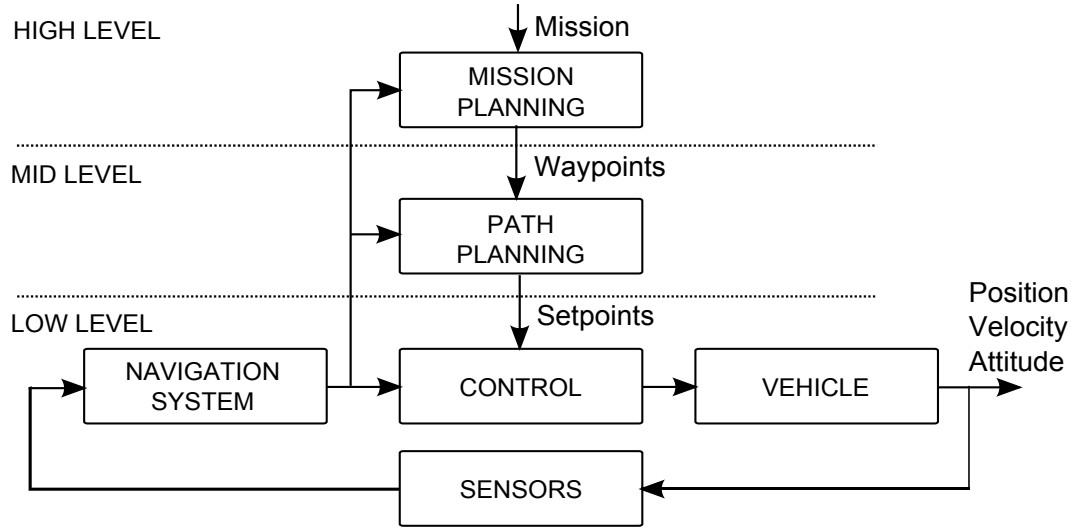


Figure 2. Control structure for an underwater vehicle.

The Automation and Design (A+D) Group from the Universidad Pontificia Bolivariana has developed an ROV called Visor3; used for surveillance and maintenance of ship and underwater structures of Colombian port facilities and oceanographic research. The mechanical/naval design was performed through an iterative process by using computational tools CAD/CAE/CFD [15]. Visor3 has a 3-layer hardware architecture:

instrumentation, communications and control [16]. Although much work has been done in mechanics and electronics, a closed-loop control system was not developed for the ROV Visor3, so the capabilities of the vehicle are still completely dependent on the pilot skills.

1.1. MATHEMATICAL MODEL

The design of some controllers is based in the mathematical model of the system. Having accurate models for prediction and control is desirable, however, this is not a simple task due to the highly non-linear behavior that appears in the fluid-vehicle interaction [17]. This mathematical model that represents the dynamic behavior is highly dependent on the hydrodynamic parameters caused by interaction with the environment in which the vehicle moves [18]. These parameters are important for the design of the control system, and it is possible to find in the literature several works that show different methodologies for the determination and identification of the mathematical model. Chin et al. [19] developed a computational toolbox for the analysis and design of an ROV which can simulate the behavior of the vehicle and the control system. Tiano et al. [20] used a Kalman Filter based method for the experimental evaluation of the dynamic behavior of an AUV. Chen [21] developed a system to identify ROVs parameters using a vision system for measurements, which is useful when there is no access to data for experimental modelling. Avila and Adamowski [22] developed an experimental identification system of hydrodynamic coefficients using the onboard sensors and signals from the thrusters of an ROV .

In order to improve the performance of the mathematical model, several works consider the dynamics and the configuration of thrusters. Akmal et al. [23] presented a model of forces and moments produced by four x-shape arranged thrusters over an ROV, which allow the vehicle to move in three DOFs (surge, sway and yaw).

1.2. NAVIGATION SYSTEM

One of the main elements located on the lower level of the control structure is the navigation system. It allows one to estimate the position, velocity, and attitude of the vehicle with respect to an inertial system located in the surface control station, from measurements made with different sensors (IMU, magnetometer, depth, DVL, USBL, among others). Given the characteristics of water, the development of underwater localization systems is not trivial and presents a number of challenges [24]. Therefore, for certain operating depths, knowing the vehicle's position is not a simple issue, and this should be taken into account from the design stage in order to achieve a synchronized operation between the surface station (usually located on a ship) and the underwater vehicle. The need to implement location systems for ROVs was born in 1963, with the loss and difficulty to find the USS Thresher submarine, which sank to 2560 m deep, and with the loss of an atomic bomb at the coast of Spain in 1966 [4]. Important information about determining the location of underwater vehicles can be found in [24, 25, 26, 27, 28].

The Kalman Filter is an estimator, statistically optimal with respect to a quadratic error function, which allows one to determine the state of the vehicle [3]. Armstrong et al. [29] presented an Extended Kalman Filter (EKF) used for navigation of an AUV. The AUV contains a magnetic compass and angular velocity sensor which exhibit disturbances and drift. To solve this problem, the EKF algorithm fuses information from sensors in order to produce a more accurate estimate of heading and learns a heading bias. This heading bias can correct a poorly calibrated magnetic heading sensor, and the angular velocity improves heading estimation. The test for the approach was a simulation of an artificial compass bias. A permanent magnet was placed to create magnetic field disturbances for compass, causing a deflection of 3-5 degrees. Several Kalman filter based navigation systems have been developed for years, see for reference [30, 31, 32, 33, 34, 35, 36, 37, 38].

Another method commonly used when the system is highly nonlinear and there are uncertainties in the model, is the H_∞ filtering algorithm. Different from the EKF, the design criteria for the H_∞ filter is an uniformly small estimation error for any kind of noise. H_∞ filtering has strong robustness, so it can ensure navigation accuracy, improve the system reliability, and prevent filtering divergence [39]. Batista et al. [40] presented a set of optimal filtering results for a class of kinematic systems with

particular application to the estimation of linear quantities in Integrated Navigation Systems for mobile platforms. The design was based on the Kalman or H_∞ filtering steady state solutions for an equivalent LTI system and allows one to use frequency weights to achieve disturbance rejection and attenuation of noise from sensors on the state estimates.

1.3. CONTROL SYSTEM

The control system is another component of the lower level of the control structure. It contains a set of algorithms that stabilize the state of the vehicle, so it can follow the commands generated at the path planning system. The control of an underwater vehicle is complex because there are highly nonlinear hydrodynamic effects resulting from the interaction with the environment that can not be quantified [41]. Cohan [42] states that the development of control systems for ROVs is a current and promising topic for future developments; this can be verified with the number of papers that can be found in literature.

Caccia and Veruggio [31] implemented and tested a guidance and control system for underwater vehicles using programmed controllers to regulate speed at the low level in a hierarchical three-level structure. Do et al. [43] developed a robust adaptive control strategy to ensure that a six-degree-of-freedom vehicle follows a prescribed path using four actuators. Van de Ven et al. [44] presented a qualitative assessment of the performance of control strategies using neural networks, indicating the advantages, disadvantages and application recommendations. Hoang and Kreuzer [45] designed an adaptive PD controller for dynamic positioning of ROVs when the mission is executed in places near submerged structures and requires great execution precision. Bessa et al. [46] used sliding mode controllers, combined with fuzzy adaptive algorithms for controlling depth in ROVs. Alvarez et al. [47] developed a robust PID controller for controlling an AUV used in oceanographic sampling work. Subudhi et al. [48] presented the design of a feedback controller for tracking paths in vertical planes. Ishaque et al. [49] presented a simplification of the conventional fuzzy controller for an underwater vehicle. Herman [50] presented a decoupled PD set-point controller which is expressed in terms of quasi-velocities for underwater vehicles. Petrich and Stilwell [51] presented

a robust control for an autonomous underwater vehicle that suppresses pitch and yaw coupling.

2. 6-DOF MATHEMATICAL MODEL

The behavior of the vehicle can be represented through the equations of motion. The main objective is to know the system dynamics in order to design controllers that allow one to modify the behavior of some variables of interest. This chapter state the mathematical model for Visor3, including effects like interaction with the fluid and gravitational forces.

2.1. KINEMATICS

Kinematics is the study of motion (without including forces) that is described by position, displacement, rotation, speed, velocity, and acceleration. In kinematics it is assumed that all bodies under analysis are rigid bodies, i.e., their deformation during the motion is negligible, and does not affect the behavior of the body, and the only change considered is in the position. For marine vehicles the motion components are defined according to the SNAME notation [52] as seen in Table 1.

Table 1. SNAME notation [52]

| DOF | Forces and Moments | Linear and angular velocity | Position and Euler angles |
|-------|--------------------|-----------------------------|---------------------------|
| Surge | X | u | x |
| Sway | Y | v | y |
| Heave | Z | w | z |
| Roll | K | p | ϕ |
| Pitch | M | q | θ |
| Yaw | N | r | ψ |

2.1.1. Coordinate frames

To analyze the motion of Visor3 in a three-dimensional space, two coordinate frames are defined: an inertial frame known as the Earth-fixed frame, where the motion of the vehicle is described, and the body-fixed frame, which is conveniently fixed to the vehicle and moves with it, Figure. 3. The position and orientation of the vehicle are described relative to the Earth-fixed frame as

$$\boldsymbol{\eta} = \begin{bmatrix} x & y & z & \phi & \theta & \psi \end{bmatrix}^T, \quad (1)$$

where $\mathbf{p} = [x \ y \ z]^T$ is the position and $\boldsymbol{\Theta} = [\phi \ \theta \ \psi]^T$ the orientation. The linear and angular velocities of the vehicle relative to the body-fixed frame are

$$\boldsymbol{\nu} = \begin{bmatrix} u & v & w & p & q & r \end{bmatrix}^T, \quad (2)$$

where $\mathbf{v} = [u \ v \ w]^T$ and $\boldsymbol{\omega} = [p \ q \ r]^T$ are the linear and angular velocities, respectively. The forces and moments of the vehicle relative to the body-fixed frame are

$$\boldsymbol{\tau} = \begin{bmatrix} X & Y & Z & K & M & N \end{bmatrix}^T, \quad (3)$$

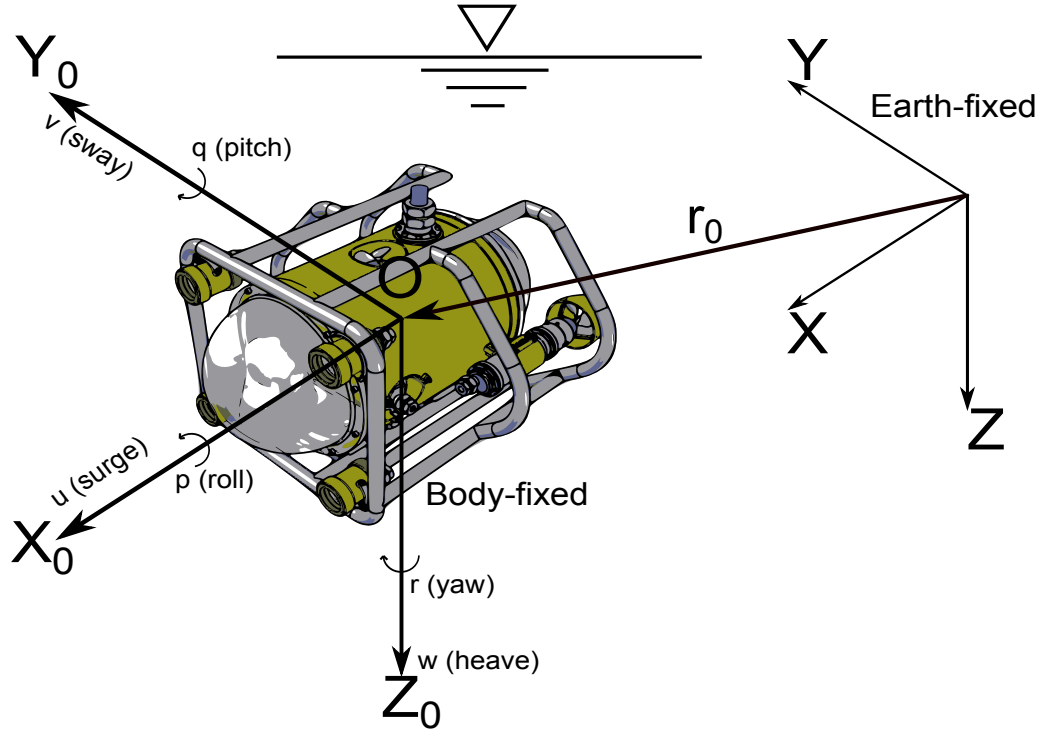


Figure 3. Coordinate frames.

where $\boldsymbol{\tau}_1 = [X \ Y \ Z]^T$ and $\boldsymbol{\tau}_2 = [K \ M \ N]^T$ are the forces and moments acting in the vehicle respectively. The frames used in this work are denoted as:

- EARTH $\{n\}$: Earth-fixed frame with axes $\{n\} = [x_n \ y_n \ z_n]$.
- BODY $\{b\}$: body-fixed frame with axes $\{b\} = [x_b \ y_b \ z_b]$.

It is common to find a third frame known as measurement frame $\{m\}$. The $\{m\}$ frame denotes the measurement of each instrument in the vehicle and it moves together with the vehicle. All measurements are assumed that are made in the body-fixed frame for this work.

2.1.2. Transformations

To obtain a vector from frame $\{a\}$ described in the components of frame $\{b\}$, a linear transformation must be applied. The rotation matrix $\boldsymbol{R} \in \mathbb{R}^{3 \times 3}$ between two frames $\{a\}$ and $\{b\}$ is denoted by \boldsymbol{R}_b^a and satisfies

$$\boldsymbol{R}^T \boldsymbol{R} = \boldsymbol{R} \boldsymbol{R}^T = \boldsymbol{I}, \quad \det \boldsymbol{R} = 1, \quad (4)$$

which implies that \boldsymbol{R} is orthogonal. The principal rotation matrices are described by

$$\boldsymbol{R}_{x,\phi} = \begin{bmatrix} 1 & 0 & 0 \\ 0 & c\phi & -s\phi \\ 0 & s\phi & c\phi \end{bmatrix}, \quad (5)$$

$$\boldsymbol{R}_{y,\theta} = \begin{bmatrix} c\theta & 0 & s\theta \\ 0 & 1 & 0 \\ -s\theta & 0 & c\theta \end{bmatrix}, \quad (6)$$

$$\boldsymbol{R}_{z,\psi} = \begin{bmatrix} c\psi & -s\psi & 0 \\ s\psi & c\psi & 0 \\ 0 & 0 & 1 \end{bmatrix}, \quad (7)$$

where $s \cdot = \sin(\cdot)$, $c \cdot = \cos(\cdot)$ and $t \cdot = \tan(\cdot)$. $\boldsymbol{R}_{x,\phi}$ denotes a rotation angle of ϕ about x -axis.

- **Linear velocity transformation:** To obtain the linear velocity in the Earth-fixed frame $\{n\}$ from the linear velocity in the body-fixed frame $\{b\}$, the three rotations described in (5), (6) and (7) must be applied in order. First, the coordinate system

rotates an angle ψ around the Z -axis. Then, this new system rotates an angle θ around the Y -axis. Finally, the coordinate system rotates an angle ϕ around the X -axis. The rotation matrix is given by

$$\mathbf{R}_b^n(\Theta_{nb}) = \mathbf{R}_{z,\psi} \mathbf{R}_{y,\theta} \mathbf{R}_{x,\phi}, \quad (8)$$

$$\mathbf{R}_b^n(\Theta_{nb}) = \begin{bmatrix} c\psi & -s\psi & 0 \\ s\psi & c\psi & 0 \\ 0 & 0 & 1 \end{bmatrix} \begin{bmatrix} c\theta & 0 & s\theta \\ 0 & 1 & 0 \\ -s\theta & 0 & c\theta \end{bmatrix} \begin{bmatrix} 1 & 0 & 0 \\ 0 & c\phi & -s\phi \\ 0 & s\phi & c\phi \end{bmatrix}, \quad (9)$$

$$\mathbf{R}_b^n(\Theta_{nb}) = \begin{bmatrix} c\psi c\theta & -s\psi c\phi + c\psi s\theta s\phi & s\psi s\phi + c\psi s\theta c\phi \\ s\psi c\theta & c\psi c\phi + s\psi s\theta s\phi & -c\psi s\phi + s\psi s\theta c\phi \\ -s\theta & c\theta s\phi & c\theta c\phi \end{bmatrix}. \quad (10)$$

Finally, the vehicle's motion relative to the Earth-fixed frame is given by the velocity transformation as

$$\dot{\mathbf{p}}_{b/n}^n = \mathbf{R}_b^n(\Theta_{nb}) \mathbf{v}_{b/n}^b, \quad (11)$$

where $\mathbf{p}_{b/n}^n$ is the position of $\{b\}$ with respect to $\{n\}$ expressed in $\{n\}$ and $\mathbf{v}_{b/n}^b$ is the linear velocity of the frame $\{b\}$ with respect to $\{n\}$ expressed in $\{n\}$. The inverse velocity transformation can be written

$$\mathbf{v}_{b/n}^b = \mathbf{R}_b^n(\Theta_{nb})^{-1} \dot{\mathbf{p}}_{b/n}^n. \quad (12)$$

- **Angular velocity transformation:** The angular rate vector $\dot{\Theta}_{nb} = [\dot{\phi} \ \dot{\theta} \ \dot{\psi}]^T$ can be obtained from the body angular velocity vector $\boldsymbol{\omega}_{b/n}^b = [p \ q \ r]^T$ by applying the next linear transformation

$$\boldsymbol{\omega}_{b/n}^b = \begin{bmatrix} \dot{\phi} \\ 0 \\ 0 \end{bmatrix} + \mathbf{R}_{x,\phi}^T \begin{bmatrix} 0 \\ \dot{\theta} \\ 0 \end{bmatrix} + \mathbf{R}_{x,\phi}^T \mathbf{R}_{y,\theta}^T \begin{bmatrix} 0 \\ 0 \\ \dot{\psi} \end{bmatrix}, \quad (13)$$

$$\boldsymbol{\omega}_{b/n}^b = \begin{bmatrix} \dot{\phi} \\ 0 \\ 0 \end{bmatrix} + \begin{bmatrix} 1 & 0 & 0 \\ 0 & c\phi & s\phi \\ 0 & -s\phi & c\phi \end{bmatrix} \begin{bmatrix} 0 \\ \dot{\theta} \\ 0 \end{bmatrix} + \begin{bmatrix} 1 & 0 & 0 \\ 0 & c\phi & s\phi \\ 0 & -s\phi & c\phi \end{bmatrix} \begin{bmatrix} c\theta & 0 & -s\theta \\ 0 & 1 & 0 \\ s\theta & 0 & c\theta \end{bmatrix} \begin{bmatrix} 0 \\ 0 \\ \dot{\psi} \end{bmatrix}, \quad (14)$$

$$\boldsymbol{\omega}_{b/n}^b = \begin{bmatrix} \dot{\phi} - \dot{\psi} s\theta \\ \dot{\theta} c\phi + \dot{\psi} c\theta s\phi \\ \dot{\psi} c\theta c\phi - \dot{\theta} s\phi \end{bmatrix}, \quad (15)$$

$$\boldsymbol{\omega}_{b/n}^b = \begin{bmatrix} 1 & 0 & -s\theta \\ 0 & c\phi & c\theta s\phi \\ 0 & -s\phi & c\theta c\phi \end{bmatrix} \begin{bmatrix} \dot{\phi} \\ \dot{\theta} \\ \dot{\psi} \end{bmatrix}, \quad (16)$$

$$\boldsymbol{\omega}_{b/n}^b = \mathbf{T}_{\Theta}^{-1}(\boldsymbol{\Theta}_{nb}) \dot{\boldsymbol{\Theta}}_{nb}. \quad (17)$$

The inverse angular velocity transformation can be written as

$$\dot{\boldsymbol{\Theta}}_{nb} = \mathbf{T}_{\Theta}(\boldsymbol{\Theta}_{nb}) \boldsymbol{\omega}_{b/n}^b, \quad (18)$$

where

$$\mathbf{T}_{\Theta}(\boldsymbol{\Theta}_{nb}) = \begin{bmatrix} 1 & s\phi t\theta & c\phi t\theta \\ 0 & c\phi & -s\phi \\ 0 & \frac{s\phi}{c\theta} & \frac{c\phi}{c\theta} \end{bmatrix}, \quad \theta \neq \pm 90^\circ \quad (19)$$

The angular velocity transformation $\mathbf{T}_{\Theta}(\boldsymbol{\Theta}_{nb})$ has a singularity in $\theta \neq \pm 90^\circ$. Other form to express the kinematic equations of motion could be, using Euler angle representation with different singularities or using a quaternion representation [13]. More details in quaternion representation can be seen in [53]. A compilation of the kinematics equation of motion can be summarized as

$$\begin{bmatrix} \dot{\mathbf{p}}_{b/n}^n \\ \dot{\boldsymbol{\Theta}}_{nb} \end{bmatrix} = \begin{bmatrix} \mathbf{R}_b^n(\boldsymbol{\Theta}_{nb}) & \mathbf{0}_{3 \times 3} \\ \mathbf{0}_{3 \times 3} & \mathbf{T}_{\Theta}(\boldsymbol{\Theta}_{nb}) \end{bmatrix} \begin{bmatrix} \mathbf{v}_{b/n}^b \\ \boldsymbol{\omega}_{b/n}^b \end{bmatrix}, \quad (20)$$

$$\dot{\boldsymbol{\eta}} = \mathbf{J}_{\Theta}(\boldsymbol{\eta}) \boldsymbol{\nu}. \quad (21)$$

2.2. RIGID BODY DYNAMICS

The mathematical model that describes the 6-DOF differential nonlinear equation of motion for an underwater vehicle, stated in [13], is given by

$$\mathbf{M}\dot{\boldsymbol{\nu}} + \mathbf{C}(\boldsymbol{\nu})\boldsymbol{\nu} + \mathbf{D}(\boldsymbol{\nu})\boldsymbol{\nu} + \mathbf{g}(\boldsymbol{\eta}) = \boldsymbol{\tau}, \quad (22)$$

$$\dot{\boldsymbol{\eta}} = \mathbf{J}_{\Theta}(\boldsymbol{\eta}) \boldsymbol{\nu}, \quad (23)$$

where $\mathbf{M} \in \mathbb{R}^{6 \times 6}$ is the inertia matrix, which comprises the mass of the rigid body and the added mass, $\mathbf{M} = \mathbf{M}_{RB} + \mathbf{M}_A$; $\mathbf{C} \in \mathbb{R}^{6 \times 6}$ is the Coriolis and centripetal matrix, which includes the term due to rigid body and the term due to the added mass,

$\mathbf{C} = \mathbf{C}_{RB} + \mathbf{C}_A$; $\mathbf{D} \in \mathbb{R}^{6 \times 6}$ is the damping matrix; $\mathbf{g} \in \mathbb{R}^{6 \times 1}$ is the gravitational and moments vector; $\boldsymbol{\tau} \in \mathbb{R}^{6 \times 1}$ is the force vector; and $\mathbf{J}_\Theta \in \mathbb{R}^{6 \times 6}$ is the rotation matrix from the body-fixed frame to the Earth-fixed frame. The last terms are explained in the following sections.

Applying Newtonian laws, the rigid body equation of motion for the vehicle is

$$\mathbf{M}_{RB} \dot{\mathbf{v}} + \mathbf{C}_{RB}(\mathbf{v}) \mathbf{v} = \boldsymbol{\tau}_{RB}. \quad (24)$$

In (24) the rigid body inertia matrix \mathbf{M}_{RB} can be expressed as

$$\mathbf{M}_{RB} = \begin{bmatrix} m \mathbf{I}_{3 \times 3} & -m \mathbf{S}(\mathbf{r}_g^b) \\ m \mathbf{S}(\mathbf{r}_g^b) & \mathbf{I}_b \end{bmatrix}, \quad (25)$$

where m is the mass of the vehicle, $\mathbf{I}_{3 \times 3}$ the identity matrix, \mathbf{I}_b the inertia tensor with respect to an arbitrary fixed body frame given by

$$\mathbf{I}_b = \begin{bmatrix} I_x & -I_{xy} & -I_{xz} \\ -I_{yx} & I_y & -I_{yz} \\ -I_{zx} & -I_{zy} & I_z \end{bmatrix}. \quad (26)$$

In (26) I_x , I_y , and I_z are the inertia moments around the x_b , y_b , and z_b axes; and $I_{xy} = I_{yx}$, $I_{xz} = I_{zx}$ and $I_{yz} = I_{zy}$ are the products of inertia. $\mathbf{r}_g^b = [x_g \ y_g \ z_g]^T$ is the gravity vector with respect to the body-fixed frame $\{b\}$ and $\mathbf{S}(\cdot)$ a skew symmetric matrix with $\lambda = [\lambda_1 \ \lambda_2 \ \lambda_3]$ and defined by

$$\mathbf{S}(\lambda) = \begin{bmatrix} 0 & -\lambda_3 & \lambda_2 \\ \lambda_3 & 0 & -\lambda_1 \\ -\lambda_2 & \lambda_1 & 0 \end{bmatrix}. \quad (27)$$

Using (26) and (27) in (25), and expanding the expression, yields

$$\mathbf{M}_{RB} = \begin{bmatrix} m & 0 & 0 & 0 & mz_g & -my_g \\ 0 & m & 0 & -mz_g & 0 & mx_g \\ 0 & 0 & m & my_g & -mx_g & 0 \\ 0 & -mz_g & my_g & I_x & -I_{xy} & -I_{xz} \\ mz_g & 0 & -mx_g & -I_{yx} & I_y & -I_{yz} \\ -my_g & mx_g & 0 & -I_{zx} & -I_{zy} & I_z \end{bmatrix}. \quad (28)$$

According to [13], the rigid body inertia matrix (28) is unique and satisfies

$$\mathbf{M}_{RB} = \mathbf{M}_{RB}^T > 0, \quad \dot{\mathbf{M}}_{RB} = \mathbf{0}_{6 \times 6}. \quad (29)$$

The rigid body centripetal and Coriolis matrix can be parametrized in the form of a skew symmetric matrix

$$\mathbf{C}_{RB}(\boldsymbol{\nu}) = \begin{bmatrix} \mathbf{C}_{RB_{11}} & \mathbf{C}_{RB_{12}} \\ \mathbf{C}_{RB_{21}} & \mathbf{C}_{RB_{22}} \end{bmatrix}, \quad (30)$$

where

$$\mathbf{C}_{RB_{11}} = \mathbf{0}_{3 \times 3}, \quad (31)$$

$$\mathbf{C}_{RB_{12}} = -m\mathbf{S}(\boldsymbol{\nu}_1) - m\mathbf{S}(\boldsymbol{\nu}_2)\mathbf{S}(\mathbf{r}_g^b), \quad (32)$$

$$\mathbf{C}_{RB_{21}} = -m\mathbf{S}(\boldsymbol{\nu}_1) + m\mathbf{S}(\boldsymbol{\nu}_2)\mathbf{S}(\mathbf{r}_g^b), \quad (33)$$

$$\mathbf{C}_{RB_{22}} = -\mathbf{S}(\mathbf{I}_b)\boldsymbol{\nu}_2, \quad (34)$$

$$\boldsymbol{\nu}_1 = \mathbf{v}_{b/n}^b = [u \ v \ w]^T, \quad (35)$$

$$\boldsymbol{\nu}_2 = \boldsymbol{\omega}_{b/n}^b = [p \ q \ r]^T. \quad (36)$$

Therefore, $\mathbf{C}_{RB}(\boldsymbol{\nu})$ can be written as

$$\mathbf{C}_{RB}(\boldsymbol{\nu}) = \begin{bmatrix} 0 & 0 & 0 \\ 0 & 0 & 0 \\ 0 & 0 & 0 \\ -m(y_g q + z_g r) & m(y_g p + w) & m(z_g p - v) \\ m(x_g q - w) & -m(z_g r + x_g p) & m(z_g q + u) \\ m(x_g r + v) & m(y_g r - u) & -m(x_g p + y_g q) \\ m(y_g q + z_g r) & -m(x_g q - w) & -m(x_g r + v) \\ -m(y_g p + w) & m(z_g r + x_g p) & -m(y_g r - u) \\ -m(z_g p - v) & -m(z_g q + u) & m(x_g p + y_g q) \\ 0 & -I_{yz}q - I_{xz}p + I_z r & I_{yz}r + I_{xy}p - I_y q \\ I_{yz}q + I_{xz}p - I_z r & 0 & -I_{xz}r - I_{xy}q + I_x p \\ -I_{yz}r - I_{xy}p + I_y q & I_{xz}r + I_{xy}q - I_x p & 0 \end{bmatrix}. \quad (37)$$

Using (28) and (37) in (24), the general 6-DOF rigid body equations of motion can be

written as

$$X = m [\dot{u} - vr + wq - x_g (q^2 + r^2) + y_g (pq - \dot{r}) + z_g (pr + \dot{q})], \quad (38)$$

$$Y = m [\dot{v} - wp + ur - y_g (r^2 + p^2) + z_g (qr - \dot{p}) + x_g (qp + \dot{r})], \quad (39)$$

$$Z = m [\dot{w} - uq + vp - z_g (p^2 + q^2) + x_g (rp - \dot{q}) + y_g (rq + \dot{p})], \quad (40)$$

$$K = I_x \dot{p} + (I_z - I_y) qr - (\dot{r} + pq) I_{xz} + (r^2 - q^2) I_{yz} + (pr - \dot{q}) I_{xy} \\ + m [y_g (\dot{w} - uq + vp) - z_g (\dot{v} - wp + ur)], \quad (41)$$

$$M = I_y \dot{q} + (I_x - I_z) rp - (\dot{p} + qr) I_{xy} + (p^2 - r^2) I_{zx} + (qp - \dot{r}) I_{yz} \\ + m [z_g (\dot{u} - vr + wq) - x_g (\dot{w} - uq + vp)], \quad (42)$$

$$N = I_z \dot{r} + (I_y - I_x) pq - (\dot{q} + rp) I_{yz} + (q^2 - p^2) I_{xy} + (rp - \dot{p}) I_{zx} \\ + m [x_g (\dot{v} - wp + ur) - y_g (\dot{u} - vr + wq)]. \quad (43)$$

2.3. HYDRODYNAMIC FORCES AND MOMENTS

The hydrodynamic forces and moments appear when the vehicle interacts with the fluid. These forces and moments can be linearly superposed according to [53], and are described as the sum of three components [13]:

- **Added mass:** due to the inertia of the fluid that interacts when the vehicle is moving.
- **Potential damping:** appears due to the energy carried away by generated waves.
- **Restoring forces:** appears due to the weight and buoyancy of the vehicle.

Therefore, these three items can be expressed as

$$\boldsymbol{\tau}_H = -\mathbf{M}_A \dot{\boldsymbol{\nu}} - \mathbf{C}_A(\boldsymbol{\nu}) \boldsymbol{\nu} - \mathbf{D}(\boldsymbol{\nu}) \boldsymbol{\nu} - \mathbf{g}(\boldsymbol{\eta}). \quad (44)$$

2.3.1. Added mass

The concept of added mass appears when a vehicle must displace some volume of the fluid as it moves through it. This term can be derived using an energy approach. The added mass is not a finite mass of water attached to the vehicle's body, since it varies

with the shape and volume of the vehicle as well as its rate of change. The added mass due to the inertia of the surrounding fluid is given by

$$\begin{aligned} \mathbf{M}_A &= \begin{bmatrix} \mathbf{A}_{11}^{3 \times 3} & \mathbf{A}_{12}^{3 \times 3} \\ \mathbf{A}_{21}^{3 \times 3} & \mathbf{A}_{22}^{3 \times 3} \end{bmatrix} \\ &= - \begin{bmatrix} X_{\dot{u}} & X_{\dot{v}} & X_{\dot{w}} & X_{\dot{p}} & X_{\dot{q}} & X_{\dot{r}} \\ Y_{\dot{u}} & Y_{\dot{v}} & Y_{\dot{w}} & Y_{\dot{p}} & Y_{\dot{q}} & Y_{\dot{r}} \\ Z_{\dot{u}} & Z_{\dot{v}} & Z_{\dot{w}} & Z_{\dot{p}} & Z_{\dot{q}} & Z_{\dot{r}} \\ K_{\dot{u}} & K_{\dot{v}} & K_{\dot{w}} & K_{\dot{p}} & K_{\dot{q}} & K_{\dot{r}} \\ M_{\dot{u}} & M_{\dot{v}} & M_{\dot{w}} & M_{\dot{p}} & M_{\dot{q}} & M_{\dot{r}} \\ N_{\dot{u}} & N_{\dot{v}} & N_{\dot{w}} & N_{\dot{p}} & N_{\dot{q}} & N_{\dot{r}} \end{bmatrix}, \end{aligned} \quad (45)$$

where the hydrodynamic parameter $X_{\dot{v}}$ denotes the force along the x -axis due to an acceleration \dot{v} in the y direction given as

$$X_{\dot{v}} \triangleq \frac{\partial X}{\partial \dot{v}}. \quad (46)$$

Finding the 36 elements of \mathbf{M}_A is a difficult task, but this can be simplified exploiting symmetry properties of the vehicle. It has been proven that the parameters obtained from ideal theory are very similar to the parameters obtained with a real fluid [53]. Additionally, for completely submerged vehicles that move with low speed, the added inertia mass matrix is positive definite:

$$\mathbf{M}_A = \mathbf{M}_A^T > 0 \quad (47)$$

The inertia tensor obtained through CAD model, is given by

$$\mathbf{I} = \begin{bmatrix} 2.9 & -7.0 \times 10^{-3} & -2.1 \times 10^{-3} \\ -7.0 \times 10^{-3} & 2.5 & -7.2 \times 10^{-3} \\ -2.1 \times 10^{-3} & -7.2 \times 10^{-3} & 3.0 \end{bmatrix}. \quad (48)$$

For this work, Visor3 is assumed to have symmetry about xy , xz and yz planes, due to the I_{xy} , I_{xz} , and I_{yz} are approximately zero. Therefore, the added mass matrix can be computed as

$$\mathbf{M}_A = -\text{diag} \{X_{\dot{u}}, Y_{\dot{v}}, Z_{\dot{w}}, K_{\dot{p}}, M_{\dot{q}}, N_{\dot{r}}\}. \quad (49)$$

The hydrodynamic centripetal and Coriolis matrix can also be parametrized as

$$\mathbf{C}_A(\boldsymbol{\nu}) = \begin{bmatrix} \mathbf{0}_{3 \times 3} & -\mathbf{S}(\mathbf{A}_{11}\boldsymbol{\nu}_1 + \mathbf{A}_{12}\boldsymbol{\nu}_2) \\ -\mathbf{S}(\mathbf{A}_{11}\boldsymbol{\nu}_1 + \mathbf{A}_{12}\boldsymbol{\nu}_2) & -\mathbf{S}(\mathbf{A}_{21}\boldsymbol{\nu}_1 + \mathbf{A}_{22}\boldsymbol{\nu}_2) \end{bmatrix}. \quad (50)$$

Substituting (35), (36) and (45) into (50), allows one to describe $\mathbf{C}_A(\boldsymbol{\nu})$ as

$$\mathbf{C}_A(\boldsymbol{\nu}) = \begin{bmatrix} 0 & 0 & 0 & 0 & -a_3 & a_2 \\ 0 & 0 & 0 & a_3 & 0 & -a_1 \\ 0 & 0 & 0 & -a_2 & a_1 & 0 \\ 0 & -a_3 & a_2 & 0 & -b_3 & b_2 \\ a_3 & 0 & -a_1 & b_3 & 0 & -b_1 \\ -a_2 & a_1 & 0 & -b_2 & b_1 & 0 \end{bmatrix}, \quad (51)$$

where

$$a_1 = X_{\dot{u}}u + X_{\dot{v}}v + X_{\dot{w}}w + X_{\dot{p}}p + X_{\dot{q}}q + X_{\dot{r}}r, \quad (52)$$

$$a_2 = X_{\dot{v}}u + Y_{\dot{v}}v + Y_{\dot{w}}w + Y_{\dot{p}}p + Y_{\dot{q}}q + Y_{\dot{r}}r, \quad (53)$$

$$a_3 = X_{\dot{w}}u + Y_{\dot{w}}v + Z_{\dot{w}}w + Z_{\dot{p}}p + Z_{\dot{q}}q + Z_{\dot{r}}r, \quad (54)$$

$$b_1 = X_{\dot{p}}u + Y_{\dot{p}}v + Z_{\dot{p}}w + K_{\dot{p}}p + K_{\dot{q}}q + K_{\dot{r}}r, \quad (55)$$

$$b_2 = X_{\dot{q}}u + Y_{\dot{q}}v + Z_{\dot{q}}w + K_{\dot{q}}p + M_{\dot{q}}q + M_{\dot{r}}r, \quad (56)$$

$$b_3 = X_{\dot{r}}u + Y_{\dot{r}}v + Z_{\dot{r}}w + K_{\dot{r}}p + M_{\dot{r}}q + N_{\dot{r}}r. \quad (57)$$

Visor3's Coriolis and centripetal force due to the added mass can be found by substituting (49) into (51), which yields

$$\mathbf{C}_A(\boldsymbol{\nu}) = \begin{bmatrix} 0 & 0 & 0 & 0 & -Z_{\dot{w}}w & -Y_{\dot{v}}v \\ 0 & 0 & 0 & Z_{\dot{w}}w & 0 & -X_{\dot{u}}u \\ 0 & 0 & 0 & -Y_{\dot{v}}v & X_{\dot{u}}u & 0 \\ 0 & -Z_{\dot{w}}w & Y_{\dot{v}}v & 0 & -N_{\dot{r}}r & M_{\dot{q}}q \\ Z_{\dot{w}}w & 0 & -X_{\dot{u}}u & N_{\dot{r}}r & 0 & -K_{\dot{p}}p \\ -Y_{\dot{v}}v & X_{\dot{u}}u & 0 & -M_{\dot{q}}q & K_{\dot{p}}p & 0 \end{bmatrix}. \quad (58)$$

2.3.2. Hydrodynamic damping

According to [13] the hydrodynamic damping is mainly caused by:

- Potential damping due to forced body oscillations mainly caused by the waves.
- Linear skin friction due to the laminar boundary layers when the vehicle is moving at low speed.
- Quadratic skin friction due to the turbulent boundary layers.

- Wave drift damping, that is the resistance to advance due to waves.
- Damping due to the vortex shedding.

For underwater vehicles damping is mainly caused by skin friction and vortex shedding. One approximation commonly used [13, 53, 54] is a linear and quadratic damping term given as

$$\begin{aligned} \mathbf{D}(\boldsymbol{\nu}) = & -\text{diag}\{X_u, Y_v, Z_w, K_p, M_q, N_r\} \\ & -\text{diag}\{X_{u|u}|u|, Y_{v|v}|v|, Z_{w|w}|w|, K_{p|p}|p|, \\ & M_{q|q}|q|, N_{r|r}|r|\}. \end{aligned} \quad (59)$$

2.3.3. Restoring forces and moments

The gravitational force \mathbf{f}_g^b acts through the center of gravity of the vehicle, defined by the vector $\mathbf{r}_g^b = [x_g \ y_g \ z_g]^T$. The buoyant force \mathbf{f}_b^b acts through the center of buoyancy of the vehicle, defined by the vector $\mathbf{r}_b^b = [x_b \ y_b \ z_b]^T$. The force vectors that act on the vehicle (see Figure 4) expressed in the $\{n\}$ frame are

$$\mathbf{f}_g^n = \begin{bmatrix} 0 \\ 0 \\ W \end{bmatrix}, \text{ and } \mathbf{f}_b^n = -\begin{bmatrix} 0 \\ 0 \\ B \end{bmatrix}. \quad (60)$$

These two forces can be obtained in the body-fixed frame $\{b\}$ by applying the rotation matrix and expressed by

$$\mathbf{f}_g^b = \mathbf{R}_b^n (\boldsymbol{\Theta}_{nb})^{-1} \mathbf{f}_g^n, \quad (61)$$

$$\mathbf{f}_b^b = \mathbf{R}_b^n (\boldsymbol{\Theta}_{nb})^{-1} \mathbf{f}_b^n. \quad (62)$$

Using the previous result, the restoring forces can be calculated as

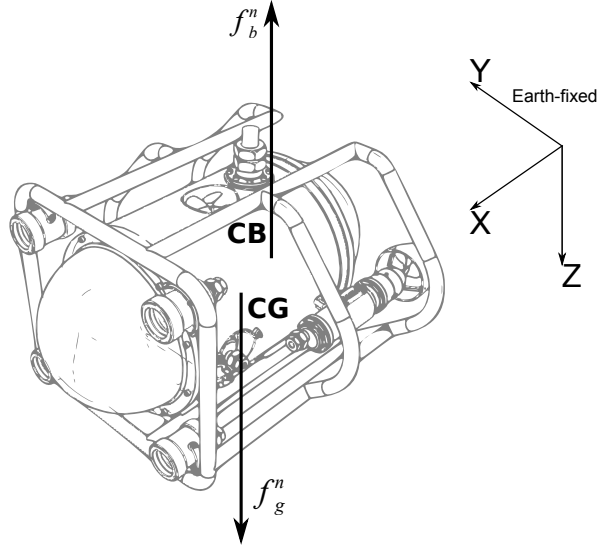


Figure 4. Center of gravity and center of buoyancy.

$$\mathbf{g}(\boldsymbol{\eta}) = - \begin{bmatrix} \mathbf{f}_g^b + \mathbf{f}_b^b \\ \mathbf{r}_g^b \times \mathbf{f}_g^b + \mathbf{r}_b^b \times \mathbf{f}_b^b \end{bmatrix} \quad (63)$$

$$= - \begin{bmatrix} \mathbf{R}_b^n (\boldsymbol{\Theta}_{nb})^{-1} (\mathbf{f}_g^n + \mathbf{f}_b^n) \\ \mathbf{r}_g^b \times \mathbf{R}_b^n (\boldsymbol{\Theta}_{nb})^{-1} \mathbf{f}_g^n + \mathbf{r}_b^b \times \mathbf{R}_b^n (\boldsymbol{\Theta}_{nb})^{-1} \mathbf{f}_b^n \end{bmatrix} \quad (64)$$

$$= \begin{bmatrix} (W - B) \sin \theta \\ -(W - B) \cos \theta \sin \phi \\ -(W - B) \cos \theta \cos \phi \\ -(y_g W - y_b B) \cos \theta \cos \phi + (z_g W - z_b B) \cos \theta \sin \phi \\ (z_g W - z_b B) \sin \theta + (x_g W - x_b B) \cos \theta \cos \phi \\ -(x_g W - x_b B) \cos \theta \sin \phi - (y_g W - y_b B) \sin \theta \end{bmatrix}, \quad (65)$$

where $W = mg$ is the weight of the vehicle. $B = \rho g \nabla$ is the buoyancy, where ρ is the density of the fluid, g is the acceleration of the gravity, and ∇ the volume of fluid displaced by the vehicle.

2.4. THRUSTER MODEL

The propulsion system is defined as the set of parts which enable the ROV to move. The system takes energy given by the power source and then transforms it into mechanical energy that moves the propeller and impulse the vehicle. According to [55] the propulsion system is divided into four main parts (see Figure 6): the low-level thruster controller which regulates the power given to the motor in order to maintain the velocity in the shaft; the motor dynamics which transforms the electricity into mechanical energy; shaft dynamics which transmits the torque given by the motor to the propeller; and finally the propeller transforms the torque given by the shaft into thrust.

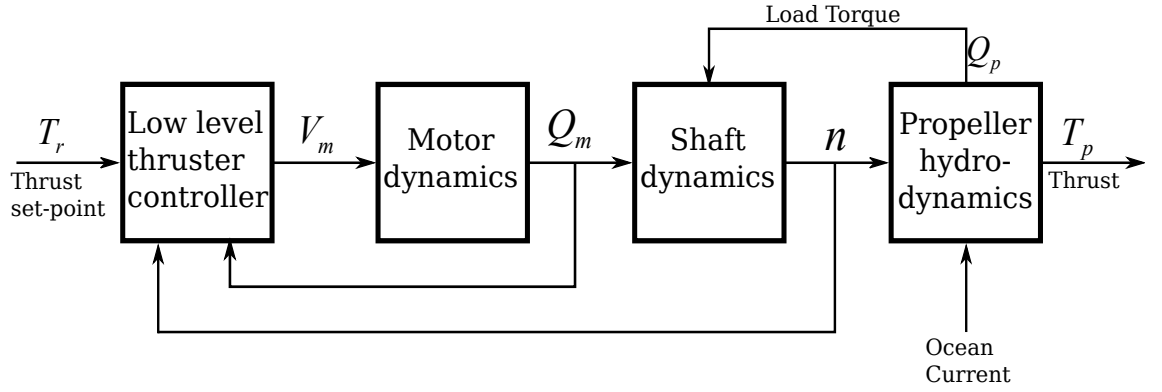


Figure 5. Propulsion system scheme [55].

Different types of propellers exist, but there are two main types: fixed pitch propellers (FPP) and controllable pitch propellers (CPP). FPP can be only controlled through the speed of the shaft, instead CPP can be controlled by speed and the angle of the propellers blades. Additionally, the propeller can be ducted or open. In a ducted propeller, the propeller is surrounded by a duct or nozzle, which increases the efficiency of the propeller [55].

Visor3 has four thrusters with ducted fixed pitch propellers that allow the vehicle to move in four independent directions, see Figure 6.

- **Motor dynamics:** The main objective for a DC motor is to provide speed and torque. The torque given by the motor can be regulated through the current in the motor winding. The relation between the voltage source and the motor speed

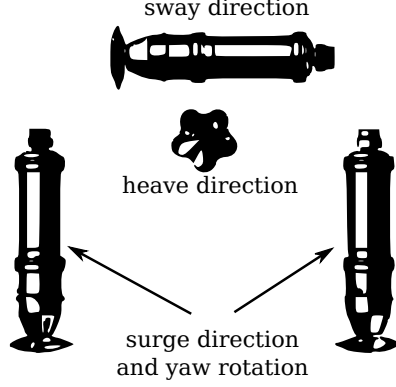


Figure 6. Propulsion system configuration for Visor3 [56].

is given by

$$\frac{di}{dt} = \frac{1}{L} (u - Ri - K_v n), \quad (66)$$

$$\frac{dn}{dt} = \frac{1}{J} (K_m i - Q_p - \beta n), \quad (67)$$

where i is the current in the armature, L the inductance, u the voltage input, R the rotor resistor, K_v the speed constant, n the shaft velocity, J the inertia of the shaft, K_m the torque constant, β the friction coefficient, and Q_p the load torque. Visor3 uses EC 45 DC motors from MAXON. These motors are brushless and work at 48 VDC; Table 2 shows the parameters from motor.

Table 2. MAXON Parameters

| Parameter | Symbol | Value |
|-------------------------|---------|--|
| Armature resistor | R | $3.85 \, \Omega$ |
| Armature inductance | L | $1.19 \times 10^{-3} \, \text{H}$ |
| Motor torque constant | K_m | $77.10 \times 10^{-3} \, \text{Nm/A}$ |
| Motor velocity constant | K_v | $7.70 \times 10^{-2} \, \text{V s/rad}$ |
| Motor friction constant | β | $1.98 \times 10^{-5} \, \text{Nm s/rad}$ |
| Inertia shaft | J | $1.19 \times 10^{-5} \, \text{kgm}^2$ |

- **Propeller:** the propeller function is to transform rotational speed given by the motor into thrust that allows the ROV to move through the water. The force and moment generated by the propeller is a function of the vehicle's velocity vector and

the shaft velocity expressed by

$$\boldsymbol{\tau} = \mathbf{b}(\boldsymbol{\nu}, \mathbf{n}), \quad (68)$$

where $\mathbf{b}(\cdot)$ is a nonlinear function describing the relationship between $\boldsymbol{\nu}$ and \mathbf{n} . A first order approximation of the thrust T and torque Q , is given by

$$T = \rho D^4 K_T(J_0) |n|n, \quad (69)$$

$$Q = \rho D^5 K_Q(J_0) |n|n, \quad (70)$$

where ρ the water density, D the propeller diameter, K_T is the thrust coefficient, K_Q the torque coefficient, J_0 the advance number, and n denotes the propeller revolution. According to [55], K_T is a four quadrant nonlinear function that depends on the advance number. The advance number J_0 is given by

$$J_0 = \frac{V_a}{nD}, \quad (71)$$

where V_a is the advance speed related to the velocity of the vehicle V according to:

$$V_a = (1 - w) V. \quad (72)$$

w is the wake fraction number that relates the relative velocity. For underwater vehicles the wake fraction can be approximated to zero $w \approx 0$. According to [13], the thrust coefficient can be approximated to a linear behavior such as

$$K_T = k_1 + k_2 \frac{V_a}{nD}. \quad (73)$$

For underwater vehicles that are moving at low speed, the advance number can be approximated to zero $J \approx 0$. For this work this is assumed, hence, the thrust coefficient is simply a constant k_1 (for more details [54]).

2.5. OCEAN CURRENT

The forces generated by the ocean current are included in the model through the ocean current velocity in the body-fixed frame. In the model this is simply included through the relative velocity as

$$\mathbf{M}_{RB} \dot{\boldsymbol{\nu}} + \mathbf{C}_{RB}(\boldsymbol{\nu}) \boldsymbol{\nu} + \mathbf{M}_A \dot{\boldsymbol{\nu}}_r + \mathbf{C}_A(\boldsymbol{\nu}_r) \boldsymbol{\nu}_r + \mathbf{D}(\boldsymbol{\nu}_r) \boldsymbol{\nu}_r + \mathbf{g}(\boldsymbol{\eta}) = \boldsymbol{\tau}. \quad (74)$$

$\boldsymbol{\nu}_r \in \mathbb{R}^{6 \times 1}$ is the relative velocity vector with respect to the water and it is calculated as

$$\boldsymbol{\nu}_r = \boldsymbol{\nu} - \boldsymbol{\nu}_c, \quad (75)$$

where $\boldsymbol{\nu}_c \in \mathbb{R}^{6 \times 1}$ is the ocean current velocity vector decomposed in the body frame. For irrotational ocean currents, the velocity can be decomposed as

$$\boldsymbol{\nu}_c = [u_c \ v_c \ w_c \ 0 \ 0 \ 0]^T. \quad (76)$$

3. NONLINEAR MODEL BASED OBSERVER

Underwater navigation is one of the problems more studied in the navigation area, in order to build more autonomous underwater vehicles (AUV). The difference with a vessel navigation system, is that for underwater vehicles GPS signals do not penetrate the surface of the water, therefore, another system must be installed to the vehicle to improve the performance of the navigation system.

There are two main types of navigation systems: sensor navigation systems, which use the information provided by all sensors in the system and estimate the position and attitude of the vehicle through these measures; and the model-based navigation system that are very efficient at filtering noise and estimating states when there is a good knowledge of the vehicle's dynamic parameters. However, unmodelled dynamics and disturbances in the vehicle can cause error in the position and attitude estimation.

This chapter addresses the first approach to develop the navigation system for the ROV Visor3 that will help operators to determine the position and attitude of the vehicle under certain scenarios where there is no visual information from the water surface such as in ports or dams inspection tasks. The first part presents concepts about random processes and stochastic systems, the second part shows the structure of the Kalman filter, then the extended Kalman filter version for nonlinear systems is presented.

3.1. STATISTICS AND STOCHASTIC SYSTEMS

The basic concept of statistics is the study of interpretation and organization of data. From these data, statistical characteristics such as mean, variance, covariance, among others, can be obtained. The focus of this subsection is the statistical properties of the system and to describe its dynamics as a random process.

3.1.1. Gaussian probability distribution

A Gaussian probability distribution is a function that expresses the probability that a measure will fall between two limits, as the curve approaches to zero. The middle of this two limits is known as the mean [3]. The notation used to express a Gaussian distribution is $\mathcal{N}(\bar{x}, \sigma^2)$ and its density function described by

$$p(x) = \frac{1}{\sqrt{2\pi}\sigma} \exp \left[-\frac{1}{2} \frac{(x - \bar{x})^2}{\sigma^2} \right], \quad (77)$$

where

$$\bar{x} = E \langle x \rangle \quad (78)$$

is the expected value or the mean, and σ^2 is the variance. The expected value or the expectancy $E \langle x \rangle$ or Ex denotes the expected value of the possible values from the random variable x . Figure 7(a) represents changes in the variance from equation (77) and the Figure 7(b) changes in the expected value.

- **Random processes (RPs):** a random process is the collection of random variables that represent the evolution of some system over the time. If the random variable is a function for each outcome of an experiment, the random process will be formed by these outcomes over time. Theses RPs can be represented by $x(t, s)$ and in discrete time by $x(k, s)$, where s is each outcome of the experiment.

3.1.2. Some statistics definitions

- **Mean:** is the probability weighted average of all possible values, i.e., each possible value is multiplied by its probability, and the results are summed to obtain the mean. The expected value can be described by

$$Ex(t) = \int_{-\infty}^{\infty} x(t) p[x(t)] dx(t), \quad (79)$$

or in discrete time by

$$Ex(k) = \sum_{i=1}^{\infty} x_i p_i. \quad (80)$$

- **Correlation:** is the relationship between two random processes. The correlation

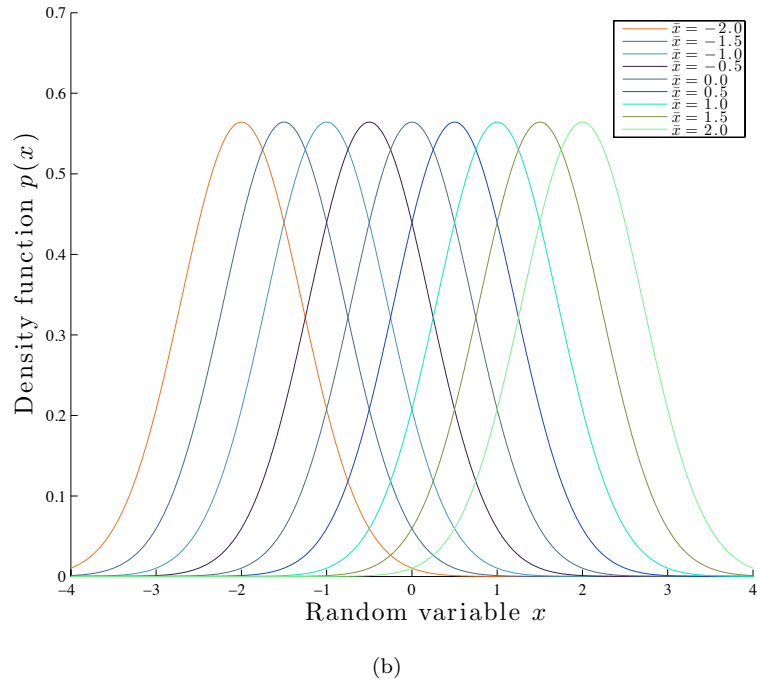
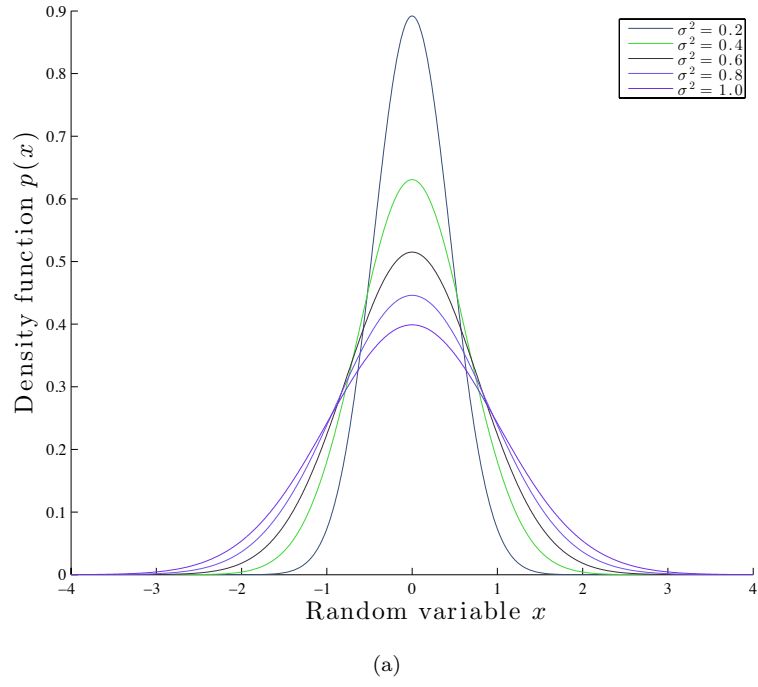


Figure 7. Gaussian probability distribution. (a) change in the variance σ^2 . (b) change in the expected value \bar{x} .

of the vector process $x(t)$ is defined by

$$E \langle x(t_1) x^T(t_2) \rangle = \begin{bmatrix} E \langle x_1(t_1) x_1(t_2) \rangle & \dots & E \langle x_1(t_1) x_n(t_2) \rangle \\ \vdots & \ddots & \vdots \\ E \langle x_n(t_1) x_1(t_2) \rangle & \dots & E \langle x_n(t_1) x_n(t_2) \rangle \end{bmatrix}, \quad (81)$$

where

$$E x_i(t_1) x_j(t_2) = \int_{-\infty}^{\infty} \int_{-\infty}^{\infty} x_i(t_1) x_j(t_2) p[x_i(t_1) x_j(t_2)] dx_i(t_1) dx_j(t_2). \quad (82)$$

Two random processes are orthogonal if their correlation matrix is identically to zero.

- **Covariance:** the covariance is a measure of how much two random variables change together and is defined by

$$E \langle [x(t_1) - E x(t_1)] [x(t_2) - E x(t_2)]^T \rangle = E \langle x(t_1) x^T(t_2) \rangle - E \langle x(t_1) \rangle E \langle x^T(t_2) \rangle. \quad (83)$$

The covariance between two RPs is called cross-covariance, and is the covariance of each process with the other at the same time periods. When the cross-covariance is zero for all t_1 and t_2 , these processes are called uncorrelated. A random process $x(t)$ is called uncorrelated if

$$E \langle [x(t_1) - E \langle x(t_1) \rangle] [x(t_2) - E \langle x(t_2) \rangle]^T \rangle = Q(t_1, t_2) \delta(t_1 - t_2), \quad (84)$$

where $\delta(t)$ is the Dirac delta function. A random sequence x_k is called uncorrelated if

$$E \langle [x_k - E x(t_1)] [x(t_2) - E x(t_2)]^T \rangle = Q(k, j) \Delta(k - j), \quad (85)$$

where $\Delta(\cdot)$ is the Kronecker delta function, defined by

$$\Delta(k) = \begin{cases} 1 & \text{if } k = 0 \\ 0 & \text{otherwise.} \end{cases} \quad (86)$$

3.2. KALMAN FILTER

The Kalman filter, also known as linear quadratic estimator (LQE), is an algorithm that uses a series of measurements with noise, and produces estimates of the unknown

states with more precision than those based on a single measurement. The Kalman filter generates a statistically optimal estimate of the system state. It is optimal in the sense that minimizes the expected value of a quadratic loss function.

The system is modelled by the state transition equation given by

$$\mathbf{x}_k = \Phi_{k-1}\mathbf{x}_{k-1} + \Gamma_{k-1}\mathbf{u}_{k-1} + \mathbf{w}_{k-1}, \quad (87)$$

where \mathbf{x}_{k-1} is the state vector, Φ_{k-1} is the state transition matrix, Γ_{k-1} is the input-coupling matrix, \mathbf{u}_{k-1} is the input control vector, and \mathbf{w}_{k-1} is the process noise. The system measurements or the output can be represented by the linear equation

$$\mathbf{z}_k = \mathbf{H}_k\mathbf{x}_k + \mathbf{v}_k, \quad (88)$$

where \mathbf{z}_k is the measurement, \mathbf{H}_k is the measurement sensitivity matrix, and \mathbf{v}_k is the measurement noise. The plant (\mathbf{w}_{k-1}) and the measurement (\mathbf{v}_k) are assumed to be zero-mean Gaussian white noise processes with covariance matrices \mathbf{Q}_k and \mathbf{R}_k and uncorrelated, given by

$$E \langle \mathbf{w}_k \rangle = 0, \quad (89)$$

$$E \langle \mathbf{w}_k \mathbf{w}_i^T \rangle = \Delta(k-i) \mathbf{Q}_k, \quad (90)$$

$$E \langle \mathbf{v}_k \rangle = 0, \quad (91)$$

$$E \langle \mathbf{v}_k \mathbf{v}_i^T \rangle = \Delta(k-i) \mathbf{R}_k. \quad (92)$$

The initial value \mathbf{x}_0 is Gaussian variate with known mean and covariance matrix \mathbf{P}_0 . The objective of the Kalman filter is to find an estimate of the state vector $\hat{\mathbf{x}}_k$ in a finite time k , given the measurements z_i, \dots, z_k that minimizes the weighted mean-square error

$$E \left\langle [\mathbf{x}_k - \hat{\mathbf{x}}_k]^T M [\mathbf{x}_k - \hat{\mathbf{x}}_k] \right\rangle, \quad (93)$$

where M is a square symmetric non-negative definite weighting matrix. The estimator is unbiased, therefore, the expectation of its output is the expectation of the estimation

$$\hat{x} = E \langle x(t) | z(t) \rangle. \quad (94)$$

- **Prediction step:** The Kalman filter is executed in two steps: the prediction, where a first approximation of the current state and covariance matrix is yielded;

then the correction, which improves the first approximation through the measurements. Then, the a priori predicted state ($\hat{\mathbf{x}}_k(-)$) according to (94) is given by

$$\begin{aligned}\hat{\mathbf{x}}_k(-) &= E \langle \mathbf{x}_k | z_i \dots z_k \rangle, \\ &= E \langle \mathbf{x}_k | \mathbf{Z}_k \rangle.\end{aligned}\tag{95}$$

Substituting (87) into (95) yields

$$\begin{aligned}\hat{\mathbf{x}}_k(-) &= E \langle \Phi_{k-1} \mathbf{x}_{k-1} + \Gamma_{k-1} \mathbf{u}_{k-1} + \mathbf{w}_{k-1} | \mathbf{Z}_k \rangle, \\ &= E \langle \Phi_{k-1} \mathbf{x}_{k-1} | \mathbf{Z}_k \rangle + E \langle \Gamma_{k-1} \mathbf{u}_{k-1} | \mathbf{Z}_k \rangle + E \langle \mathbf{w}_{k-1} | \mathbf{Z}_k \rangle, \\ &= \Phi_{k-1} E \langle \mathbf{x}_{k-1} | \mathbf{Z}_k \rangle + \Gamma_{k-1} \mathbf{u}_{k-1}, \\ &= \Phi_{k-1} \hat{\mathbf{x}}_{k-1}(+) + \Gamma_{k-1} \mathbf{u}_{k-1},\end{aligned}\tag{96}$$

where $\hat{\mathbf{x}}_k(+)$ is the a posteriori estimate of the state given by the measurement vector. The input is known all the time, therefore, the expected value of the input is the same input. The expected value of the plant noise is zero according to (89). To define the estimate covariance matrix, let's define the errors as

$$\tilde{\mathbf{x}}_k(+) = \hat{\mathbf{x}}_k(+) - \mathbf{x}_k,\tag{97}$$

$$\tilde{\mathbf{x}}_k(-) = \hat{\mathbf{x}}_k(-) - \mathbf{x}_k,\tag{98}$$

$$\begin{aligned}\tilde{\mathbf{z}}_k &= \hat{\mathbf{z}}_k(-) - \mathbf{z}_k \\ &= \mathbf{H}_k \hat{\mathbf{x}}_k(-) - \mathbf{z}_k.\end{aligned}\tag{99}$$

Using the results obtained in (96) and (87), and substituting into (98) yields

$$\begin{aligned}\tilde{\mathbf{x}}_k(-) &= \Phi_{k-1} \hat{\mathbf{x}}_{k-1}(+) + \Gamma_{k-1} \mathbf{u}_{k-1} - (\Phi_{k-1} \mathbf{x}_{k-1} + \Gamma_{k-1} \mathbf{u}_{k-1} + \mathbf{w}_{k-1}), \\ &= \Phi_{k-1} (\hat{\mathbf{x}}_{k-1}(+) - \mathbf{x}_{k-1}) - \mathbf{w}_{k-1}, \\ &= \Phi_{k-1} \tilde{\mathbf{x}}_{k-1}(+) - \mathbf{w}_{k-1}.\end{aligned}\tag{100}$$

Using (100) and the definition of the a priori estimate covariance matrix [3], $\mathbf{P}_k(-)$ can be calculated as

$$\begin{aligned}\mathbf{P}_k(-) &= E [\tilde{\mathbf{x}}_k(-) \tilde{\mathbf{x}}_k^T(-) | \mathbf{Z}_k] \\ &= E \left[(\Phi_{k-1} \tilde{\mathbf{x}}_{k-1}(+) - \mathbf{w}_{k-1}) (\Phi_{k-1} \tilde{\mathbf{x}}_{k-1}(+) - \mathbf{w}_{k-1})^T | \mathbf{Z}_k \right] \\ &= E \left[(\Phi_{k-1} \tilde{\mathbf{x}}_{k-1}(+) - \mathbf{w}_{k-1}) (\tilde{\mathbf{x}}_{k-1}^T(+) \Phi_{k-1}^T - \mathbf{w}_{k-1}^T) | \mathbf{Z}_k \right] \\ &= \Phi_{k-1} E [\tilde{\mathbf{x}}_{k-1}(+) \tilde{\mathbf{x}}_{k-1}^T(+) | \mathbf{Z}_k] \Phi_{k-1}^T + E [\mathbf{w}_{k-1} \mathbf{w}_{k-1}^T] \\ &= \Phi_{k-1} \mathbf{P}_{k-1}(+) \Phi_{k-1}^T + \mathbf{Q}_{k-1}.\end{aligned}\tag{101}$$

- **Correction step:** in the second the step, the prediction can be improved using a new measure of the system \mathbf{z}_k , in order to correct the first approximation, i.e., the a posteriori estimation of the state denoted by $\hat{\mathbf{x}}_k(+)$ can be found. It is assumed that the estimate is a weighted sum of the new measure and the result obtained in the prediction, described by the equation

$$\hat{\mathbf{x}}_k(+) = \mathbf{K}'_k \hat{\mathbf{x}}_k(-) + \bar{\mathbf{K}}_k \mathbf{z}_k, \quad (102)$$

where \mathbf{K}'_k and $\bar{\mathbf{K}}_k$ are weighted matrices. To find \mathbf{K}'_k and $\bar{\mathbf{K}}_k$ that minimize the conditional mean squared estimation error, the new estimate $\hat{\mathbf{x}}_k(+)$ must satisfy the orthogonality principle [3]

$$E \langle [\mathbf{x}_k - \hat{\mathbf{x}}_k(+)] | \mathbf{Z}_k \rangle = 0 \quad (103)$$

Using (87) and (102) in (103)

$$\begin{aligned} E \langle [\Phi_{k-1} \mathbf{x}_{k-1} + \mathbf{w}_{k-1} - (\mathbf{K}'_k \hat{\mathbf{x}}_k(-) + \bar{\mathbf{K}}_k \mathbf{z}_k)] | \mathbf{Z}_k \rangle &= 0, \\ \Phi_{k-1} E \langle \mathbf{x}_{k-1} | \mathbf{Z}_k \rangle - \mathbf{K}'_k E \langle \hat{\mathbf{x}}_k(-) | \mathbf{Z}_k \rangle - \bar{\mathbf{K}}_k \mathbf{H}_k \Phi_{k-1} E \langle \mathbf{x}_{k-1} | \mathbf{Z}_k \rangle - \bar{\mathbf{K}}_k E \langle \mathbf{v}_k | \mathbf{Z}_k \rangle &= 0, \\ \Phi_{k-1} E \langle \mathbf{x}_{k-1} | \mathbf{Z}_k \rangle - \mathbf{K}'_k E \langle \hat{\mathbf{x}}_k(-) | \mathbf{Z}_k \rangle - \bar{\mathbf{K}}_k \mathbf{H}_k \Phi_{k-1} E \langle \mathbf{x}_{k-1} | \mathbf{Z}_k \rangle &= 0, \\ E \langle [\mathbf{x}_k - \bar{\mathbf{K}}_k \mathbf{H}_k \mathbf{x}_k - \mathbf{K}'_k \mathbf{x}_k] - \mathbf{K}'_k (\hat{\mathbf{x}}_k(-) - \mathbf{x}_k) | \mathbf{Z}_k \rangle &= 0, \\ [I - \mathbf{K}'_k - \bar{\mathbf{K}}_k \mathbf{H}_k] E \langle \mathbf{x}_k | \mathbf{Z}_k \rangle &= 0. \end{aligned} \quad (104)$$

To satisfy (104), \mathbf{K}'_k must be

$$\mathbf{K}'_k = I - \bar{\mathbf{K}}_k \mathbf{H}_k. \quad (105)$$

With this choice of \mathbf{K}'_k the orthogonality principle is satisfied. Substituting (105) into (102), the a posteriori state estimation (correction of the state) is given by

$$\begin{aligned} \hat{\mathbf{x}}_k(+) &= (I - \bar{\mathbf{K}}_k \mathbf{H}_k) \hat{\mathbf{x}}_k(-) + \bar{\mathbf{K}}_k \mathbf{z}_k, \\ &= \hat{\mathbf{x}}_k(-) - \bar{\mathbf{K}}_k \mathbf{H}_k \hat{\mathbf{x}}_k(-) + \bar{\mathbf{K}}_k \mathbf{z}_k, \\ &= \hat{\mathbf{x}}_k(-) + \bar{\mathbf{K}}_k [\mathbf{z}_k - \mathbf{H}_k \hat{\mathbf{x}}_k(-)], \end{aligned} \quad (106)$$

where $\bar{\mathbf{K}}_k$ is known as the Kalman gain. The Kalman filter gain choice depends on minimizing the mean square error of our loss function. The objective will be

$$\begin{aligned} L &= \min_{\bar{\mathbf{K}}_k} E \langle \tilde{\mathbf{x}}_k^T(+) \tilde{\mathbf{x}}_k(+) | \mathbf{Z}_k \rangle, \\ &= \min_{\bar{\mathbf{K}}_k} \text{trace} (E \langle \tilde{\mathbf{x}}_k^T(+) \tilde{\mathbf{x}}_k(+) | \mathbf{Z}_k \rangle), \\ &= \min_{\bar{\mathbf{K}}_k} \text{trace} (\mathbf{P}_k(+)). \end{aligned} \quad (107)$$

From Linear Algebra, for any \mathbf{A} and a symmetric \mathbf{B} matrix

$$\frac{\partial}{\partial \mathbf{A}} (\text{trace}(\mathbf{A}\mathbf{B}\mathbf{A}^T)) = 2\mathbf{A}\mathbf{B}. \quad (108)$$

Using (108) in (107)

$$\frac{\partial L}{\partial \bar{\mathbf{K}}_k} = \frac{\partial}{\partial \bar{\mathbf{K}}_k} \text{trace}(\mathbf{P}_k(+)) = 0 \quad (109)$$

Before finding $\bar{\mathbf{K}}_k$, the update of the error covariance must be calculated as

$$\begin{aligned} \mathbf{P}_k(+) &= E \langle [\tilde{\mathbf{x}}_k(+) \tilde{\mathbf{x}}_k^T(+)] | \mathbf{Z}_k \rangle \\ &= (\mathbf{I} - \bar{\mathbf{K}}_k \mathbf{H}_k) E \langle \tilde{\mathbf{x}}_k(-) \tilde{\mathbf{x}}_k^T(-) \rangle (\mathbf{I} - \bar{\mathbf{K}}_k \mathbf{H}_k)^T + \bar{\mathbf{K}}_k E \langle \mathbf{v}_k \mathbf{v}_k^T \rangle \bar{\mathbf{K}}_k^T \\ &\quad + 2(\mathbf{I} - \bar{\mathbf{K}}_k \mathbf{H}_k) E \langle \tilde{\mathbf{x}}_k(-) \mathbf{v}_k^T \rangle \bar{\mathbf{K}}_k^T. \end{aligned} \quad (110)$$

Given that the states and the measurement noise are uncorrelated, and (92) and using (101) in (110), yields

$$\mathbf{P}_k(+) = (\mathbf{I} - \bar{\mathbf{K}}_k \mathbf{H}_k) \mathbf{P}_k(-) (\mathbf{I} - \bar{\mathbf{K}}_k \mathbf{H}_k)^T + \bar{\mathbf{K}}_k \mathbf{H}_k \bar{\mathbf{K}}_k^T. \quad (111)$$

Substituting (111) into (109) yields

$$-2(\mathbf{I} - \bar{\mathbf{K}}_k \mathbf{H}_k) \mathbf{P}_k(-) \mathbf{H}_k^T + 2\bar{\mathbf{K}}_k \mathbf{R}_k = 0; \quad (112)$$

rearranging, the Kalman gain is given by

$$\bar{\mathbf{K}}_k = \mathbf{P}_k(-) \mathbf{H}_k^T [\mathbf{H}_k \mathbf{P}_k(-) \mathbf{H}_k^T + \mathbf{R}_k]^{-1}. \quad (113)$$

The Kalman filter result can be used in (111) to reduce the expression to

$$\mathbf{P}_k(+) = (\mathbf{I} - \bar{\mathbf{K}}_k \mathbf{H}_k) \mathbf{P}_k(-). \quad (114)$$

- **Summary:** the Kalman filter algorithm can be summarized in two set of equations: the prediction step given by

$$\hat{\mathbf{x}}_k(-) = \Phi_{k-1} \hat{\mathbf{x}}_{k-1}(+) + \Gamma_{k-1} \mathbf{u}_{k-1}, \quad (115)$$

$$\mathbf{P}_k(-) = \Phi_{k-1} \mathbf{P}_{k-1}(+) \Phi_{k-1}^T + \mathbf{Q}_{k-1}; \quad (116)$$

and the correction step

$$\hat{\mathbf{x}}_k(+) = \hat{\mathbf{x}}_k(-) + \bar{\mathbf{K}}_k [\mathbf{z}_k - \mathbf{H}_k \hat{\mathbf{x}}_k(-)], \quad (117)$$

$$\mathbf{P}_k(+) = (\mathbf{I} - \bar{\mathbf{K}}_k \mathbf{H}_k) \mathbf{P}_k(-). \quad (118)$$

Figure 8 shows the structure of how to construct the discrete Kalman filter.

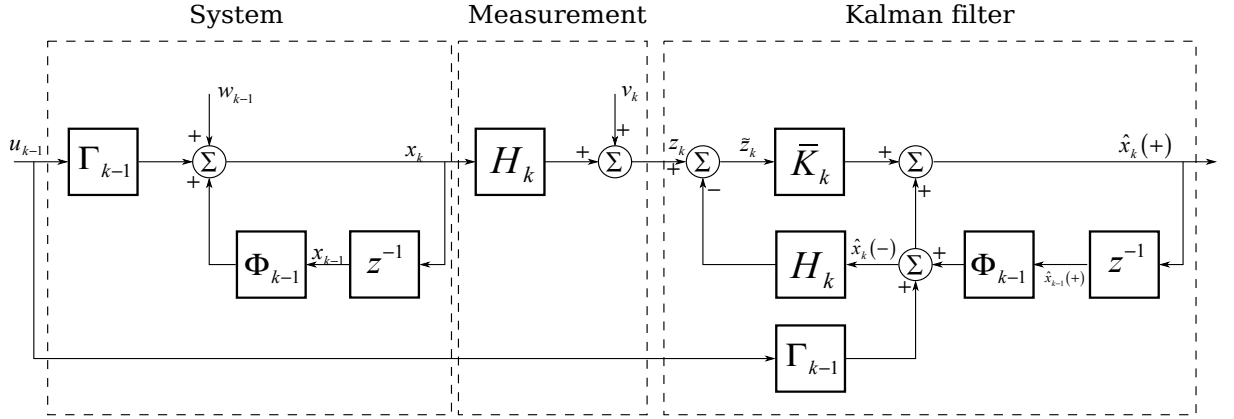


Figure 8. Kalman filter structure with the dynamic system and the observation model.

3.3. EXTENDED KALMAN FILTER

The objective of the Kalman filter algorithm is to estimate the unknown state of the system through measurements and knowledge of the input applied to the system. This concept is based on the fact that the system can be represented in a linear state space form, however, in real life almost all problems are described by non-linear equations. The objective is to extend the methods of linear estimation to non-linear problems.

The first solution that may appear, is the linearization of the system about a nominal trajectory. This trajectory is a particular solution of the system, in which the state variables take a particular value in the state space. The trajectory is a vector of values from each state variable; it is called nominal to refer the trajectory in which the state variables assume their expected values. For example, a nominal trajectory can be the ROV with a fixed position and attitude $\boldsymbol{\eta}_1$, and zero linear and angular velocity.

A non-linear discrete system can be represented in a state space realization by

$$\mathbf{x}_k = g_{k-1}(\mathbf{x}_{k-1}) + \mathbf{\Gamma}_{k-1}u_{k-1} + w_{k-1}, \quad (119)$$

$$\mathbf{z}_k = h_k(\mathbf{x}_k) + v_k, \quad (120)$$

where $g_{k-1}(\cdot)$ and $h_k(\cdot)$ are non-linear functions of the state \mathbf{x}_k . To apply the result obtained for linear systems, a linearization process must be applied. Using a represen-

tation of a first-order approximation Taylor series, $g_{k-1}(\cdot)$ is of the form

$$\begin{aligned}\Phi_{k-1}^{[1]} &= \left. \frac{\partial g_{k-1}(\mathbf{x}_{k-1})}{\partial \mathbf{x}} \right|_{\mathbf{x}=\mathbf{x}_{k-1}^{\text{nom}}} \\ &= \left[\begin{array}{ccc} \frac{\partial g_1}{\partial x_1} & \cdots & \frac{\partial g_1}{\partial x_n} \\ \vdots & \ddots & \vdots \\ \frac{\partial g_n}{\partial x_1} & \cdots & \frac{\partial g_n}{\partial x_n} \end{array} \right] \bigg|_{\mathbf{x}=\mathbf{x}_{k-1}^{\text{nom}}},\end{aligned}\quad (121)$$

and $h_k(\cdot)$ is given by

$$\begin{aligned}\mathbf{H}_k^{[1]} &= \left. \frac{\partial h_k(\mathbf{x}_k)}{\partial \mathbf{x}} \right|_{\mathbf{x}=\mathbf{x}_k^{\text{nom}}} \\ &= \left[\begin{array}{ccc} \frac{\partial h_1}{\partial x_1} & \cdots & \frac{\partial h_1}{\partial x_n} \\ \vdots & \ddots & \vdots \\ \frac{\partial h_n}{\partial x_1} & \cdots & \frac{\partial h_n}{\partial x_n} \end{array} \right] \bigg|_{\mathbf{x}=\mathbf{x}_k^{\text{nom}}}.\end{aligned}\quad (122)$$

The solution of the linearization about the nominal trajectory may diverge when deviation of the actual trajectory from the nominal trajectory occurs. Another factor that affects the performance of this approach, is that the deviation increase the significance of the higher order terms in the Taylor series expansion. To resolve this problem, the linearization can be about the estimated state, in spite of the nominal trajectory. The new equivalent equations for (121) and (122), are

$$\Phi_{k-1}^{[1]} = \left. \frac{\partial g_{k-1}(\mathbf{x}_{k-1})}{\partial \mathbf{x}} \right|_{\mathbf{x}=\hat{\mathbf{x}}_k(-)} \quad (123)$$

$$\mathbf{H}_k^{[1]} = \left. \frac{\partial h_k(\mathbf{x}_k)}{\partial \mathbf{x}} \right|_{\mathbf{x}=\hat{\mathbf{x}}_k(-)} \quad (124)$$

Figure 9 shows the structure of how to construct the discrete extended Kalman filter (EKF).

3.4. EKF FOR THE ROV

The development of the observer needs to account for the ROV high non-linearities and coupled dynamics. Therefore, an extended 6-DOF Kalman filter (EKF) that considers

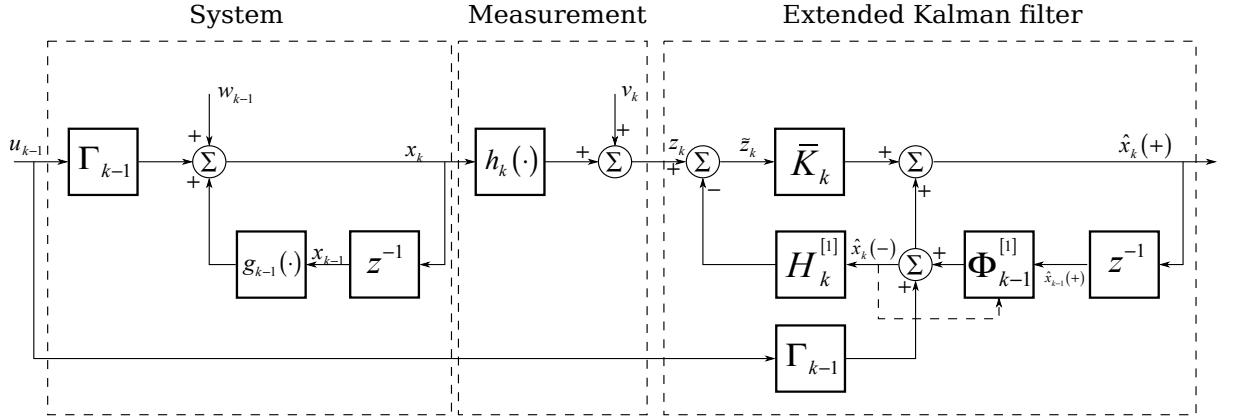


Figure 9. Extended Kalman filter structure with the dynamic system and the observation model.

Coriolis, damping and restoring forces has been developed. Equations (22) and (23) can be written as a state space realization, as follows

$$\dot{\mathbf{x}} = f(\mathbf{x}, t) + \mathbf{B}u(t) + w(t), \quad (125)$$

$$\mathbf{z} = h(\mathbf{x}, t) + v(t), \quad (126)$$

where $w(t)$ and $v(t)$ are plant and measurement noises, respectively; they are assumed to be zero-mean Gaussian white noise processes with covariance matrix $\mathbf{Q}(t)$ and $\mathbf{R}(t)$ given by

$$E\langle w(t) \rangle = 0, \quad (127)$$

$$E\langle w(t) w^T(s) \rangle = \delta(t - s) \mathbf{Q}(t), \quad (128)$$

$$E\langle v(t) \rangle = 0, \quad (129)$$

$$E\langle v(t) v^T(s) \rangle = \delta(t - s) \mathbf{R}(t). \quad (130)$$

In (125), $f(\mathbf{x}, t)$ is a function of the state vector $\mathbf{x} = [\nu \ \eta]^T$, and is given by

$$f(\mathbf{x}, t) = \begin{bmatrix} \mathbf{M}^{-1}(-\mathbf{C}(\nu)\nu - \mathbf{D}(\nu)\nu - \mathbf{g}(\eta)) \\ \mathbf{J}(\eta)\nu \end{bmatrix}, \quad (131)$$

and \mathbf{B} is the input coupling matrix given by

$$\mathbf{B} = \begin{bmatrix} \mathbf{M}^{-1} \\ \mathbf{0}_{6 \times 6} \end{bmatrix}. \quad (132)$$

In (125), $u(t)$ is the input vector given by thruster forces, and $h(\mathbf{x}, t)$ is the measurement sensitivity matrix, which depends on the ROV sensors. The continuous-time model in (125) and (126) is discretized using a 1st-order approximation Euler method as follows

$$\mathbf{x}_k = g_{k-1}(\mathbf{x}_{k-1}) + \mathbf{\Gamma}u_{k-1} + w_{k-1}, \quad (133)$$

$$\mathbf{z}_k = h_k(\mathbf{x}_k) + v_k, \quad (134)$$

where

$$g_{k-1}(\mathbf{x}_{k-1}) = \mathbf{x}_{k-1} + hf(\mathbf{x}_{k-1}, t_{k-1}), \quad (135)$$

$$\mathbf{\Gamma} = h\mathbf{B}, \quad (136)$$

and h is the step time. The discretized system is given by

$$\begin{aligned} \boldsymbol{\nu}_k &= \boldsymbol{\nu}_{k-1} + h\mathbf{M}^{-1}[\boldsymbol{\tau}_{k-1} - \mathbf{C}(\boldsymbol{\nu}_{k-1})\boldsymbol{\nu}_{k-1} \\ &\quad - \mathbf{D}(\boldsymbol{\nu}_{k-1})\boldsymbol{\nu}_{k-1} - \mathbf{g}(\boldsymbol{\eta}_{k-1})], \end{aligned} \quad (137)$$

$$\boldsymbol{\eta}_k = \boldsymbol{\eta}_{k-1} + h[\mathbf{J}(\boldsymbol{\eta}_{k-1})\boldsymbol{\nu}_k]. \quad (138)$$

The objective of the EKF is to use a linearized version of the system's model to estimate the current state. The EKF is executed in two steps: the predictor which calculates a approximation of the state and covariance; and the corrector which improves the initial approximation. The predictor equations for the EKF are

$$\hat{\mathbf{x}}_k(-) = g_{k-1}(\hat{\mathbf{x}}_{k-1}(+)) + \mathbf{\Gamma}u_{k-1}, \quad (139)$$

$$\hat{\mathbf{z}}_k = h_k(\hat{\mathbf{x}}_k(-)), \quad (140)$$

$$\mathbf{P}_k(-) = \boldsymbol{\Phi}_{k-1}^{[1]}\mathbf{P}_{k-1}(+)\boldsymbol{\Phi}_{k-1}^{[1]\text{T}} + \mathbf{Q}_{k-1}. \quad (141)$$

$\hat{\mathbf{x}}_k(-)$ is the a priori estimate of the state, $\hat{\mathbf{x}}_k(+)$ the a posteriori estimate of the state, $\hat{\mathbf{z}}_k$ the predicted measurement, $\mathbf{P}_k(-)$ a priori covariance matrix, $\mathbf{P}_k(+)$ a posteriori covariance matrix, and $\boldsymbol{\Phi}_{k-1}^{[1]}$ is the state transition matrix defined by the Jacobian matrix in (123). The corrector equations for the EKF algorithm are

$$\hat{\mathbf{x}}_k(+) = \hat{\mathbf{x}}_k(-) + \bar{\mathbf{K}}_k(\mathbf{z}_k - \hat{\mathbf{z}}_k), \quad (142)$$

$$\mathbf{P}_k(+) = \left[\mathbf{I} - \bar{\mathbf{K}}_k\mathbf{H}_k^{[1]} \right] \mathbf{P}_k(-), \quad (143)$$

where $\bar{\mathbf{K}}_k$ is the Kalman filter gain calculated as

$$\bar{\mathbf{K}}_k = \mathbf{P}_k(-) \mathbf{H}_k^{[1]\text{T}} \left[\mathbf{H}_k^{[1]} \mathbf{P}_k(-) \mathbf{H}_k^{[1]\text{T}} + \mathbf{R}_k \right]^{-1}, \quad (144)$$

where the observation matrix is defined by the Jacobian matrix in (124).

It is important to state that the EKF is not an optimal filter, due to the linearization process of the system. Furthermore, the matrices $\Phi_{k-1}^{[1]}$ and $\mathbf{H}_k^{[1]}$ depend on the previous state estimation and the measurement noise. Therefore, the EKF may diverge if the consecutive linearizations are not a good approximation of the linear model in the whole domain. Additionally, the Kalman gain is not a static matrix, it changes in each iteration of the algorithm

4. CONTROL ALGORITHMS

The control system is a component of the lowest level of the control structure. It contains a set of algorithms that stabilize the state of the vehicle, so the vehicle can follow the commands generated at the path planning system or by the vehicle's operator. The control of an underwater vehicle is complex because there are highly nonlinear hydrodynamic effects resulting from the interaction with the environment that can not be quantified [41]. Additionally, perturbations from the environment that require robust control laws, may appear. Problems like obtaining all the state variables of the vehicle, can limit the design of such control algorithms.

In classical control, it is common to classify the control algorithms in two types: open-loop and closed-loop control systems. Currently, Visor3 is driven through a joystick that sends power commands to a main-board installed in the vehicle, which translates to an input signal for each motor. Figure 10 shows the current open-loop control system implemented in Visor3.

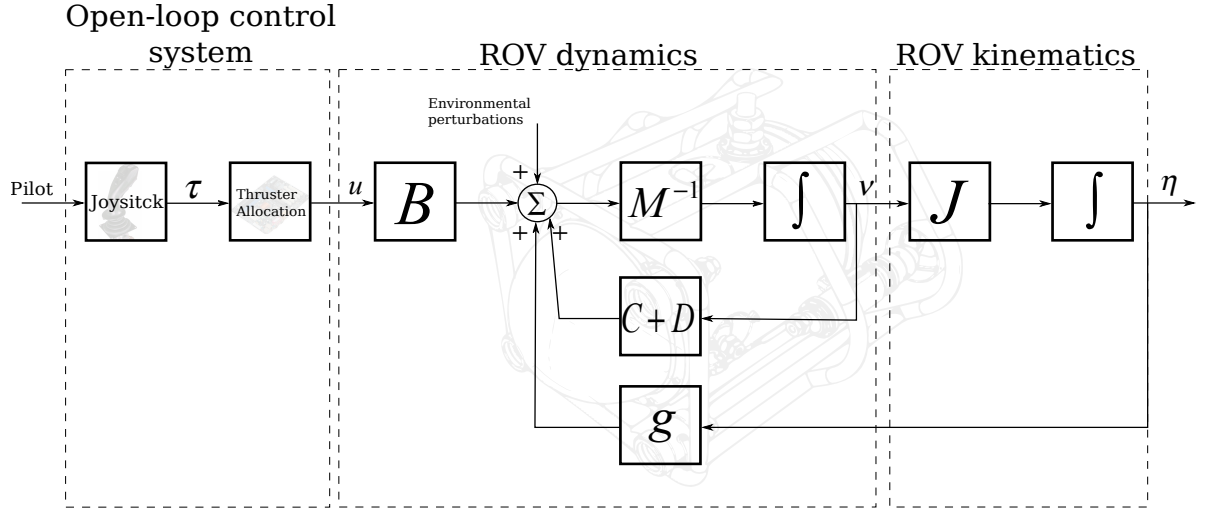


Figure 10. Open-loop control system implemented in Visor3.

The Joystick must have as many degrees of freedom as controllable DOFs the vehicle has. Visor3 has 4 motors, that allow the vehicle to move in: surge, sway, heave and yaw

directions. The surge direction is controlled by two thrusters (T1 and T2) on either side of the vehicle; the sway direction by one thruster (T3) located in the middle of the vehicle and rotated $\theta = \pi/2$; the heave direction by one thruster (T4) located near to T3 and rotated $\psi = \pi/2$; and for yaw it uses T1 and T2 with the motors operating one forward and one reverse. Figure 11 shows the position of thrusters in Visor3.

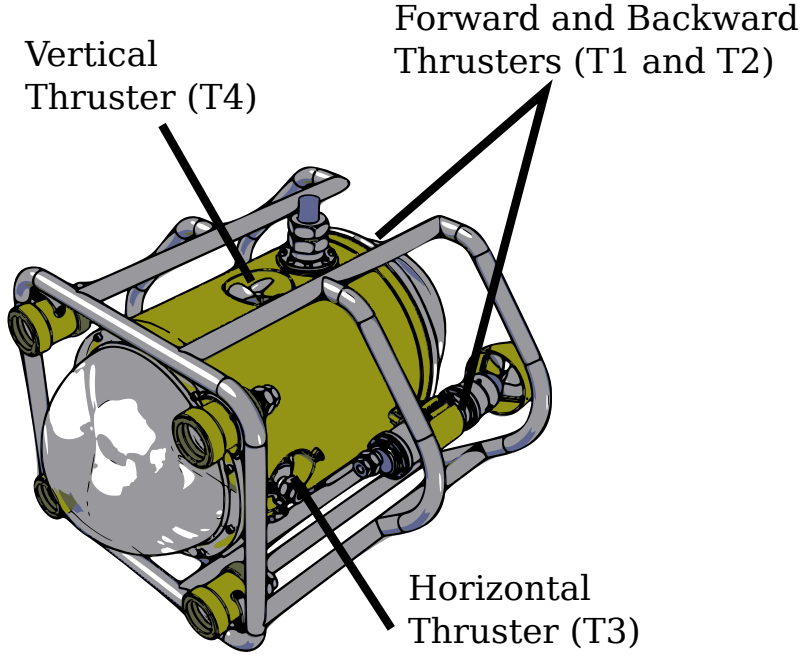


Figure 11. Thrusters positions in Visor3.

In this control scheme (the operator is the only one that give commands to the thrusters), when no command is given to the system, the vehicle can be moved in any direction, because of the environmental disturbances or by difference between the buoyancy and weight. To improve the performance of the operation in the presence of environmental disturbances, a closed-loop control system can be used. This new scheme receives commands from the operator, but uses feedback to stabilize the system in the presence of disturbances, Figure 12.

This scheme reads data from sensors, compares them with the reference, and decides what is the best action to follow the reference. When the reference is static or do not change in time, it is known as a problem of set-point regulation. If the reference change

in time, i.e, the operator wants the vehicle to follow a predetermined path, it is known as a tracking problem. Additionally, when there are uncertainties in the measurements and unknown state variables, it is necessary to have a navigation system capable of estimating the state variables of the vehicle.

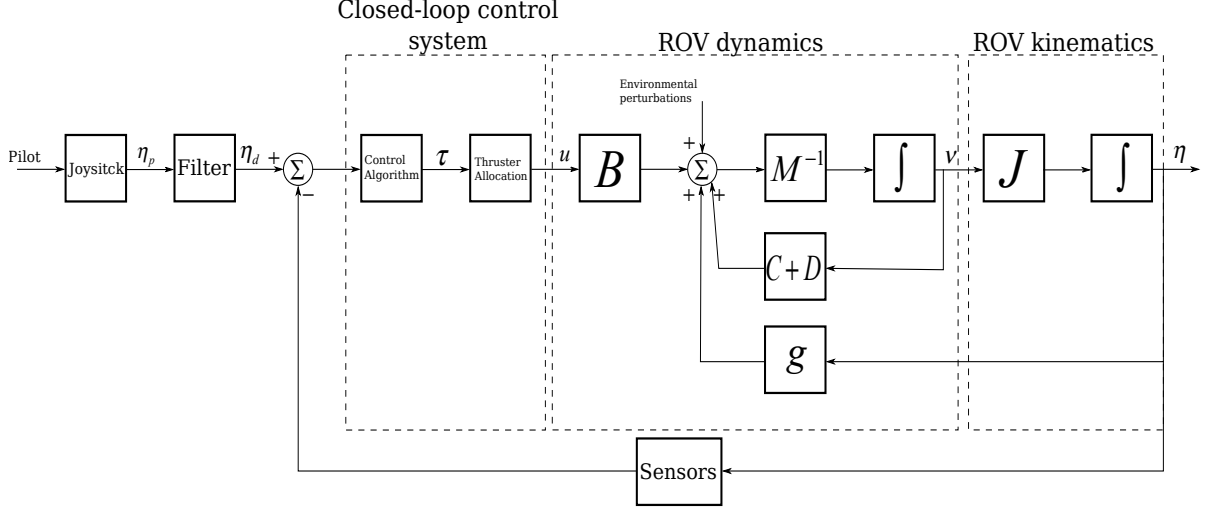


Figure 12. Closed-loop control system to be implemented in Visor3.

4.1. THRUSTER ALLOCATION PROBLEM

When the pilot wants to move the vehicle in one direction, a command is given to the thrusters. This force τ must be translated into a signal for the motor. The objective of the thruster allocation is to find the distribution of the propulsion for each thruster that can generate the needed force. The thrust vector that describe the force f_i generated by the thruster i is given by

$$\mathbf{f} = [f_1 \ f_2 \ \dots \ f_r]^T, \quad (145)$$

where r is the total number of thrusters. The total force and moment generated by the thrusters will be

$$\boldsymbol{\tau} = \mathbf{T}\mathbf{f}, \quad (146)$$

where \mathbf{T} is the thruster configuration matrix, which is a function of the thrusters position $\mathbf{r}_{ti/b}^b$ and heading and pitch angles, ψ and θ , respectively. This vector is referenced

to the body-fixed frame. The thruster configuration matrix describes how the thrust of each motor contributes to the force or moment of each direction. \mathbf{T} is given by

$$\mathbf{T} = [\mathbf{t}_1, \mathbf{t}_2, \dots, \mathbf{t}_r], \quad (147)$$

where \mathbf{t}_i is the column vector of the i -th thruster, computed as

$$\mathbf{t}_i = \begin{bmatrix} \mathbf{I}_{3 \times 3} \\ -\mathbf{S}^T(\mathbf{r}_{ti/b}^b) \end{bmatrix} \mathbf{R}(\psi, \theta) \begin{bmatrix} 1 \\ 0 \\ 0 \end{bmatrix} f_i. \quad (148)$$

The rotation matrix $\mathbf{R}(\psi, \theta)$ is defined by the product of two rotation matrices

$$\mathbf{R}(\psi, \theta) = \mathbf{R}_{z,\psi} \mathbf{R}_{y,\theta}, \quad (149)$$

where $\mathbf{R}_{z,\psi}$ and $\mathbf{R}_{y,\theta}$ are described by (7) and (6) respectively. Visor3 has fixed heading and pitch angles for each thruster.

Now that the thrust provided by each thruster is known using (146), the input that must be sent to each motor has to be computed. The input could be the revolution speed of the motor or a voltage for the driver. Equation (146) is then rewritten as

$$\boldsymbol{\tau} = \mathbf{T} \mathbf{K} \mathbf{u}, \quad (150)$$

where $\mathbf{K} = \text{diag}\{K_1, K_2, \dots, K_r\}$ is a diagonal matrix with the thrust coefficients described by the equation

$$K_i = K_T(J) \rho D^4. \quad (151)$$

\mathbf{u} is a column vector with elements $u_i = |n|n$, where n is the propeller velocity rate. The thruster allocation problem is solved finding \mathbf{u} as

$$\mathbf{u} = \mathbf{K}^{-1} \mathbf{T}^{-1} \boldsymbol{\tau}. \quad (152)$$

\mathbf{T} may not be square or invertible. This problem can be solved using the Moore-Penrose pseudo inverse given by

$$\mathbf{T}^\dagger = \mathbf{T}^T (\mathbf{T} \mathbf{T}^T)^{-1}. \quad (153)$$

Substituting (152) into (153) yields

$$\mathbf{u} = \mathbf{K}^{-1} \mathbf{T}^\dagger \boldsymbol{\tau}. \quad (154)$$

The voltage for each driver calculated from \mathbf{u} is given by

$$v_i = (1/G_{m_i}) (1/G_{d_i}) \operatorname{sgn}(u_i) \sqrt{|u_i|}, \quad (155)$$

where G_{m_i} and G_{d_i} are the gain of the i -th motor and driver respectively. This last equation fails when saturation occurs in the actuators. For example, Figure 13 shows how to change v_i according to u_i , with different values from multiplication $M_g = (1/G_{m_i}) (1/G_{d_i})$.

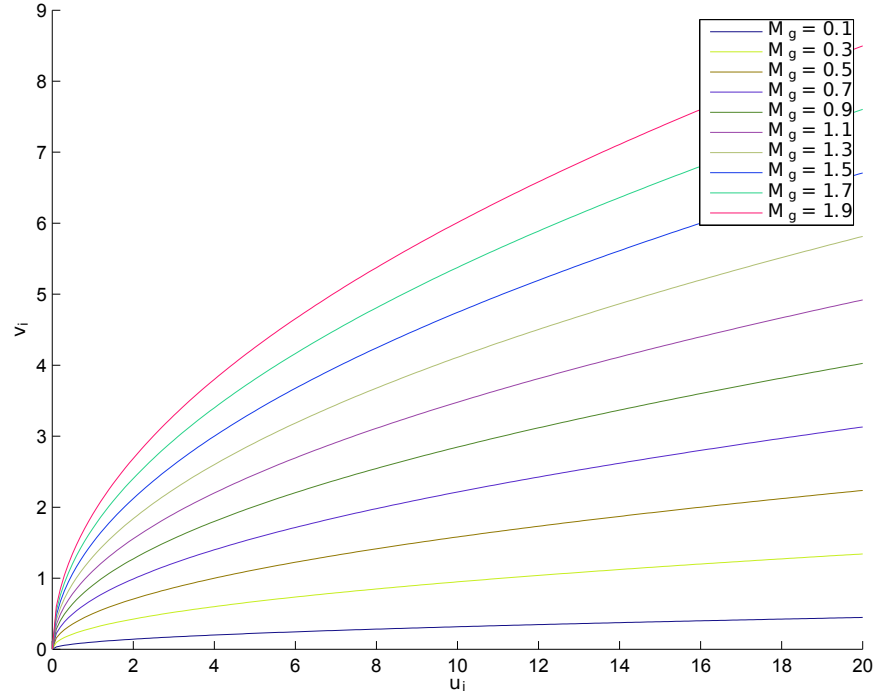


Figure 13. Change of voltage according to u_i in the thruster allocation problem.

4.2. MULTIVARIABLE PID-CONTROL

The PID is the most common algorithm used in industry, because its robustness and structure, consisting of only three tuning parameters, hence, it is easy to implement and many different techniques are nowadays available for their tuning through experiments

or theoretical models.

In the control of underwater vehicles the PID is also widely used. Several controllers are simple P or PI, and they are designed independently for each degree of freedom. Another technique commonly used, is to decouple the dynamic system, in two or three non-interacting subsystems, for example, diving and steering subsystems.

The parallel non-interacting structure of the PID is given by

$$\boldsymbol{\tau}_{PID} = \mathbf{K}_p \mathbf{e}(t) + \mathbf{K}_d \dot{\mathbf{e}}(t) + \mathbf{K}_i \int_0^t \mathbf{e}(\tau) d\tau, \quad (156)$$

where \mathbf{K}_p is the proportional gain, \mathbf{K}_d the derivative gain, \mathbf{K}_i the integral gain, and $\mathbf{e}(t)$ is the error defined by

$$\mathbf{e} = \boldsymbol{\eta}_d - \boldsymbol{\eta}. \quad (157)$$

For Visor3 each controller is designed for the control of one DOF, this implies that \mathbf{K}_p , \mathbf{K}_i and \mathbf{K}_d are diagonal and positive matrices. Heuristic methods were used to tune the gains of the PID controller. A high proportional gain, acts rapidly to correct changes in the references. Due to the vehicle's dynamics and the interaction with the fluid, a high derivative action is used to slow down the movement of the vehicle, when is reaching the set-point. Finally, it is decided that a small integral action can correct the steady state error. This PID control can be improved according to [13] by using gravity compensation and vehicle kinematics. The PID control signal is transformed by

$$\boldsymbol{\tau} = \mathbf{J}^T(\boldsymbol{\eta}) \boldsymbol{\tau}_{PID} + \mathbf{g}(\boldsymbol{\eta}). \quad (158)$$

Figure 12 shows the implementation of (158). The controller needs the error and the position estimation to calculate the output.

4.3. LINEAR QUADRATIC REGULATOR (LQR)

The linear quadratic regulator (LQR) is an optimal controller that stabilizes the state of the system as fast as possible. It is a controller based on the minimization of a linear quadratic performance index. The LQR controller needs full state feedback and knowledge of the system's dynamics. Additionally, the objective of the LQR is to

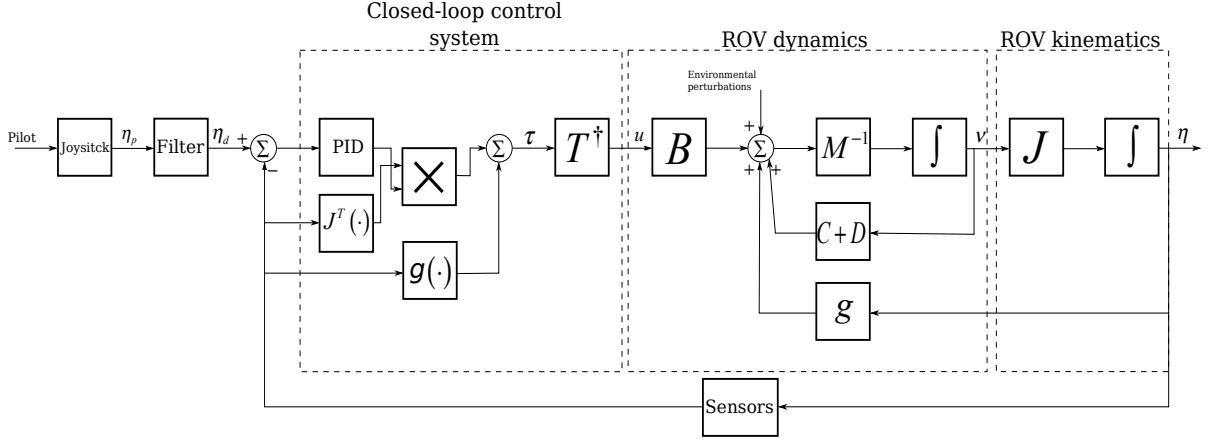


Figure 14. Closed-loop control system implemented in Visor3.

solve the regulation problem. To improve the performance of the LQR, an integral feedback with state augmentation can solve the tracking problem and compensate for disturbances that affect the system.

Consider the dynamics of the vehicle as state space realization given by

$$\dot{\mathbf{x}} = \mathbf{A}\mathbf{x} + \mathbf{B}\mathbf{u}. \quad (159)$$

In some time t_1 the initial state of the system $\mathbf{x} = \mathbf{0}$ is displaced to $\mathbf{x}(t_1) = \mathbf{x}_0$. The regulator controller tries to return the state to zero. To stabilize the system, it is necessary to design a state feedback control given by

$$\mathbf{u} = -\mathbf{k}\mathbf{x}. \quad (160)$$

According to [57], the design of \mathbf{k} is a trade-off between the rate of decay of \mathbf{x} and the control effort or the energy of the input. This matrix can be obtained by choosing \mathbf{u} that minimizes

$$\mathbf{J} = \int_0^\infty [\mathbf{x}^T(t) \mathbf{Q} \mathbf{x}(t) + \mathbf{u}^T(t) \mathbf{R} \mathbf{u}(t)] dt, \quad (161)$$

where $\mathbf{Q} \in \mathbb{R}^{n \times n}$ is a symmetric positive semidefinite matrix, n is the number of state variables, $\mathbf{R} \in \mathbb{R}^{m \times m}$ symmetric positive definite matrix, and m is the number of control inputs. These matrices can give different weightings to the control cost and deviations from the desired state. The optimal control to solve this problem, assuming that the pair (\mathbf{A}, \mathbf{B}) is stabilizable, is given by

$$\mathbf{u} = -\mathbf{R}^{-1} \mathbf{B}^T \mathbf{P} \mathbf{x}, \quad (162)$$

where $\mathbf{P} \in \mathbb{R}^{n \times n}$ is the symmetric positive semidefinite solution of the Algebraic Riccati Equation (ARE)

$$\mathbf{P}\mathbf{A} + \mathbf{A}^T\mathbf{P} + \mathbf{Q} - \mathbf{P}\mathbf{B}\mathbf{R}^{-1}\mathbf{B}^T\mathbf{P} = \mathbf{0}. \quad (163)$$

The selection of \mathbf{Q} and \mathbf{R} depends on how much we want to penalize the control effort or the deviation of the state. Figure 15 shows the scheme of the state feedback.

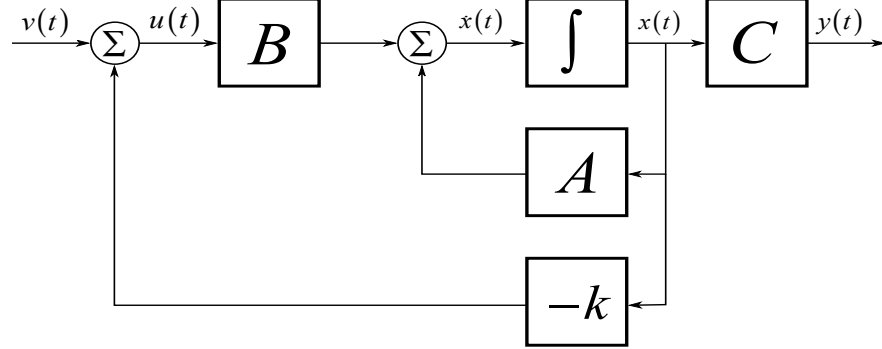


Figure 15. State feedback control.

The success of this algorithm depends on the whole knowledge of the vehicle's state and its dynamics. Additionally, the presence of disturbances or uncertainties in the parameters of the model, can cause a steady state value different from zero. This effects can be eliminated by using integral error feedback. The integral introduces a new state variable given by

$$\dot{\mathbf{q}}(t) = \mathbf{e}(t), \quad (164)$$

where the use of feedback becomes

$$\mathbf{u}(t) = -\mathbf{k}\mathbf{x}(t) - \mathbf{K}_i\mathbf{q}(t). \quad (165)$$

The augmented closed-loop system is

$$\begin{bmatrix} \dot{\mathbf{x}}(t) \\ \dot{\mathbf{q}}(t) \end{bmatrix} = \begin{bmatrix} \mathbf{A} - \mathbf{B}\mathbf{k} & \mathbf{B}\mathbf{K}_i \\ -\mathbf{C} & \mathbf{0} \end{bmatrix} \begin{bmatrix} \mathbf{x}(t) \\ \mathbf{q}(t) \end{bmatrix} + \begin{bmatrix} \mathbf{0} \\ \mathbf{1} \end{bmatrix} \mathbf{u}(t). \quad (166)$$

According to this new system, the LQR controller is calculated again. With the integral action, a change in the desired reference, can be obtained with a nonzero set-point. In the regulation problem, the goal is to return the state to zero, and therefore the external

force is taken to be zero. If it is desired that the vehicle has an output \mathbf{y}_d , this can be accomplished by a constant command input \mathbf{v}_d such that

$$\dot{\mathbf{x}} = (\mathbf{A} - \mathbf{B}\mathbf{k}) \mathbf{x}_d + \mathbf{B}\mathbf{v}_d = 0 \quad (167)$$

$$\begin{aligned} \mathbf{y}_d &= \mathbf{C}\mathbf{x}_d \\ &= \mathbf{C} \left(-(\mathbf{A} - \mathbf{B}\mathbf{k})^{-1} \mathbf{B}\mathbf{v}_d \right) \\ &= -\mathbf{C}(\mathbf{A} - \mathbf{B}\mathbf{k})^{-1} \mathbf{B}\mathbf{v}_d \\ &= \mathbf{H}_k(0) \mathbf{v}_d, \end{aligned} \quad (168)$$

where $\mathbf{H}_k(s)$ is the closed loop transfer matrix given by

$$\mathbf{H}_k(s) = \mathbf{C}(s\mathbf{I} - \mathbf{A} + \mathbf{B}\mathbf{k})^{-1} \mathbf{B}. \quad (169)$$

Finally, the command input \mathbf{v}_d can be obtained as

$$\mathbf{v}_d = \mathbf{H}_k^{-1}(0) \mathbf{y}_d \quad (170)$$

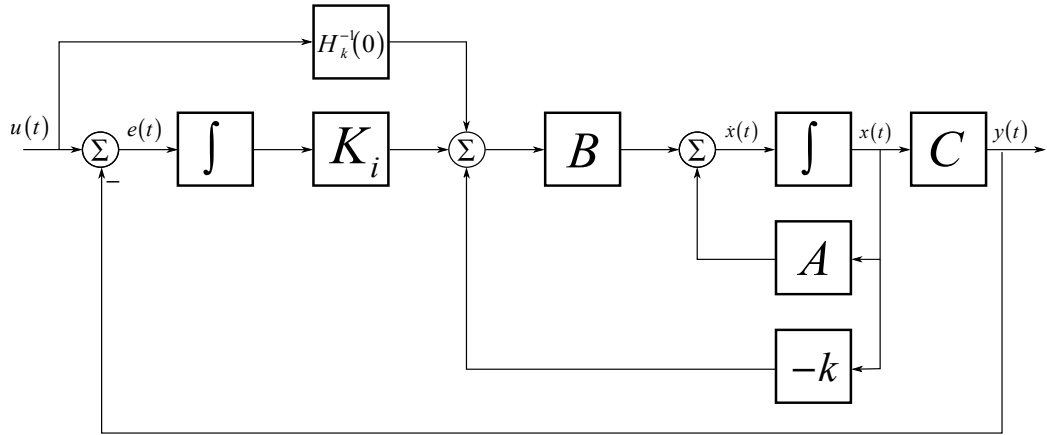


Figure 16. State feedback control with integral action and open loop gain.

5. SIMULATION AND RESULTS

The simulation of the ROV dynamics, the observer algorithm, and the controller were implemented in Simulink®. This is a platform for simulation and model based design of dynamic systems. It provides an interactive graphical environment where continuous and discrete time differential equations can be simulated. Additionally, several functions can be constructed using conventional Matlab® code, providing great flexibility for high level programming.

5.1. DESCRIPTION OF THE VEHICLE

Visor3 system is divided into three main subsystems: the surface station, the ROV and the communication system which communicates the ROV with the surface station. The surface station contains the control devices such as: surface computer with man/machine interface, a joystick used to control vehicle's movement and an electric power plant. The communication system is composed of an umbilical cable which is made up of four fiber optics and AC power conductors that transmit all the energy to the vehicle. Finally, the ROV contains the instrumentation and the controller board.

Visor3 parameters were obtained using CAD models (Solid-Edge® software) and CFD simulation (ANSYS® software). Table 3 contains all the model parameters used in the simulation to represent the dynamics of the vehicle. These parameters are saved in a file called `Visor3_parameters.m`.

5.2. DYNAMIC SIMULATION

For the dynamic simulation a Simulink block was created. This block implements the equations (22) and (23) with the parameters shown in Table 3. This block is divided as follows: the dynamics (see Figure 17), which contains inertia forces, the centripetal

Table 3. ROV Visor3 parameters for simulation

| Parameter | Value |
|-------------------|---|
| m | 64.5 kg |
| I_{xx} | 2.9 kg m ² |
| I_{yy} | 2.5 kg m ² |
| I_{zz} | 3.0 kg m ² |
| I_{xy} | -7.0×10^{-3} kg m ² |
| I_{xz} | -2.1×10^{-3} kg m ² |
| I_{yz} | -7.2×10^{-3} kg m ² |
| ∇ | 1.8×10^{-2} m ³ |
| $[x_g, y_g, z_g]$ | [0, 0, 0] m |
| $[x_b, y_b, z_b]$ | $[1.7, 1.8, 68] \times 10^{-3}$ m |
| $X_{\dot{u}}$ | 6.5 kg |
| $Y_{\dot{v}}$ | 59.8 kg |
| $Z_{\dot{w}}$ | 59.8 kg |
| $K_{\dot{p}}$ | 0 kg m ² |
| $M_{\dot{q}}$ | 2.2 kg m ² |
| $N_{\dot{r}}$ | 2.2 kg m ² |
| $X_{u u }$ | -10.3 kg/m |
| $Y_{v v }$ | -100.8 kg/m |
| $Z_{w w }$ | -100.8 kg/m |
| $K_{p p }$ | -400.3 kg m ² |
| $M_{q q }$ | -100.8 kg m ² |
| $N_{r r }$ | -100.8 kg m ² |

and Coriolis forces, the damping forces, and the restoring forces; and the kinematics (see Figure 18), with the velocity transformation matrices.

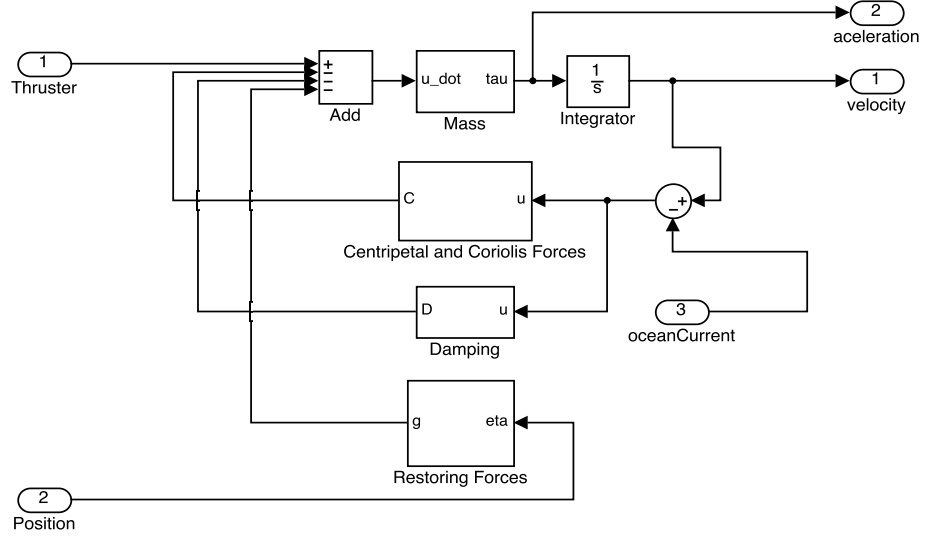


Figure 17. Dynamic vehicle simulation.

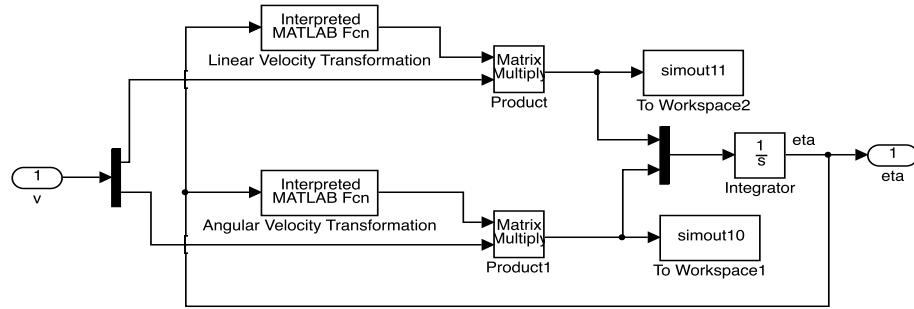


Figure 18. Velocity transformation.

5.3. THRUSTER SIMULATION

The thruster simulation is divided in three steps: the driver, the motor dynamics, and the propeller dynamics. The low level control of the system is managed by the driver. The driver regulates the torque by increasing or decreasing the current in order to maintain the velocity of the motor shaft. For this work it is assumed that the load

changes generated for the propellers are regulated by the driver. In that order, only the thrust will be considered. For this work, the dynamic of the motor will not be considered, due to its fast time response in comparison with the dynamic of the vehicle. Figure 19 shows the dynamic response of the MAXON DC motor. The steady state value is reached in less than 40 ms. The simulation model is represented only by a constant gain G_m , which is the relationship between the maximum velocity Vel_{\max} and the nominal voltage V_{nom} , and is described by

$$G_m = \frac{\text{Vel}_{\max}}{V_{\text{nom}}}. \quad (171)$$

The driver function is to regulate the velocity before changes in the load. The driver receives an input voltage between 0~5V (saturation) and transforms it to 0~48V. Additionally, the driver can be configured to have an acceleration curve, in order to decrease the current consumed by the motor in the initial operation. Figure 20 shows the block diagram implemented to simulate the driver. The parameters for a thruster are shown in Table 4.

- **Thruster allocation Visor3:** Figure 21 shows the position of each thruster respect to the center of the body-fixed frame (the same as the center of gravity).

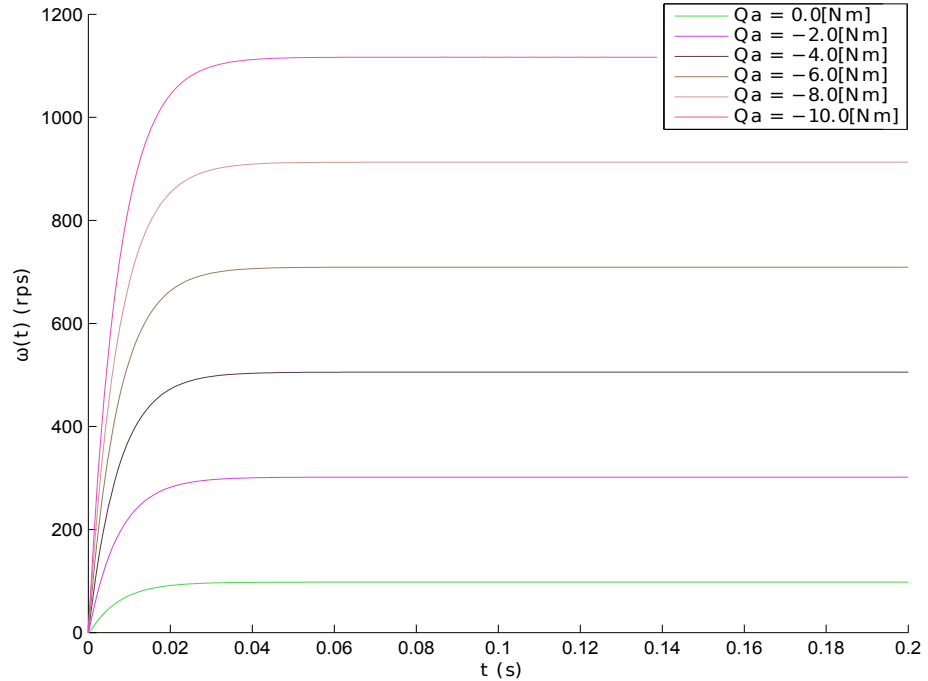


Figure 19. Time response for a MAXON DC motor.

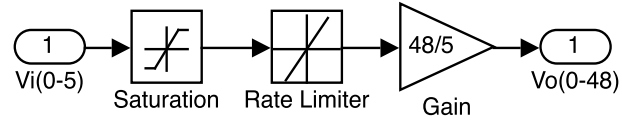


Figure 20. Motor driver block.

Table 4. Thruster Visor3 parameters for simulation

| Parameter | Value |
|------------------------------------|------------------------|
| High/Low voltage driver saturation | ± 5 V |
| Slew rate | 1200 V s |
| Driver gain | 9.6 |
| Motor gain | 20.83 rpm/V |
| Seawater density | 1027 kg/m ³ |
| Propeller diameter | 8.8 cm |
| Thrust coefficients | 0.5 |
| Torque coefficients | 0.08 |

All values are measured in mm. Table 5 summarizes the parameters from thruster allocation needed for the simulation.

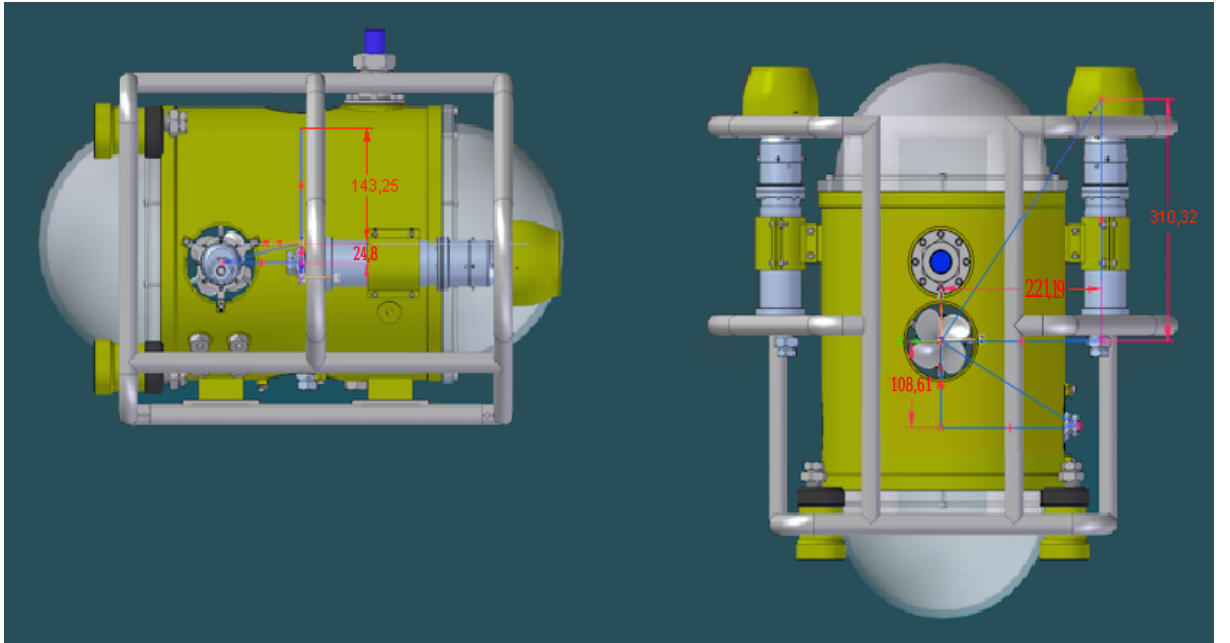


Figure 21. Measure of the thruster position.

Table 5. Thruster allocation

| Thruster | Vector position | ψ | θ |
|----------|-----------------------|---------|----------|
| T1 | $[-0.31, -0.22, 0]$ m | 0 | 0 |
| T2 | $[-0.31, 0.22, 0]$ m | 0 | 0 |
| T3 | $[0, 0, 0]$ m | 0 | $\pi/2$ |
| T4 | $[0.11, 0, 0]$ m | $\pi/2$ | 0 |

5.4. NAVIGATION SYSTEM

The navigation system simulated is an extended Kalman filter (EKF). The EKF runs in discrete time with a 0.05s fixed sample time. The implementation was done using four main functions, see Figure 22:

- **ROV_Nonlinear_Discrete**: calculates the next state of the ROV described by (137) and (138).
- **ROVSaI_Nonlinear_Discrete**: calculates the output of the ROV according to the sensors.
- **ROV_linear_Discrete**: evaluates the Jacobian in each state estimation described by (123).
- **ROVSaI_linear_Discrete**: evaluates the output of the ROV given the Jacobian described by (124)

To test the performance of the EKF algorithm and its implementation, several experiments were conducted, using a PID controller. It is assumed that Visor3 has a position sensor (USBL, LBL, among others), which provides the position of the vehicle in the Earth-fixed frame. In that order, the measurement matrix is given by

$$\mathbf{H}_k = \begin{bmatrix} \mathbf{0}_{6 \times 6} & \mathbf{I}_{6 \times 6} \end{bmatrix}. \quad (172)$$

Also, it is assumed that the sensor has zero-mean Gaussian white noise of 0.05 m and 0.05 rad to linear position and attitude respectively. First, two different position references were commanded to the ROV: in the surge direction a position of 2 m (see Fig. 23), in sway 1 m (see Fig. 23). Figure 23 shows the estimation of the position in

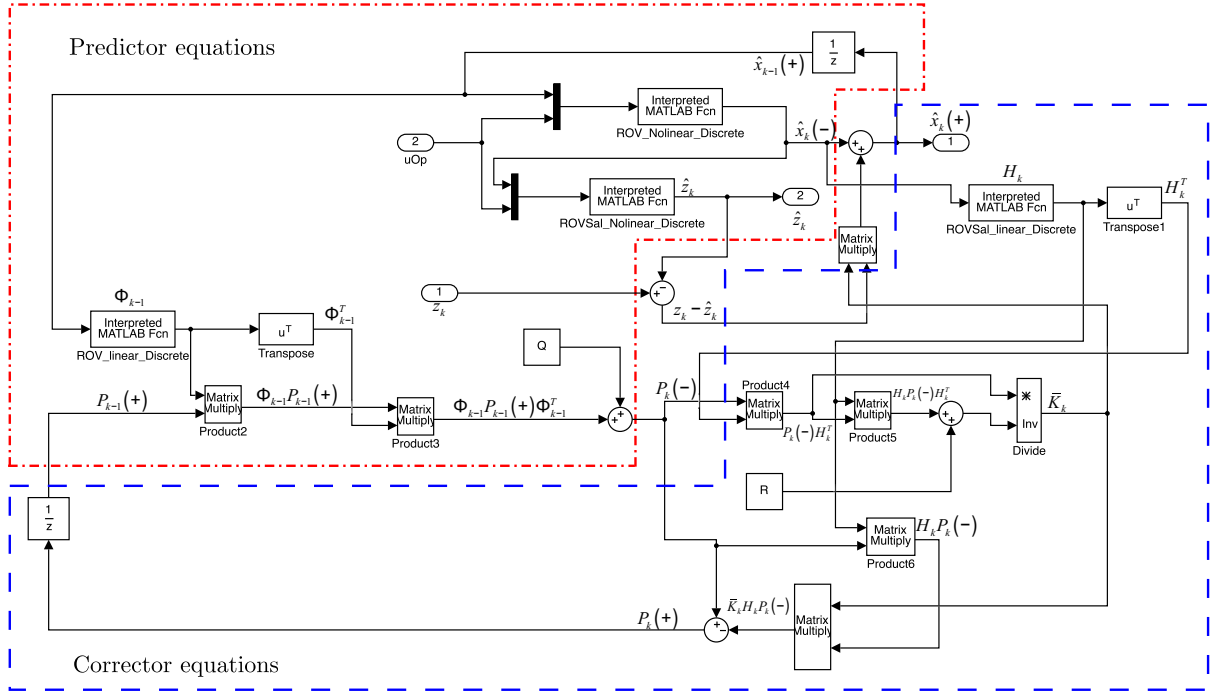


Figure 22. EKF Simulink® implementation.

the Earth-fixed frame. Figure 24 shows the estimation of the velocity. Figure 25 and 26 show the error in the position and velocity estimation, respectively. As it can be seen from Figures 24 and 26, the navigation systems provides a good estimation of the vehicle's velocities in its four DOF controllable directions. This will be a helpful tool for Visor3's operators since the pilot does not have feedback of such variables in the surface control station.

5.5. CONTROLLERS

5.5.1. PID and PID with gravity compensation

The first controller implemented and tested was the PID structure with thruster allocation. The thruster allocation provides the voltage needed in each thruster to move the vehicle with the forces and moments generated by the control (PID). The PID controller is improved through the use of gravity compensation and using the kinematics of

the vehicle. Two different task were tested: first, the planar motion control, where the vehicle moves in the x-y plane and maintain the depth. Second, a depth control, where the vehicle must maintain the position in x-y plane and the attitude while is moving in the heave direction. The comparison was made with the following gain matrices

$$\mathbf{K}_p = \text{diag} \{10, 10, 10, 0, 0, 10\}, \quad (173)$$

$$\mathbf{K}_i = \text{diag} \{0.01, 0.01, 0.01, 0, 0, 0.01\}, \quad (174)$$

$$\mathbf{K}_d = \text{diag} \{50, 50, 50, 0, 0, 50\}. \quad (175)$$

The first experiment was conducted with a trajectory reference that describes changes in the x, y and yaw directions. Figure 27 shows the result of both controllers. The PID with gravity compensation cancels the effects of the restoring forces while the vehicle is moving. This PID with compensation has a better performance, but it requires a good

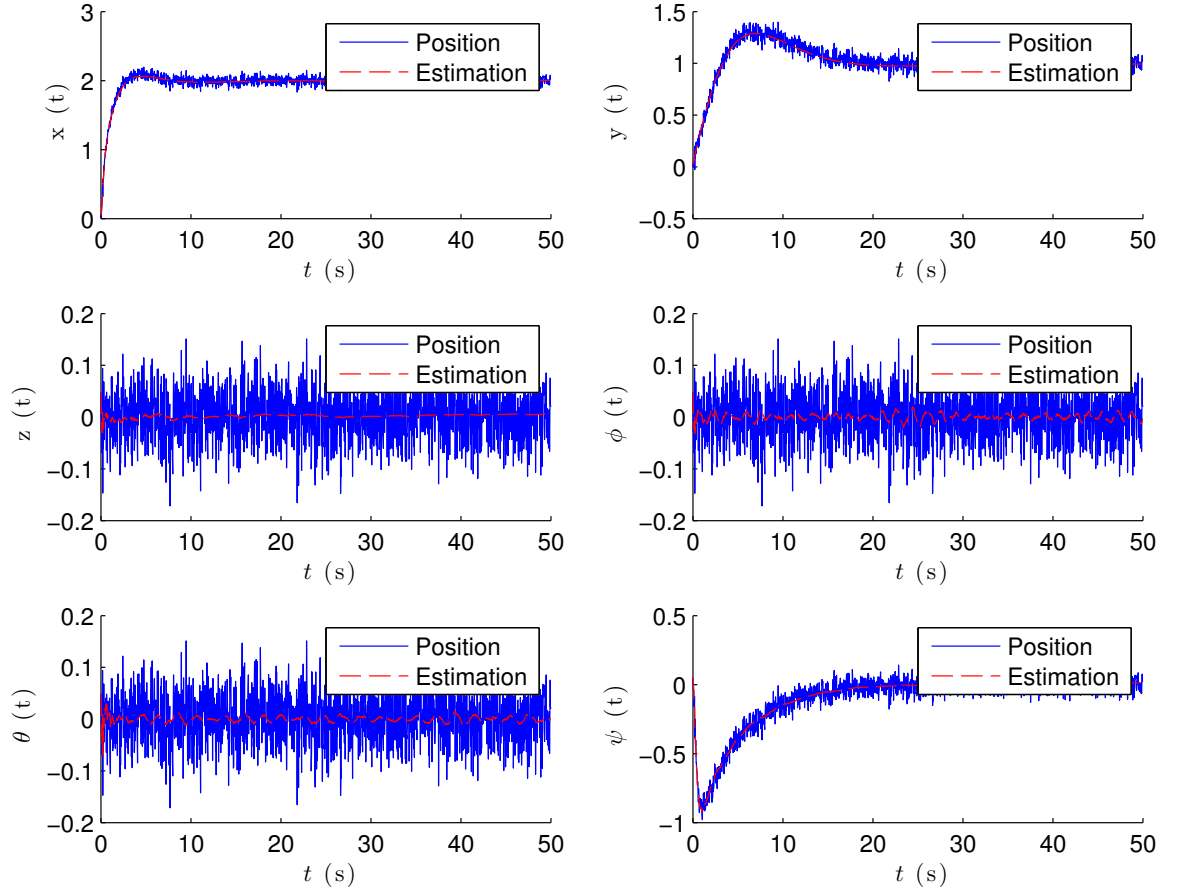


Figure 23. Position estimation in Earth-fixed frame.

estimation of the vehicle attitude. Additionally, Figure 28 shows that the simple PID is less energy efficient, due to the high changes in the control signal. This changes in the control signal, can reduce duty life of the thruster. Finally the simple PID structure is unstable, when the vehicle moves far away from the origin, due to the restoring forces and propagation error.

The second experiment was conducted with a trajectory references that describes changes in heave direction. First a position in heave of 10 m, then maintain this depth and finally return to the initial position (see Figure 29). PID and PID plus compensation controllers have similar behavior, due to the restoring forces affect the vehicle just a few.

The third and fourth experiments (Figure 31 and Figure 32) were conducted to see the

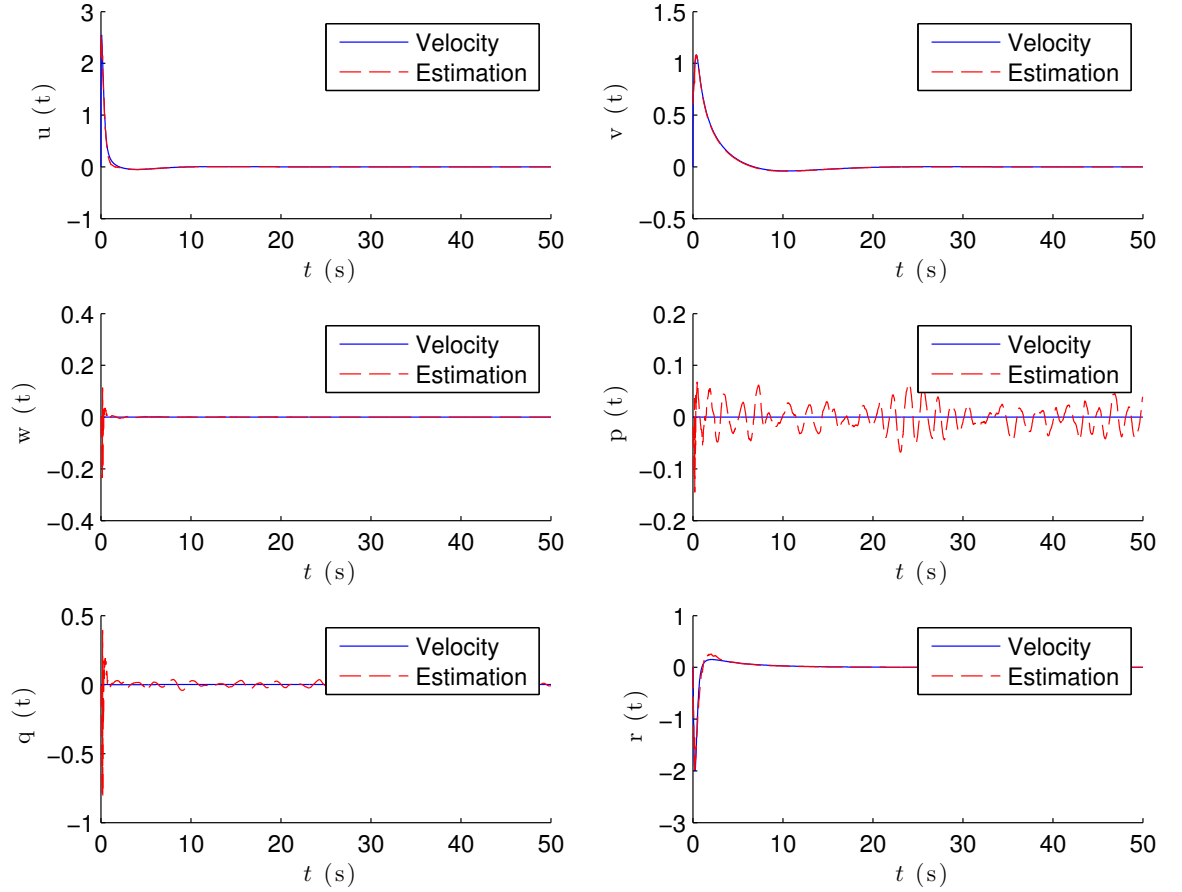


Figure 24. Velocity estimation in body-fixed frame.

effects of disturbances (ocean current). The ocean current is included in the simulation according to the equation (74), with velocity of 0.1 m/s in surge, sway and heave directions. These three ocean current components are varying in time, using a sine function with frequency of 0.1 rad/s. To improve the dynamic model of the ocean current see [54], where the dynamics is modelled as a Markov process. The PID without compensation in the last part of the trajectory shows an unstable response. Additionally, the control signal will saturate the driver, and the observer will fail.

5.5.2. LQR controller

The third tested controller was the LQR. First the non-linear model is linearized around the origin. Then, to this system an optimal feedback control that stabilizes the vehicle

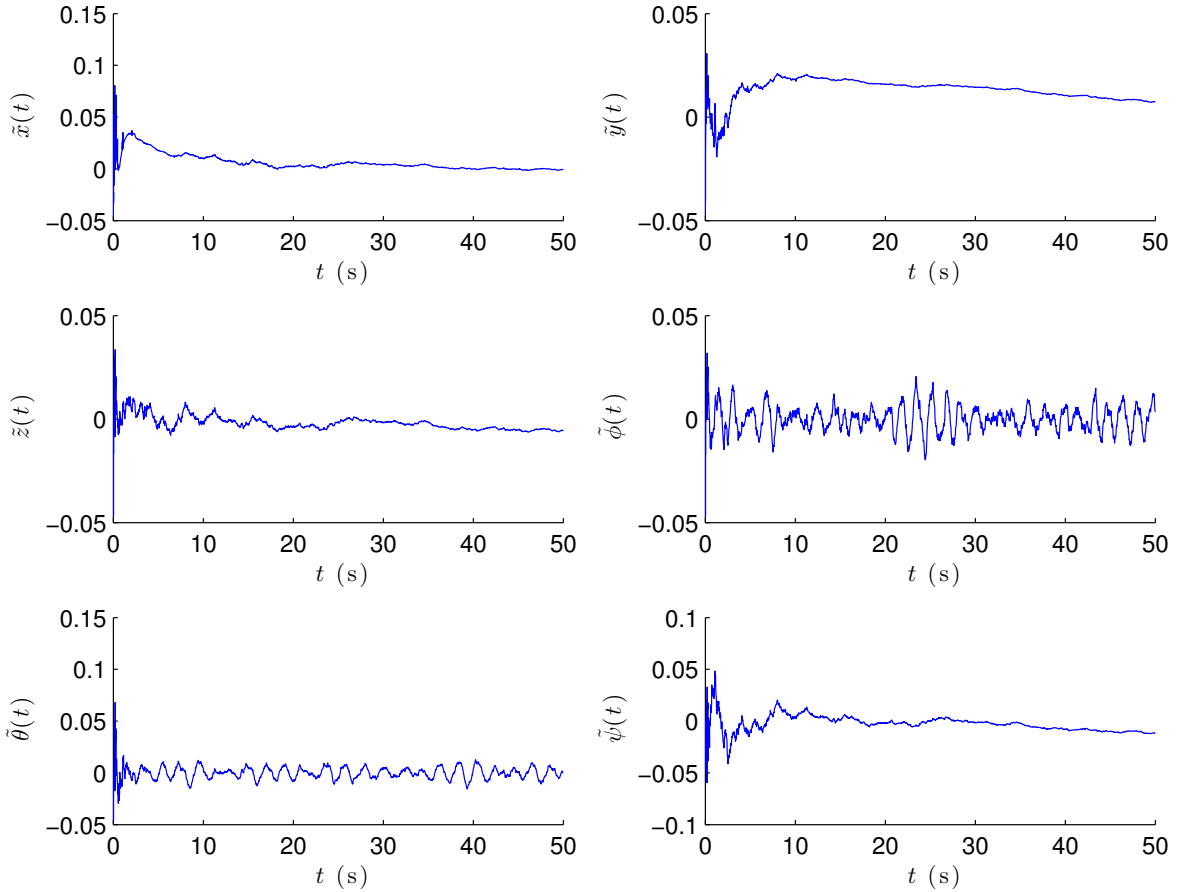


Figure 25. Error in position estimation.

is designed. This optimal controller was developed using the cost function described by (161), with weight matrix for the control signal as

$$\mathbf{R} = 0.1\mathbf{I}_{6 \times 6}. \quad (176)$$

and for state deviation of

$$\mathbf{Q} = 10\mathbf{I}_{12 \times 12}. \quad (177)$$

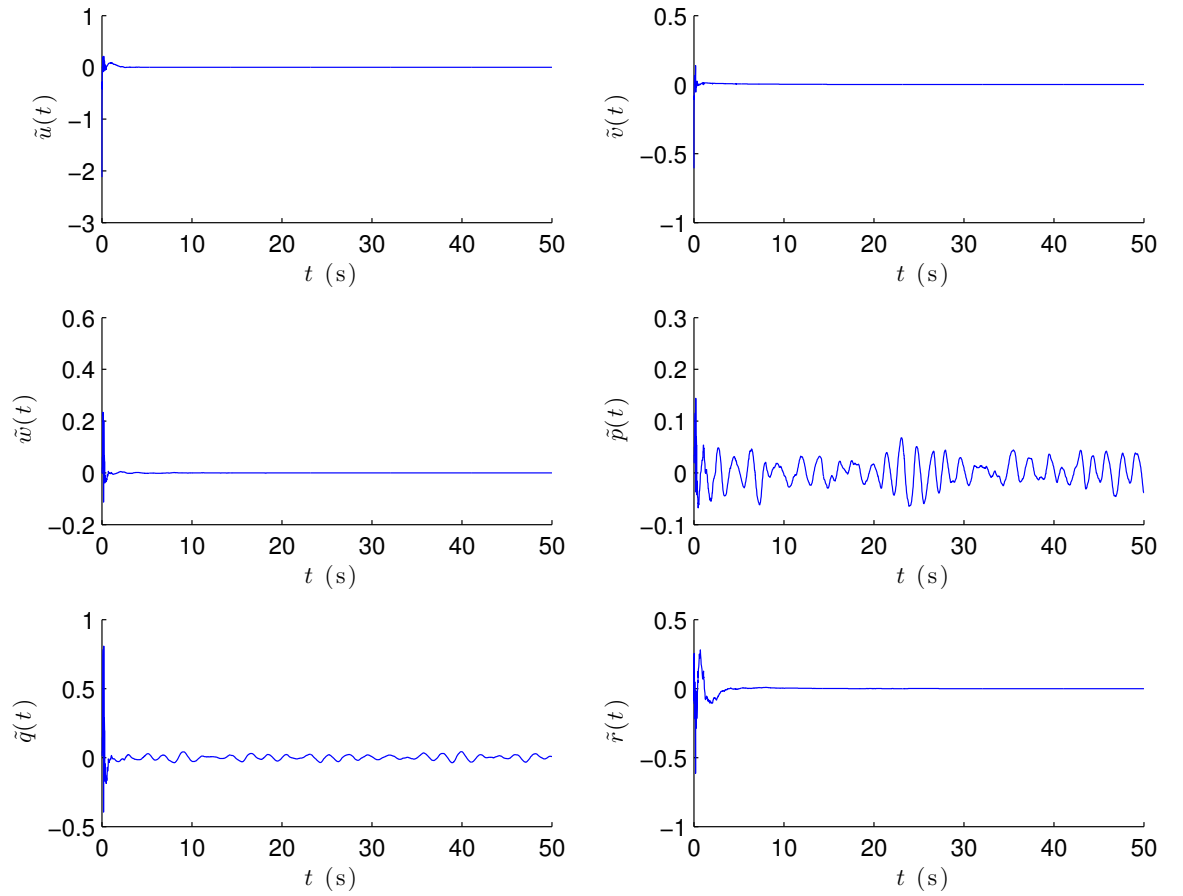


Figure 26. Error in velocity estimation.

Using the the linear dynamic model and the weight matrices (176) and (177), the LQR controller with feedback gain

$$\mathbf{k} = \begin{bmatrix} 38.98 & 0 & 0 & 0 & 0 & 0 \\ 0 & 50.85 & 0 & 0 & 0 & 0 \\ 0 & 0 & 50.85 & 0 & 0 & 0 \\ 0 & 0 & 0 & 12.56 & -5.30 \times 10^{-3} & -1.60 \times 10^{-3} \\ 0 & 0 & 0 & -5.30 \times 10^{-3} & 13.91 & -5.10 \times 10^{-3} \\ 0 & 0 & 0 & -1.60 \times 10^{-3} & -5.10 \times 10^{-3} & 14.26 \end{bmatrix}, \quad (178)$$

and integral

$$\mathbf{K}_i = -\text{diag} \{10, 10, 10, 10, 10, 10\}, \quad (179)$$

is obtained. The open-loop gain is found through the use of the linear model and the equation (169). This gain is given by

$$\mathbf{H}_k^{-1}(0) = \begin{bmatrix} 25.64 \times 10^{-3} & 0 & 0 \\ 0 & 19.66 \times 10^{-3} & 0 \\ 0 & 0 & 19.66 \times 10^{-3} \\ 0 & 0 & 0 \\ 0 & 0 & 0 \\ 0 & 0 & 0 \\ 0 & 0 & 0 \\ 0 & 0 & 0 \\ 0 & 0 & 0 \\ 79.65 \times 10^{-3} & 30.25 \times 10^{-6} & 8.74 \times 10^{-6} \\ 30.25 \times 10^{-6} & 71.90 \times 10^{-3} & 25.77 \times 10^{-6} \\ 8.74 \times 10^{-6} & 25.77 \times 10^{-6} & 70.11 \times 10^{-3} \end{bmatrix}. \quad (180)$$

The first experiment was performed by moving Visor3 in three dimensions (surge, sway and heave). Three different velocity references were commanded to the ROV: in the surge direction a reference of 0.6 m/s (see Figure 33(a)), in sway 0.4 m/s (see Figure 33(b)), and heave 0.5 m/s (see Figure 33(c)). The second experiment was performed assuming that the vehicle is rotating (change in heading) with constant velocity of 0.5 rad/s (see Figure 33(d)). As it can be seen from Figures 33(a), 33(b), 33(c), and 33(d), the controller follows the references to the desired vehicle's velocities in its four DOF controllable directions. To see the penalization over the control signals, Figure 34 shows the controls signals for each motor for the second LQR. These control signals are softer than the PID controller.

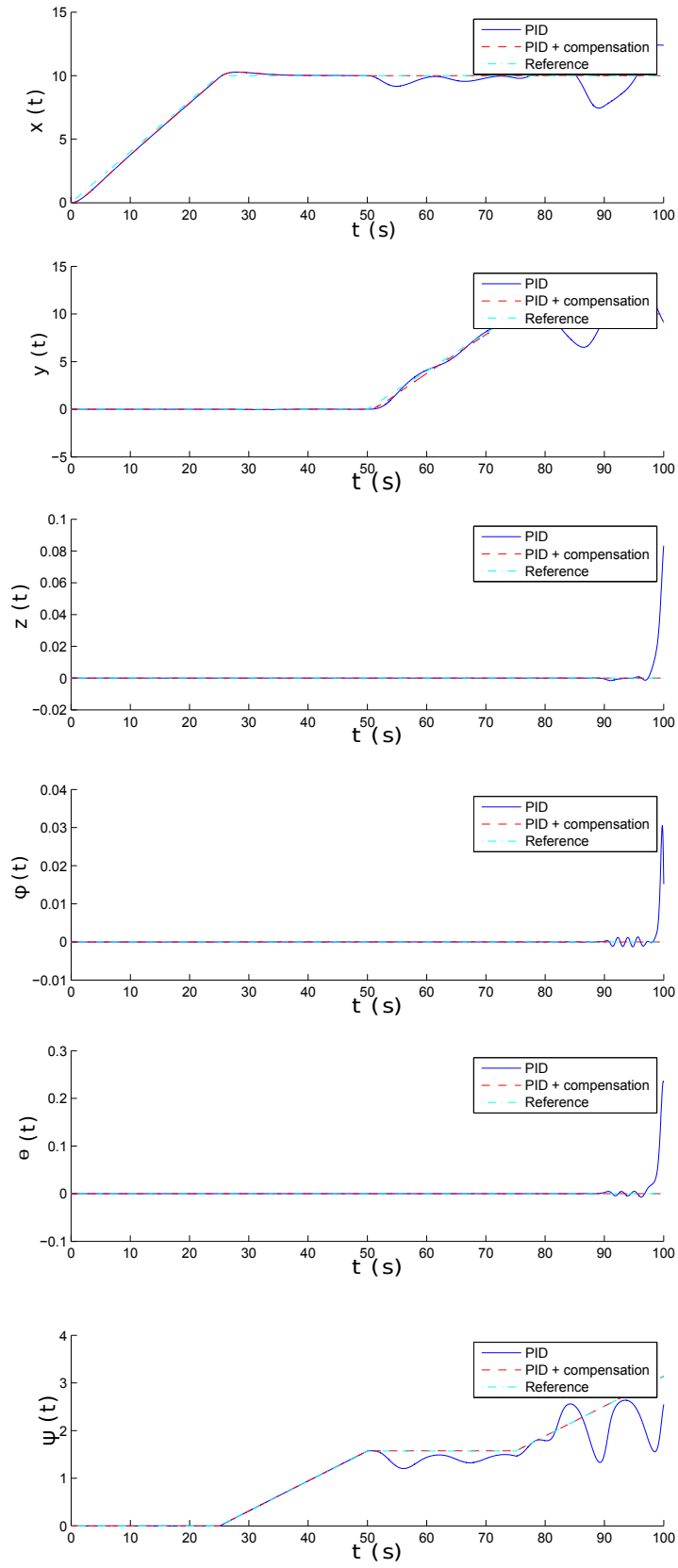


Figure 27. PID controllers with and without compensation, for planar motion control

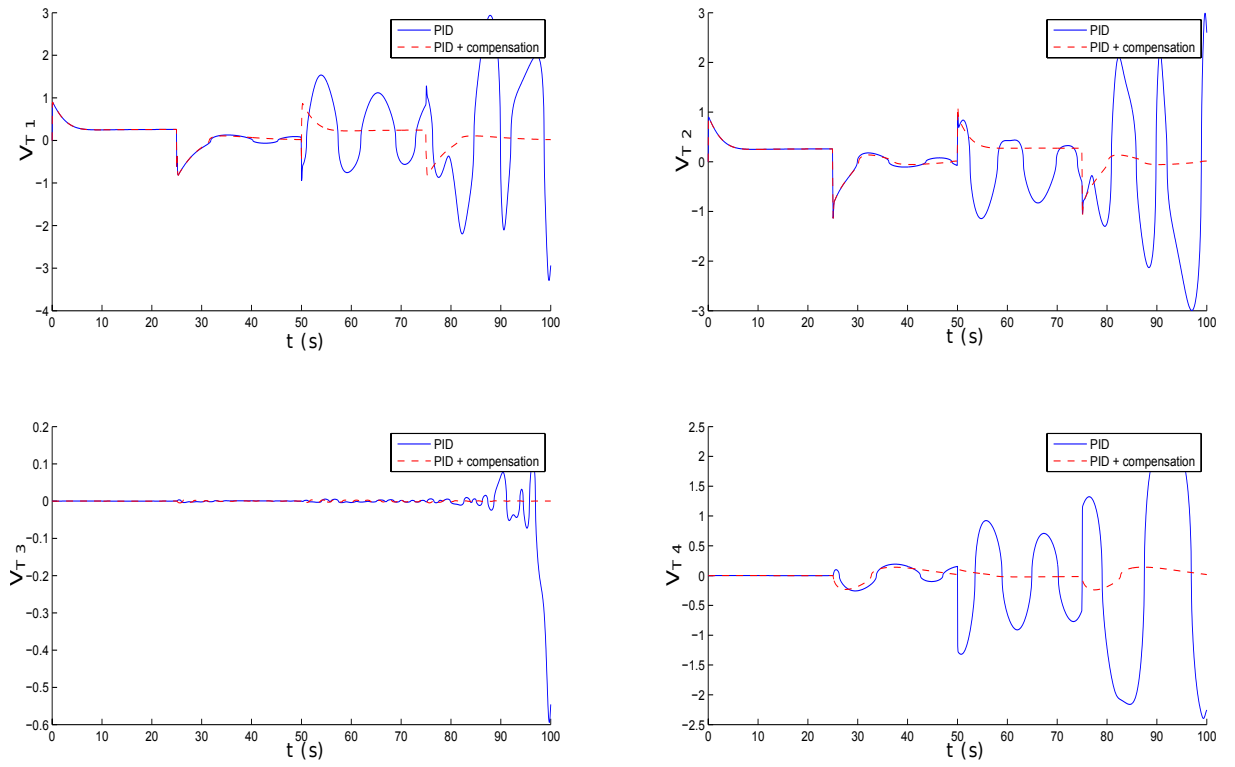


Figure 28. Control signal for each thruster, for planar motion control

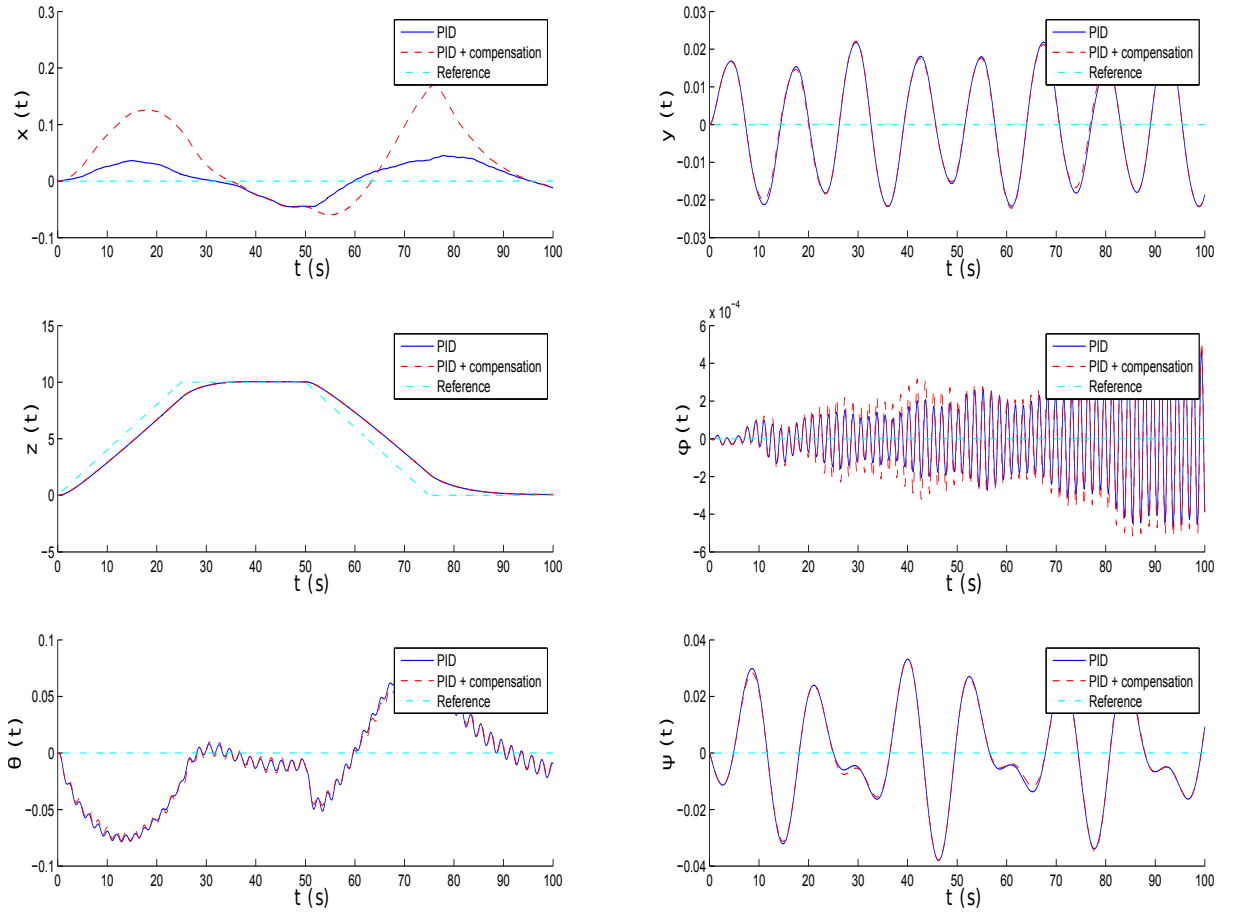


Figure 29. PID controllers with and without compensation, for depth control

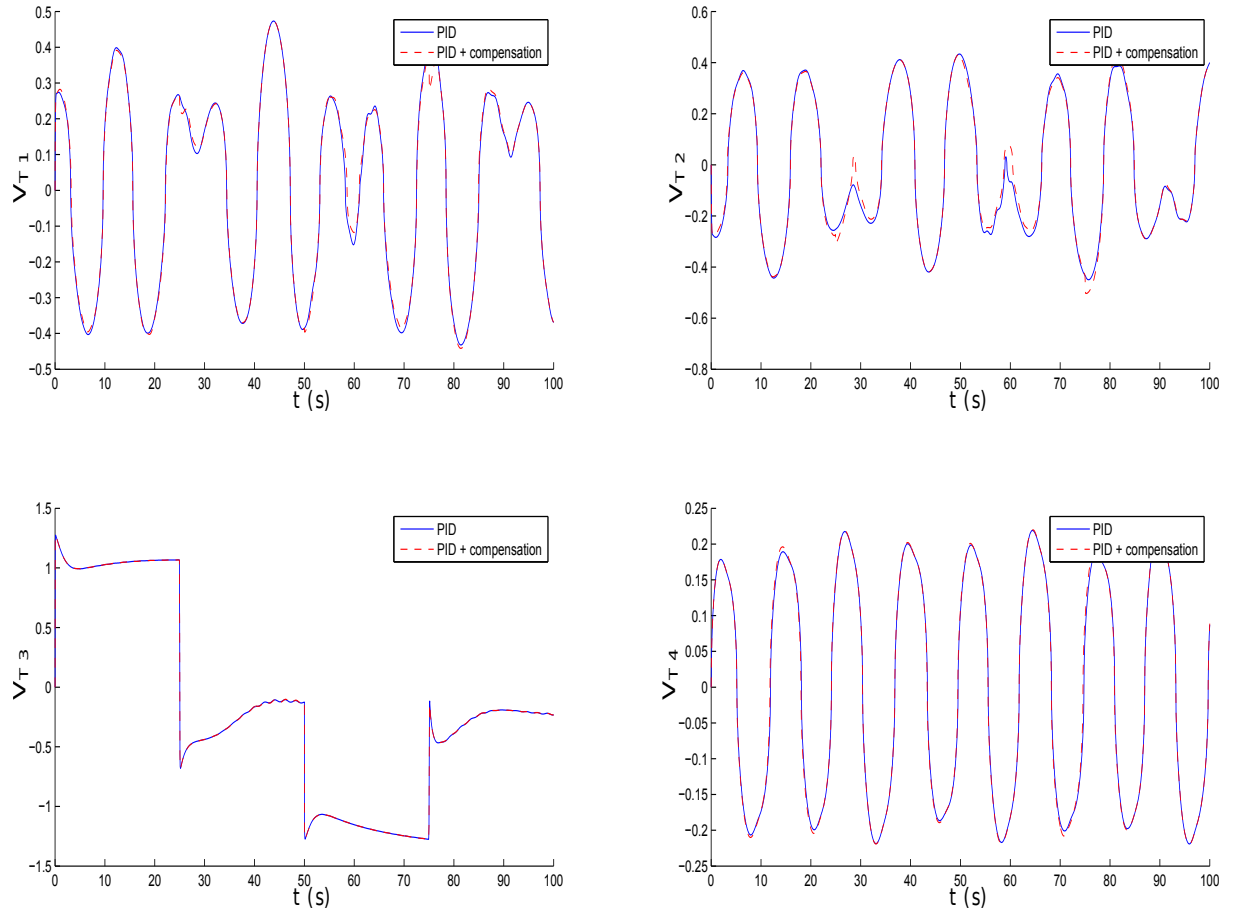


Figure 30. Control signal for each thruster, for depth control

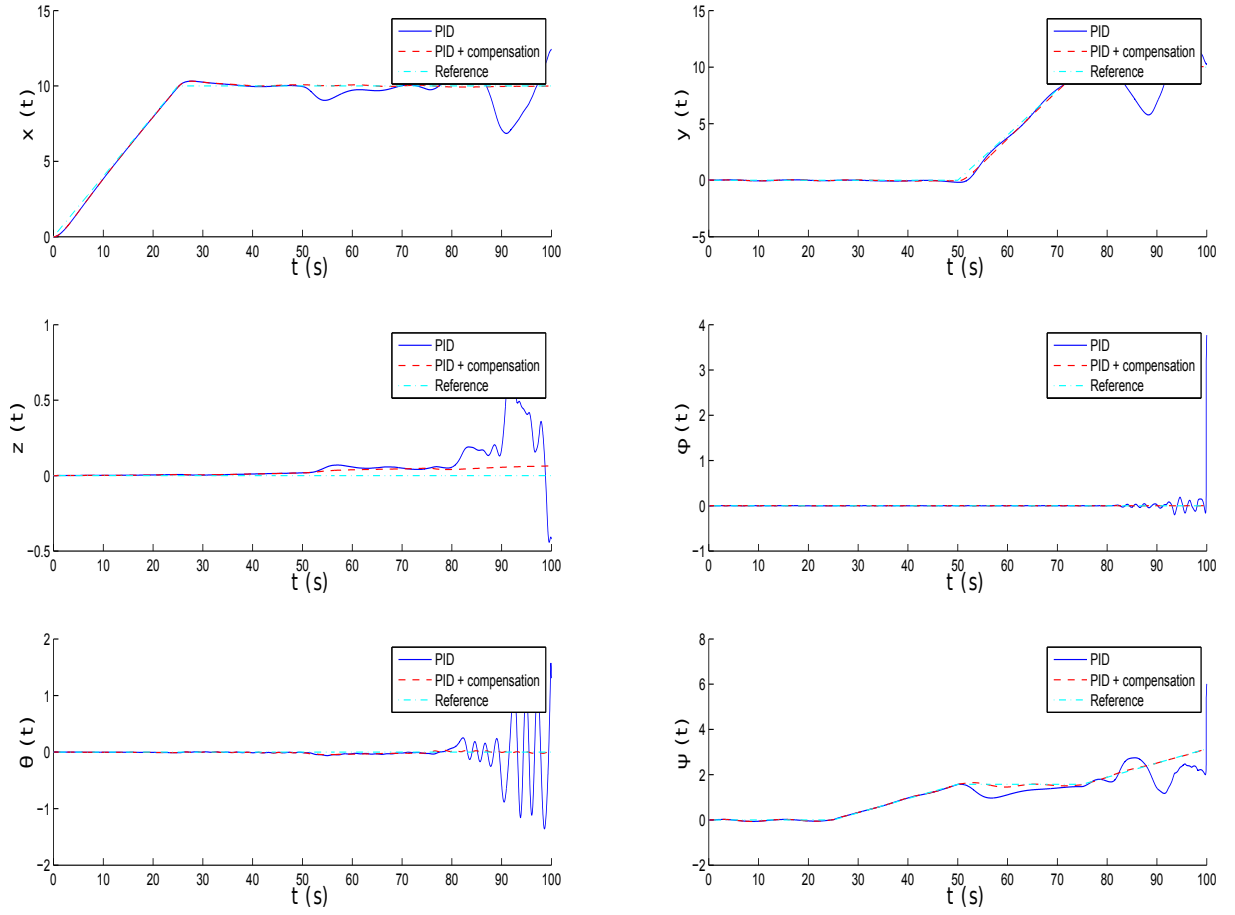


Figure 31. PID controllers with and without compensation, for planar motion control with perturbation

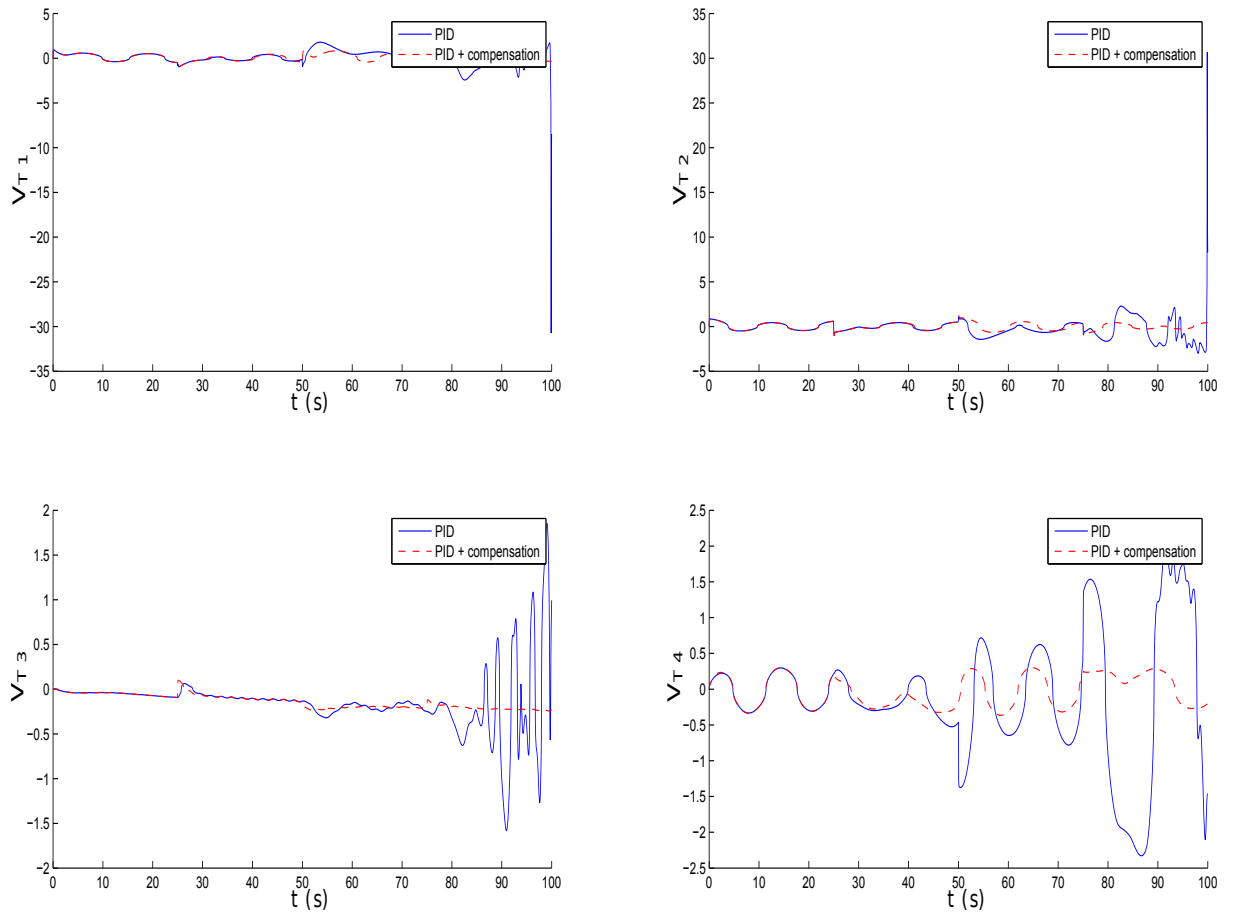
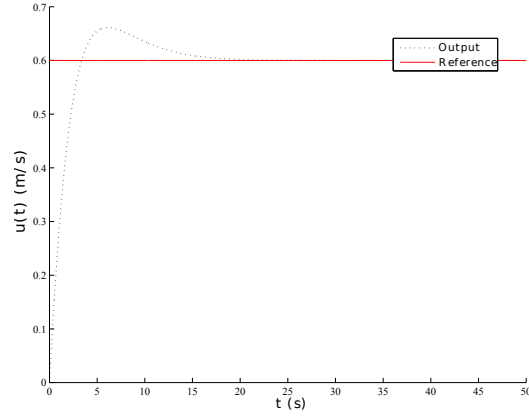
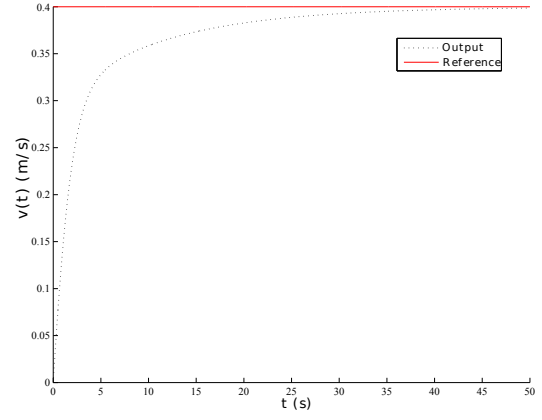


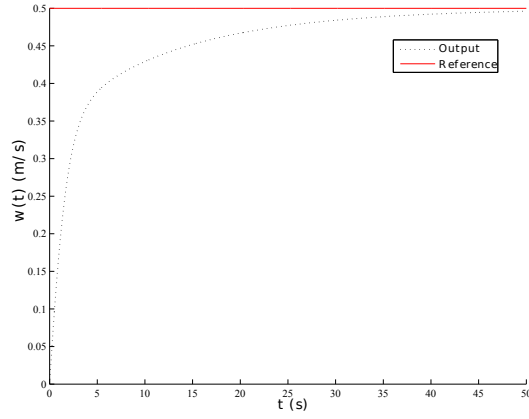
Figure 32. Control signal for each thruster, for planar motion control with perturbation



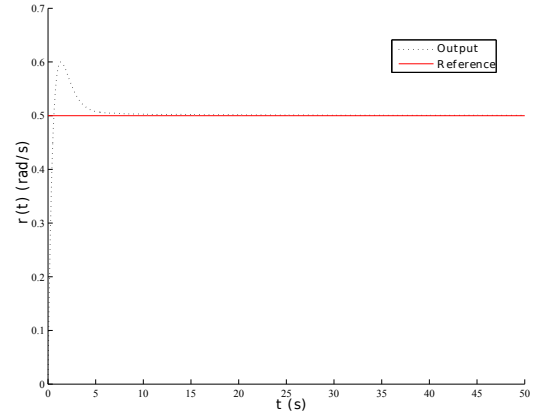
(a)



(b)



(c)



(d)

Figure 33. LQR controller performance. (a) Command velocity in surge motion. (b) Command velocity in sway motion. (c) Command velocity in heave motion. (d) Command velocity in yaw motion.

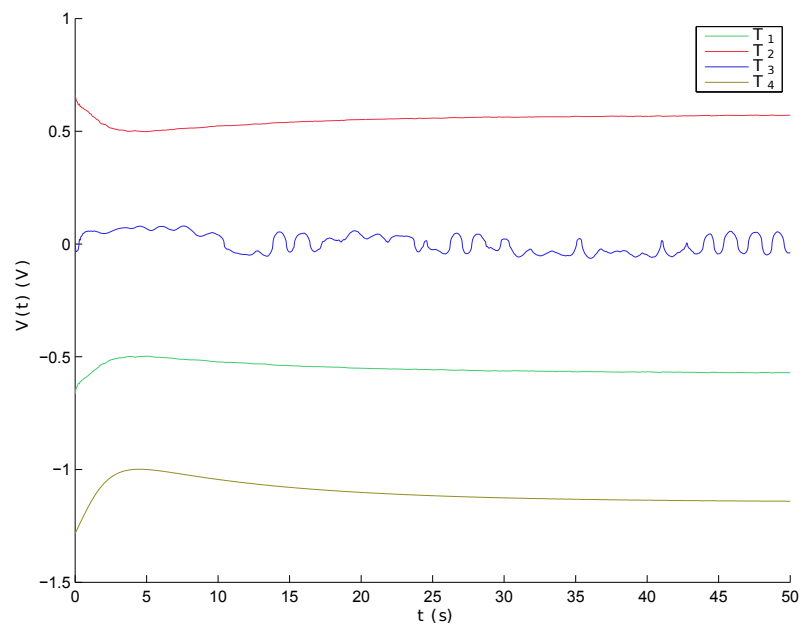


Figure 34. Control signal for each thruster in LQR controller.

CONCLUSIONS

The dynamic model of the underwater remotely operated vehicle Visor3 has been presented. This model considers forces and moments generated by the motion of the vehicle within the fluid, damping, and the restoring forces. The model was defined using body-fixed and Earth-fixed coordinate systems, and Visor3's parameters were obtained using CAD models and CFD simulations.

To improve the simulation, the thruster dynamic also has been presented. This model considers three main parts: driver, motor and propeller. The driver is simulated with a constant gain, saturation and a acceleration curve. The motor is modelled by a gain, and the dynamic will be neglected due to the low level control provided. Finally, the propeller dynamic model considers water density, the propeller diameter, and the thrust coefficient.

The navigation system (EKF) was tested assuming that Visor3 has a positioning acoustic system in the water. The navigation system was executed in discrete time with 0.05s fixed sample time. Also, the EKF was tested assuming the use of the IMU. First, the accelerometer measurement is integrated to obtain the linear velocity in the body-fixed frame. Then, the output matrix of the system was formed with the linear and angular velocity. It is important to state that the estimation in large periods of time, can diverge due to the integration of the noise coming from acceleration measurements to obtain the velocity of the vehicle in the body-fixed frame. More sensors (such a USBL) can be used in Visor3 to overcome such problem. Large sample time choice can cause divergence in estimation of the state, and short sample time can demand high performance computing on board the vehicle.

As it was shown, the EKF-based navigation system is capable to filter the noise in the measurement and accurately estimate the state of the vehicle, which is important since a noisy signal that enters into the feedback system, can cause greater efforts in the thrusters and more energy consumption.

Three different control algorithms were tested with the simulation of the ROV: PID, PID + gravity compensation, and LQR. The PID with gravity compensation is capable

to stabilize the system in less time than the PID, and decrease the energy consumption. Finally, these two algorithms were tested with disturbances in the system (ocean currents). The PID goes unstable after some time period, while the other not. However, the PID with gravity compensation needs a good estimation of the position and attitude.

The LQR algorithm was tested as a velocity controller. LQR controller was designed using a linear approximation of the vehicle's model over the origin (zero state). Then, it was tested to follow a predetermined path. With the addition of the integral and the open-loop gain, the controller is useful to track the reference. However, when the system moves away from the origin, the non-linearities are more stronger, and the LQR has a worse performance. The use of nonlinear control techniques such as gain scheduling can be used to overcome the problem of high non-linearities.

Implementing the proposed navigation system and the controller in Visor3's digital system requires the knowledge of the dynamic response of the vehicle and appropriate selection of the sample time since it affects the EKF algorithm's convergence. Moreover, many operations are in matrix form and with floating-point format, so the implementation of such navigation system and controllers requires a high computation capacity of the on-board processor. These algorithms are the first approximation to the real closed-loop control system that will be implemented in Visor3.

REFERENCES

- [1] S. Vijay, “Autonomous underwater vehicles,” internet, 2010.
- [2] M. I. Ribeiro, “Kalman and extended kalman filters: Concept, derivation and properties,” Instituto Superior Técnico, February 2004.
- [3] M. S. Grewal and A. P. Andrews, *Kalman Filtering Theory and Practice using MATLAB*, 2nd ed. Wiley, 2001.
- [4] R. D. Christ and R. L. W. Sr, *The ROV Manual, a user guide for Remotely Operated Vehicles*. Oxford: Butterworth-Heinemann, 2014.
- [5] G. A. Terejanu, “Unscented kalman filter tutorial,” *Department of Computer Science and Engineering, University of Buffalo, Buffalo, NY14260*, vol. 1, pp. 1–6, 2011.
- [6] L. Whitcomb, M. Jakuba, J. Kinsey, S. Martin, S. Webster, J. Howland, C. Taylor, D. Gomez-Ibanez., and D. Yoerger, “Navigation and control of the nereus hybrid underwater vehicle for global ocean science to 10,903 m depth: Preliminary results,” in *Robotics and Automation (ICRA), 2010 IEEE International Conference on*, 2010, pp. 594–600.
- [7] H. Shim, B.-H. Jun, P.-M. Lee, H. Baek, and J. Lee, “Workspace control system of underwater tele-operated manipulators on an ROV,” *Ocean Engineering*, vol. 37, no. 11-12, pp. 1036 – 1047, 2010.
- [8] R. B. Wynn, V. A. Huvenne, T. P. L. Bas, B. J. Murton, D. P. Connelly, B. J. Bett, H. A. Ruhl, K. J. Morris, J. Peakall, D. R. Parsons, E. J. Sumner, S. E. Darby, R. M. Dorrell, and J. E. Hunt, “Autonomous underwater vehicles (auvs): Their past, present and future contributions to the advancement of marine geoscience,” *Marine Geology*, vol. 352, no. 0, pp. 451 – 468, 2014, 50th Anniversary Special Issue.
- [9] G. Roberts, “Trends in marine control systems,” *Annual Reviews in Control*, vol. 32, no. 2, pp. 263 – 269, 2008.

- [10] M. Chyba, T. Haberkorn, R. Smith, and S. Choi, “Design and implementation of time efficient trajectories for autonomous underwater vehicles,” *Ocean Engineering*, vol. 35, no. 1, pp. 63 – 76, 2008.
- [11] S. bo FAN, L. LIAN, P. REN, and G. liang HUANG, “Oblique towing test and maneuver simulation at low speed and large drift angle for deep sea open-framed remotely operated vehicle,” *Journal of Hydrodynamics, Ser. B*, vol. 24, no. 2, pp. 280 – 286, 2012.
- [12] J. Luo, Z. Tang, Y. Peng, S. Xie, T. Cheng, and H. Li, “Anti-disturbance control for an underwater vehicle in shallow wavy water,” *Procedia Engineering*, vol. 15, no. 0, pp. 915 – 921, 2011.
- [13] T. I. Fossen, *Guidance and Control of Ocean Vehicles*. John Wiley and Sons, 1994.
- [14] J.-H. Li, B.-H. Jun, P.-M. Lee, and S.-W. Hong, “A hierarchical real-time control architecture for a semi-autonomous underwater vehicle,” *Ocean Engineering*, vol. 32, no. 13, pp. 1631 – 1641, 2005.
- [15] J. A. Ramírez, R. E. Vásquez, L. B. Gutiérrez, and D. A. Flórez, “Mechanical/naval design of an underwater remotely operated vehicle (ROV) for surveillance and inspection of port facilities,” in *Proceedings of the ASME IMECE2007*, 2007.
- [16] L. B. Gutiérrez, C. A. Zuluaga, J. A. Ramírez, R. E. Vásquez, D. A. Flórez, E. A. Taborda, and R. A. Valencia, “Development of an underwater remotely operated vehicle (ROV) for surveillance and inspection of port facilities,” in *Proceedings of the ASME IMECE2010*, 2010.
- [17] F. Xu, Z.-J. Zou, J.-C. Yin, and J. Cao, “Identification modeling of underwater vehicles’ nonlinear dynamics based on support vector machines,” *Ocean Engineering*, vol. 67, no. 0, pp. 68 – 76, 2013.
- [18] J. P. Avila, D. C. Donha, and J. C. Adamowski, “Experimental model identification of open-frame underwater vehicles,” *Ocean Engineering*, vol. 60, no. 0, pp. 81 – 94, 2013.

- [19] C. Chin, M. Lau, E. Low, and G. Seet, “Software for modelling and simulation of a remotely-operated vehicle (ROV),” *International Journal of Simulation Modeling*, vol. 5, no. 3, pp. 114–125, 2006.
- [20] A. Tiano, R. Sutton, A. Lozowicki, and W. Naeem, “Observer Kalman filter identification of an autonomous underwater vehicle,” *Control Engineering Practice*, vol. 15, no. 6, pp. 727 – 739, 2007.
- [21] H.-H. Chen, “Vision-based tracking with projective mapping for parameter identification of remotely operated vehicles,” *Ocean Engineering*, vol. 35, no. 10, pp. 983 – 994, 2008.
- [22] J. P. J. Avila and J. C. Adamowski, “Experimental evaluation of the hydrodynamic coefficients of a ROV through morison’s equation,” *Ocean Engineering*, vol. 38, no. 17-18, pp. 2162 – 2170, 2011.
- [23] M. Akmal, M. Yusoff, and M. Arshad, “Active fault tolerant control of a remotely operated vehicle propulsion system,” *Procedia Engineering*, vol. 41, no. 0, pp. 622 – 628, 2012.
- [24] H.-P. Tan, R. Diamant, W. K. Seah, and M. Waldmeyer, “A survey of techniques and challenges in underwater localization,” *Ocean Engineering*, vol. 38, no. 14-15, pp. 1663 – 1676, 2011.
- [25] J. C. Kinsey and L. L. Whitcomb, “Preliminary field experience with the DVL-NAV integrated navigation system for oceanographic submersibles,” *Control Engineering Practice*, vol. 12, no. 12, pp. 1541 – 1549, 2004.
- [26] A. Alcocer, P. Oliveira, and A. Pascoal, “Study and implementation of an EKF GIB-based underwater positioning system,” *Control Engineering Practice*, vol. 15, no. 6, pp. 689 – 701, 2007.
- [27] H.-H. Chen, “In-situ alignment calibration of attitude and ultra short baseline sensors for precision underwater positioning,” *Ocean Engineering*, vol. 35, no. 15, pp. 1448 – 1462, 2008.
- [28] X. Bian, J. Zhou, Z. Yan, H. Jia, and S. Peng, “Simulation research of H_∞ filter for the pitch control of AUV,” in *Control and Decision Conference (CCDC), 2010*

Chinese, May 2010, pp. 1788–1792.

- [29] B. Armstrong, E. Wolbrecht, and D. Edwards, “AUV navigation in the presence of a magnetic disturbance with an extended Kalman filter,” in *OCEANS 2010 IEEE - Sydney*, May 2010, pp. 1–6.
- [30] M. Caccia, G. Casalino, R. Cristi, and G. Veruggio, “Acoustic motion estimation and control for an unmanned underwater vehicle in a structured environment,” *Control Engineering Practice*, vol. 6, no. 5, pp. 661 – 670, 1998.
- [31] M. Caccia and G. Veruggio, “Guidance and control of a reconfigurable unmanned underwater vehicle,” *Control Engineering Practice*, vol. 8, no. 1, pp. 21 – 37, 2000.
- [32] L. Drolet, F. Michaud, and J. Cote, “Adaptable sensor fusion using multiple Kalman filters,” in *Intelligent Robots and Systems, 2000. (IROS 2000). Proceedings. 2000 IEEE/RSJ International Conference on*, vol. 2, 2000, pp. 1434–1439 vol.2.
- [33] M. Blain, S. Lemieux, and R. Houde, “Implementation of a ROV navigation system using acoustic/Doppler sensors and Kalman filtering,” in *OCEANS 2003. Proceedings*, vol. 3, 2003, pp. 1255–1260 Vol.3.
- [34] D. Loebis, R. Sutton, J. Chudley, and W. Naeem, “Adaptive tuning of a Kalman filter via fuzzy logic for an intelligent AUV navigation system,” *Control Engineering Practice*, vol. 12, no. 12, pp. 1531 – 1539, 2004.
- [35] J. C. Kinsey, R. M. Eustice, and L. L. Whitcomb, “A survey of underwater vehicle navigation: Recent advances and new challenges,” in *IFAC Conference of Manoeuvring and Control of Marine Craft*, 2006.
- [36] P.-M. Lee and B.-H. Jun, “Pseudo long base line navigation algorithm for underwater vehicles with inertial sensors and two acoustic range measurements,” *Ocean Engineering*, vol. 34, no. 3-4, pp. 416 – 425, 2007.
- [37] Y. Watanabe, H. Ochi, T. Shimura, and T. Hattori, “A tracking of AUV with integration of SSBL acoustic positioning and transmitted INS data,” in *OCEANS 2009 - EUROPE*, May 2009, pp. 1–6.

- [38] Y. Geng and J. Sousa, “Hybrid derivative-free EKF for USBL/INS tightly-coupled integration in AUV,” in *Autonomous and Intelligent Systems (AIS), 2010 International Conference on*, June 2010, pp. 1–6.
- [39] L. Ning and D. Wei, “Model-Aided Strapdown Inertial Navigation Integrated Method for AUV Based on H_∞ Filtering,” in *Computational and Information Sciences (ICCIS), 2013 Fifth International Conference on*, June 2013, pp. 1088–1092.
- [40] P. Batista, C. Silvestre, and P. J. Oliveira, “Kalman and H Infinity Optimal Filtering for a Class of Kinematic Systems,” in *Proceedings of the 17th IFAC World Congress*, vol. 17, no. 1, 2008, pp. 12 528–12 533.
- [41] F. Azis, M. M. Aras, M. Rashid, M. Othman, and S. Abdullah, “Problem identification for underwater remotely operated vehicle (ROV): A case study,” *Procedia Engineering*, vol. 41, no. 0, pp. 554 – 560, 2012.
- [42] S. Cohan, “Trends in ROV development,” *Marine Technology Society Journal*, vol. 42, no. 1, pp. 38–43, 2008.
- [43] K. Do, J. Pan, and Z. Jiang, “Robust and adaptive path following for underactuated autonomous underwater vehicles,” *Ocean Engineering*, vol. 31, no. 16, pp. 1967 – 1997, 2004.
- [44] P. W. van de Ven, C. Flanagan, and D. Toal, “Neural network control of underwater vehicles,” *Engineering Applications of Artificial Intelligence*, vol. 18, no. 5, pp. 533 – 547, 2005.
- [45] N. Q. Hoang and E. Kreuzer, “Adaptive PD-controller for positioning of a remotely operated vehicle close to an underwater structure: Theory and experiments,” *Control Engineering Practice*, vol. 15, no. 4, pp. 411 – 419, 2007.
- [46] W. M. Bessa, M. S. Dutra, and E. Kreuzer, “Depth control of remotely operated underwater vehicles using an adaptive fuzzy sliding mode controller,” *Robotics and Autonomous Systems*, vol. 56, no. 8, pp. 670 – 677, 2008.
- [47] A. Alvarez, A. Caffaz, A. Caiti, G. Casalino, L. Gualdesi, A. Turetta, and R. Viviani, “Fòlaga: A low-cost autonomous underwater vehicle combining glider and

- AUV capabilities,” *Ocean Engineering*, vol. 36, no. 1, pp. 24 – 38, 2009.
- [48] B. Subudhi, K. Mukherjee, and S. Ghosh, “A static output feedback control design for path following of autonomous underwater vehicle in vertical plane,” *Ocean Engineering*, vol. 63, no. 0, pp. 72 – 76, 2013.
 - [49] K. Ishaque, S. Abdullah, S. Ayob, and Z. Salam, “A simplified approach to design fuzzy logic controller for an underwater vehicle,” *Ocean Engineering*, vol. 38, no. 1, pp. 271 – 284, 2011.
 - [50] P. Herman, “Decoupled PD set-point controller for underwater vehicles,” *Ocean Engineering*, vol. 36, no. 7, pp. 529 – 534, 2009.
 - [51] J. Petrich and D. J. Stilwell, “Robust control for an autonomous underwater vehicle that suppresses pitch and yaw coupling,” *Ocean Engineering*, vol. 38, no. 1, pp. 197 – 204, 2011.
 - [52] SNAME, “Nomenclature for treating the motion of a submerged body through a fluid,” The Society of Naval Architects and Marine Engineers, Technical and Research Bulletin 1-5, 1950.
 - [53] T. I. Fossen, *Handbook of marine craft hydrodynamics and motion control*. West Sussex, United Kingdom: John Wiley & Sons, 2011.
 - [54] F. Dukan, “ROV motion control systems,” Ph.D. dissertation, Norwegian University of Science and Technology (NTNU), 2014.
 - [55] Øyvind N. Smogeli, “Control of marine propellers,” Ph.D. dissertation, Faculty of Engineering Science & Technology Department of Marine Technology, 2006.
 - [56] J. A. Ramírez, “Diseño mecánico de un vehículo sumergible operado remotamente.” Master’s thesis, Universidad Pontificia Bolivariana, 2007.
 - [57] T. Kailath, *Linear Systems*, P. Hall, Ed. Prentice Hall, 1980.

APPENDIX

A. PAPERS

1. Development of an EKF-Based Navigation System for the ROV Visor3. Submitted to IFAC Workshop NGCUV 2015, Barcelona, Spain.

Commitment Statement

By uploading this manuscript I certify that

(1) the manuscript is submitted with the full knowledge and consent of all co-authors (if any), and that I will undertake to keep my co-authors informed of all correspondence about the manuscript.

(2) contents of this manuscript are original and it is not being considered simultaneously for consideration towards publication in another conference or journal.

I also understand that

(1) by submitting my manuscript through the IFAC conference paper management system, I am permitting the IFAC access to my contact information and research interests. I agree that this data may only be used by the IFAC designated users to contact me regarding future events sponsored by the society and to assist its editorial board to identify qualified reviewers for peer review of submissions to its conferences.

(2) if my manuscript is accepted by the conference, I or one of my co-authors or colleagues will attend the conference to present the paper and will comply with the conference registration policy. Failure to comply with above may lead to the IFAC preventing me and my co-authors from submitting manuscripts to future events.

(3) papers that are not presented at the conference will not appear on the archival system, IFAC-PapersOnLine.net.

(4) presented papers will be further screened for possible publication in the IFAC Journals (Automatica, Control Engineering Practice, Annual Reviews in Control, Journal of Process Control, and Engineering Applications of Artificial Intelligence), or in IFAC-affiliated journals. All papers presented will be recorded as an IFAC Publication. The IFAC Journals and, after these, IFAC-affiliated journals have priority access to all contributions presented. However, if the author is not contacted by an editor of these journals within three months after the meeting, he/she is free to re-submit the material for publication elsewhere. In this case, the paper must carry a reference to the IFAC meeting where it was originally presented.

(5) Copyright of the papers presented at an IFAC meeting is held by IFAC.

(6) I permit the organizing committee of the NGCUV 2015 to contact me via e-mail to send me updates and notifications pertaining to the conference.

Rafael E. Vasquez, December 19, 2014

Development of an EKF-Based Navigation System for the ROV Visor3^{*}

Santiago Rúa^{*} Rafael E. Vásquez^{*}

^{*} *Universidad Pontificia Bolivariana, Circular 1 # 70-01, School of Engineering, 050031, Medellín, Colombia (e-mail: rafael.vasquez@upb.edu.co).*

Abstract: This paper addresses the development of a navigation system for the underwater remotely operated vehicle Visor3 using a nonlinear model based observer. The 6-DOF mathematical model of Visor3 is presented using two coordinated systems: Earth-fixed and body-fixed frames. The nonlinear model based observer is developed using the extended Kalman filter (EKF) which uses the linearization of the model to estimate the current state. The behavior of the observer is verified through simulation using Simulink®. The navigation system is a fundamental part of the closed-loop control system that will allow Visor3's operators to take advantage of more advanced vehicle's capabilities during inspection tasks of port facilities, hydroelectric dams, and oceanographic research.

Keywords: Robot navigation, Navigation systems, Kalman filters.

1. INTRODUCTION

Due to the growing interest around the world to perform offshore and underwater operations, several researchers have focused their interests on the construction of underwater vehicles that allow one to explore the ocean from a surface station. Underwater vehicles are used to perform different tasks such as observation, sampling, and surveillance, among others. Regardless if they are operated by cable (ROVs) or autonomous (AUVs), it is necessary to develop control strategies to achieve the desired vehicle movements (Roberts, 2008; Chyba et al., 2008).

Several control schemes are based on the mathematical model of the system. Hence, having accurate models for prediction and control is desirable, however, this is not a simple task due to the highly non-linear behavior that appears with the fluid-vehicle interaction (Xu et al., 2013). The guidance, navigation, and control (GNC) system for an underwater vehicle can have different degrees of sophistication, depending on the type of operation that is to be performed, and the autonomy levels that need to be achieved (Chyba et al., 2008; Roberts, 2008).

The desired level of autonomy will determine what kind of algorithms are necessary to control the variables of interest, which are normally given by the position, attitude (orientation) and vehicle's speed with respect to an inertial reference system located at the surface (Fossen, 1994). Fig. 1 shows a three-level hierarchical GNC structure for

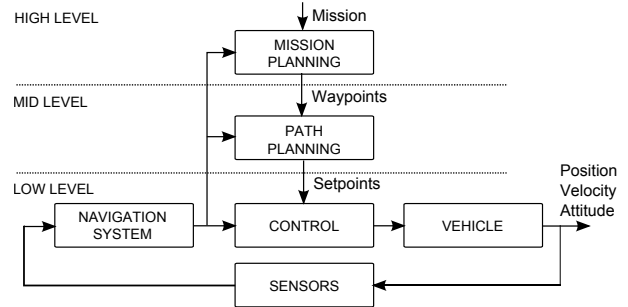


Fig. 1. Control structure for an underwater vehicle.

a underwater vehicle; this kind of structure is useful to control and stabilize the vehicle (Li et al., 2005).

One of the main components in the control structure's lower level is the navigation system. This system provides an estimate of the position, velocity, and attitude of the vehicle with respect to an inertial system located in the surface control station, from measurements made with different sensors (IMU, magnetometer, depth, DVL, USBL, among others). Given the characteristics of water, the development of underwater localization systems is not trivial and presents a number of challenges (Tan et al., 2011).

The most common algorithm to achieve this task is the Kalman filter (KF). It is an estimator, statistically optimal with respect to a quadratic error function, which allows one to estimate the state of the vehicle (Grewal and Andrews, 2001). Several Kalman-filter-based navigation systems have been developed for years. Caccia et al. (1998) developed a Kalman-filter-based acoustic navigation module to control the UUV Roby2. Caccia and Veruggio (2000) used Kalman filter techniques to estimate the state using different sampling rates of a depth-meter and altimeter.

^{*} This work was developed with the funding of the Fondo Nacional de Financiamiento para la Ciencia, la Tecnología y la Innovación, Francisco José de Caldas; the Colombian petroleum company, ECOPEPETROL; the Universidad Pontificia Bolivariana - Medellín, UPB; the Universidad Nacional de Colombia - Sede Medellín, UNALMED; through the Strategic Program for the Development of Robotic Technology for Offshore Exploration of the Colombian Sea Bottoms, project 1210-531-30550, contract 0265-2013.

Drolet et al. (2000) presented an integrated sensor fusion strategy using multiple Kalman filters allowing different combination of sensors. Blain et al. (2003) developed and tested a Kalman filter to merge data from an acoustic positioning system, a bathymeter, and a DVL. Loebis et al. (2004) implemented an intelligent navigation system, based on the integrated use of the global positioning system (GPS) and several inertial navigation system (INS) sensors for an (AUV). Kinsey et al. (2006) presented a survey with advances in underwater vehicle navigation and identified future research challenges. Lee and Jun (2007) presented a pseudo long baseline (LBL) navigation algorithm using the EKF. Watanabe et al. (2009) proposed an accurate tracking method to estimate an AUV position by using a super short baseline (USBL) from the mother ship. Geng and Sousa (2010) presented a hybrid derivative-free extended Kalman filter, taking advantage of both the linear time propagation of the Kalman filter and nonlinear measurement propagation of the derivative-free extended Kalman filter.

Gutiérrez et al. (2010) developed the underwater remotely operated vehicle Visor3 for surveillance and maintenance of ship shells and underwater structures of Colombian port facilities and oceanographic research. The mechanical/naval design was performed through an iterative process by using computational tools CAD/CAE/CFD (Ramírez et al., 2007). Visor3 has a 3-layer hardware architecture: instrumentation, communications and control. Although much work has been done in mechanics and electronics, a closed-loop control system was not developed for the ROV Visor3, so the capabilities of the vehicle are still completely dependent on the pilot skills.

This work addresses the first approach to develop the navigation system for the ROV Visor3 that will help operators to determine the position and attitude of the vehicle under certain scenarios where there is no visual information from the water surface such as in ports or dams inspection tasks. The first section presents the mathematical model of the vehicle, the second section shows the development of the nonlinear model based observer, then the simulation results are shown, and some conclusions are presented.

2. MATHEMATICAL MODEL

To analyze the motion of Visor3 in a three-dimensional space, two coordinate frames are defined: an inertial frame known as the Earth-fixed frame, where the motion of the vehicle is described, and the body-fixed frame, which is conveniently fixed to the vehicle and moves with it, Fig. 2. The acceleration of the Earth due to rotation is neglected for this work. The position and orientation of the vehicle are described relative to the Earth-fixed frame as

$$\boldsymbol{\eta} = [x \ y \ z \ \phi \ \theta \ \psi]^T, \quad (1)$$

where $\boldsymbol{\eta}_1 = [x \ y \ z]^T$ is the position and $\boldsymbol{\eta}_2 = [\phi \ \theta \ \psi]^T$ the orientation. The linear and angular velocity of the vehicle relative to the body-fixed frame are

$$\boldsymbol{\nu} = [u \ v \ w \ p \ q \ r]^T, \quad (2)$$

where $\boldsymbol{\nu}_1 = [u \ v \ w]^T$ and $\boldsymbol{\nu}_2 = [p \ q \ r]^T$ are the linear and angular velocity respectively.

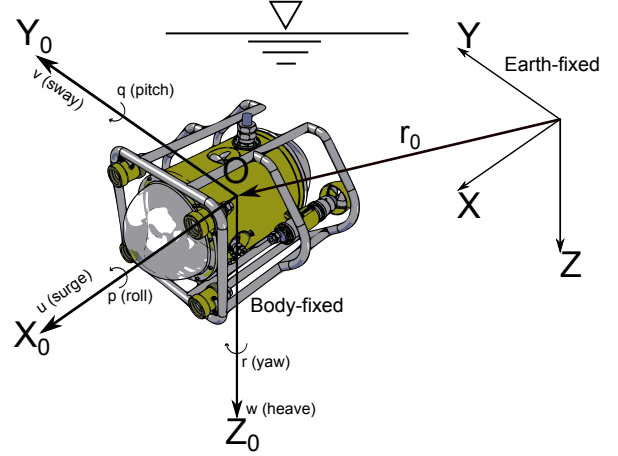


Fig. 2. Coordinate frames.

The mathematical model that describes the 6-DOF differential nonlinear equation of motion for an underwater vehicle, stated in (Fossen, 1994), is given by

$$\mathbf{M}\dot{\boldsymbol{\nu}} + \mathbf{C}(\boldsymbol{\nu})\boldsymbol{\nu} + \mathbf{D}(\boldsymbol{\nu})\boldsymbol{\nu} + \mathbf{g}(\boldsymbol{\eta}) = \boldsymbol{\tau}, \quad (3)$$

$$\dot{\boldsymbol{\eta}} = \mathbf{J}(\boldsymbol{\eta})\boldsymbol{\nu}, \quad (4)$$

where $\mathbf{M} \in \mathbb{R}^{6 \times 6}$ is the inertia matrix, which comprises the mass of the rigid body and the added mass, $\mathbf{M} = \mathbf{M}_{RB} + \mathbf{M}_A$; $\mathbf{C} \in \mathbb{R}^{6 \times 6}$ is the Coriolis and centripetal matrix, which includes the term due to rigid body and the term due to the added mass, $\mathbf{C} = \mathbf{C}_{RB} + \mathbf{C}_A$; $\mathbf{D} \in \mathbb{R}^{6 \times 6}$ is the damping matrix; $\mathbf{g} \in \mathbb{R}^{6 \times 1}$ is the gravitational and moments vector; $\boldsymbol{\tau} \in \mathbb{R}^{6 \times 1}$ is the force vector; and $\mathbf{J} \in \mathbb{R}^{6 \times 6}$ is the rotation matrix from the body-fixed frame to the earth-fixed frame. For this work, it is assumed that the origin of the body-fixed frame is located at the same point of the center of gravity.

Applying Newtonian laws, the rigid body equation of motion for the vehicle is

$$\mathbf{M}_{RB}\dot{\mathbf{v}} + \mathbf{C}_{RB}(\mathbf{v})\mathbf{v} = \boldsymbol{\tau}_{RB}. \quad (5)$$

In (5) the rigid body inertia matrix \mathbf{M}_{RB} can be expressed as

$$\mathbf{M}_{RB} = \begin{bmatrix} m\mathbf{I}_{3 \times 3} & -m\mathbf{S}(\mathbf{r}_G) \\ m\mathbf{S}(\mathbf{r}_G) & \mathbf{I}_0 \end{bmatrix}, \quad (6)$$

where m is the mass of the vehicle, $\mathbf{I}_{3 \times 3}$ the identity matrix, \mathbf{I}_0 the inertia tensor with respect to the center of gravity, \mathbf{r}_G the gravity vector in the body-fixed frame and $\mathbf{S}(\cdot)$ a skew symmetric matrix. The centripetal and Coriolis matrix can be parametrized in the form of a skew symmetric matrix

$$\mathbf{C}_{RB} = \begin{bmatrix} \mathbf{C}_{RB11} & \mathbf{C}_{RB12} \\ \mathbf{C}_{RB21} & \mathbf{C}_{RB22} \end{bmatrix}, \quad (7)$$

where

$$\mathbf{C}_{RB11} = \mathbf{0}_{3 \times 3}, \quad (8)$$

$$\mathbf{C}_{RB12} = -m\mathbf{S}(\boldsymbol{\nu}_1) - m\mathbf{S}(\boldsymbol{\nu}_2)\mathbf{S}(\mathbf{r}_G), \quad (9)$$

$$\mathbf{C}_{RB21} = -m\mathbf{S}(\boldsymbol{\nu}_1) + m\mathbf{S}(\boldsymbol{\nu}_2)\mathbf{S}(\mathbf{r}_G), \quad (10)$$

$$\mathbf{C}_{RB22} = -\mathbf{S}(\mathbf{I}_0)\boldsymbol{\nu}_2. \quad (11)$$

The added mass due to the inertia of the surrounding fluid is given by

$$\mathbf{M}_A = \begin{bmatrix} \mathbf{A}_{11}^{3 \times 3} & \mathbf{A}_{12}^{3 \times 3} \\ \mathbf{A}_{21}^{3 \times 3} & \mathbf{A}_{22}^{3 \times 3} \end{bmatrix} = - \begin{bmatrix} \frac{\partial \boldsymbol{\tau}}{\partial \dot{u}} & \frac{\partial \boldsymbol{\tau}}{\partial \dot{v}} & \frac{\partial \boldsymbol{\tau}}{\partial \dot{w}} & \frac{\partial \boldsymbol{\tau}}{\partial \dot{p}} & \frac{\partial \boldsymbol{\tau}}{\partial \dot{q}} & \frac{\partial \boldsymbol{\tau}}{\partial \dot{r}} \end{bmatrix}. \quad (12)$$

where $\boldsymbol{\tau} = [X \ Y \ Z \ K \ M \ N]$ are the hydrodynamics added mass forces and moments in each direction. Finding the 36 elements of \mathbf{M}_A is a difficult task, but this can be simplified exploiting symmetry properties of the vehicle. For this work, Visor3 is assumed to have symmetry about xy , xz and yz planes. Therefore, the added mass matrix can be computed as

$$\mathbf{M}_A = -\text{diag} \{X_{\dot{u}}, Y_{\dot{v}}, Z_{\dot{w}}, K_{\dot{p}}, M_{\dot{q}}, N_{\dot{r}}\}. \quad (13)$$

The hydrodynamic centripetal and Coriolis matrix can also be parametrized as

$$\mathbf{C}_A(\boldsymbol{\nu}) = \begin{bmatrix} \mathbf{0}_{3 \times 3} & -\mathbf{S}(\mathbf{A}_{11}\boldsymbol{\nu}_1 + \mathbf{A}_{12}\boldsymbol{\nu}_2) \\ -\mathbf{S}(\mathbf{A}_{11}\boldsymbol{\nu}_1 + \mathbf{A}_{12}\boldsymbol{\nu}_2) & -\mathbf{S}(\mathbf{A}_{21}\boldsymbol{\nu}_1 + \mathbf{A}_{22}\boldsymbol{\nu}_2) \end{bmatrix}. \quad (14)$$

For underwater vehicles damping is mainly caused by skin friction and vortex shedding. One approximation commonly used (Fossen, 1994, 2011; Dukan, 2014) is a linear and quadratic damping term given as

$$\begin{aligned} \mathbf{D}(\boldsymbol{\nu}) = & -\text{diag} \{X_u, Y_v, Z_w, K_p, M_q, N_r\} \\ & -\text{diag} \{X_{u|u}|u|, Y_{v|v}|v|, Z_{w|w}|w|, K_{p|p}|p|, \\ & M_{q|q}|q|, N_{r|r}|r|\} \end{aligned} \quad (15)$$

Restoring forces and moments, calculated from center of gravity, are given by

$$\mathbf{g}(\boldsymbol{\eta}) = \begin{bmatrix} (W - B) \sin \theta \\ -(W - B) \cos \theta \sin \phi \\ -(W - B) \cos \theta \cos \phi \\ y_b B \cos \theta \cos \phi - z_b B \cos \theta \sin \phi \\ -z_b B \sin \theta - x_b B \cos \theta \cos \phi \\ x_b B \cos \theta \sin \phi + y_b B \sin \theta \end{bmatrix}, \quad (16)$$

where $W = mg$ is the weight of the vehicle. $B = \rho g \nabla$ is the buoyancy, where ρ is the density of the fluid, g is the acceleration of the gravity, and ∇ the volume of fluid displaced by the vehicle.

2.1 Transformations

To obtain the linear velocity in the Earth-fixed frame from the linear velocity in the body-fixed frame, a linear transformation must be applied. The transformation matrix is given by

$$\mathbf{J}_1(\boldsymbol{\eta}_2) = \begin{bmatrix} c\psi c\theta & -s\psi c\phi + c\psi s\theta s\phi & s\psi s\phi + c\psi s\theta c\phi \\ s\psi c\theta & c\psi c\phi + s\psi s\theta s\phi & -c\psi s\phi + s\psi s\theta c\phi \\ -s\theta & c\theta s\phi & c\theta c\phi \end{bmatrix}, \quad (17)$$

where $s \cdot = \sin(\cdot)$ and $c \cdot = \cos(\cdot)$. The angular velocity transformation matrix is given by

$$\mathbf{J}_2(\boldsymbol{\eta}_2) = \begin{bmatrix} 1 & s\phi t\theta & c\phi t\theta \\ 0 & c\phi & -s\phi \\ 0 & s\phi/c\theta & c\phi/c\theta \end{bmatrix}, \quad (18)$$

where $t \cdot = \tan(\cdot)$.

The Kinematics equations can be expressed as

$$\begin{bmatrix} \dot{\boldsymbol{\eta}}_1 \\ \dot{\boldsymbol{\eta}}_2 \end{bmatrix} = \begin{bmatrix} \mathbf{J}_1(\boldsymbol{\eta}_2) & \mathbf{0}_{3 \times 3} \\ \mathbf{0}_{3 \times 3} & \mathbf{J}_2(\boldsymbol{\eta}_2) \end{bmatrix} \begin{bmatrix} \boldsymbol{\nu}_1 \\ \boldsymbol{\nu}_2 \end{bmatrix}. \quad (19)$$

3. NONLINEAR MODEL BASED OBSERVER

The development of the observer needs to account for the ROV high non-linearities and coupled dynamics. Therefore, an extended 6-DOF Kalman filter (EKF) that considers Coriolis, damping and restoring forces has been developed. Equations (3) and (4) can be written as a state space realization, as follows

$$\dot{\mathbf{x}} = \mathbf{f}(\mathbf{x}, t) + \mathbf{B}u(t) + \mathbf{w}(t), \quad (20)$$

$$\mathbf{z} = \mathbf{h}(\mathbf{x}, t) + \mathbf{v}(t), \quad (21)$$

where $\mathbf{w}(t)$ and $\mathbf{v}(t)$ are plant and measurement noises, respectively; they are assumed to be zero-mean Gaussian white noise processes with covariance matrix $\mathbf{Q}(t)$ and $\mathbf{R}(t)$ given by

$$E\langle \mathbf{w}(t) \rangle = 0, \quad (22)$$

$$E\langle \mathbf{w}(t) \mathbf{w}^T(s) \rangle = \delta(t - s) \mathbf{Q}(t), \quad (23)$$

$$E\langle \mathbf{v}(t) \rangle = 0, \quad (24)$$

$$E\langle \mathbf{v}(t) \mathbf{v}^T(s) \rangle = \delta(t - s) \mathbf{R}(t). \quad (25)$$

In (20), $\mathbf{f}(\mathbf{x}, t)$ is a function of the state vector $\mathbf{x} = [\boldsymbol{\nu} \ \boldsymbol{\eta}]^T$, and is given by

$$\mathbf{f}(\mathbf{x}, t) = \begin{bmatrix} \mathbf{M}^{-1}(-\mathbf{C}(\boldsymbol{\nu})\boldsymbol{\nu} - \mathbf{D}(\boldsymbol{\nu})\boldsymbol{\nu} - \mathbf{g}(\boldsymbol{\eta})) \\ \mathbf{J}(\boldsymbol{\eta})\boldsymbol{\nu} \end{bmatrix}, \quad (26)$$

and \mathbf{B} is the input coupling matrix given by

$$\mathbf{B} = \begin{bmatrix} \mathbf{M}^{-1} \\ \mathbf{0}_{6 \times 6} \end{bmatrix}. \quad (27)$$

In (20), $u(t)$ is the input vector given by thruster forces, and $\mathbf{h}(\mathbf{x}, t)$ is the measurement sensitivity matrix, which depends on the ROV sensors. The continuous-time model in (20) and (21) is discretized using a 1st-order approximation Euler method as follows

$$\mathbf{x}_k = g_{k-1}(\mathbf{x}_{k-1}) + \Delta \mathbf{u}_{k-1} + \mathbf{w}_{k-1}, \quad (28)$$

$$\mathbf{z}_k = h_k(\mathbf{x}_k) + \mathbf{v}_k, \quad (29)$$

where

$$g_{k-1}(\mathbf{x}_{k-1}) = \mathbf{x}_{k-1} + h\mathbf{f}(\mathbf{x}_{k-1}, t_{k-1}), \quad (30)$$

$$\Delta = h\mathbf{B}, \quad (31)$$

and h is the step time. The discretized system is given by

$$\boldsymbol{\nu}_k = \boldsymbol{\nu}_{k-1} + h\mathbf{M}^{-1}[\boldsymbol{\tau}_{k-1} - \mathbf{C}(\boldsymbol{\nu}_{k-1})\boldsymbol{\nu}_{k-1} - \mathbf{D}(\boldsymbol{\nu}_{k-1})\boldsymbol{\nu}_{k-1} - \mathbf{g}(\boldsymbol{\eta}_{k-1})], \quad (32)$$

$$\boldsymbol{\eta}_k = \boldsymbol{\eta}_{k-1} + h[\mathbf{J}(\boldsymbol{\eta}_{k-1})\boldsymbol{\nu}_k]. \quad (33)$$

The objective of the EKF is to use a linearized version of the system's model to estimate the current state. The EKF is executed in two steps: the predictor which calculates a approximation of the state and covariance; and the corrector which improves the initial approximation. The predictor equations for the EKF are

$$\hat{\mathbf{x}}_k(-) = g_{k-1}(\hat{\mathbf{x}}_{k-1}(+)) + \Delta \mathbf{u}_{k-1}, \quad (34)$$

$$\hat{\mathbf{z}}_k = h_k(\hat{\mathbf{x}}_k(-)), \quad (35)$$

$$\mathbf{P}_k(-) = \boldsymbol{\Phi}_{k-1}\mathbf{P}_{k-1}(+)\boldsymbol{\Phi}_{k-1}^T + \mathbf{Q}_{k-1}. \quad (36)$$

$\hat{\mathbf{x}}_k(-)$ is the a priori estimate of the state, $\hat{\mathbf{x}}_k(+)$ the a posteriori estimate of the state, $\hat{\mathbf{z}}_k$ the predicted measurement, $\mathbf{P}_k(-)$ a priori covariance matrix, $\mathbf{P}_k(+)$ a posteriori covariance matrix, and $\boldsymbol{\Phi}_{k-1}$ is the state transition matrix defined by the following Jacobian matrix

$$\boldsymbol{\Phi}_{k-1} \approx \left. \frac{\partial g_k}{\partial \mathbf{x}} \right|_{\mathbf{x}=\hat{\mathbf{x}}_{k-1}(-)}. \quad (37)$$

The corrector equations for the EKF algorithm are

$$\hat{\mathbf{x}}_k(+) = \hat{\mathbf{x}}_k(-) + \bar{\mathbf{K}}_k(\mathbf{z}_k - \hat{\mathbf{z}}_k), \quad (38)$$

$$\mathbf{P}_k(+) = [\mathbf{I} - \bar{\mathbf{K}}_k \mathbf{H}_k] \mathbf{P}_k(-), \quad (39)$$

where $\bar{\mathbf{K}}_k$ is the Kalman filter gain calculated as

$$\bar{\mathbf{K}}_k = \mathbf{P}_k(-) \mathbf{H}_k^T [\mathbf{H}_k \mathbf{P}_k(-) \mathbf{H}_k^T + \mathbf{R}_k]^{-1}. \quad (40)$$

The observation matrix is defined by the following Jacobian matrix

$$\mathbf{H}_k \approx \left. \frac{\partial \mathbf{h}_k}{\partial \mathbf{x}} \right|_{\mathbf{x}=\hat{\mathbf{x}}_k(-)}. \quad (41)$$

It is important to state that the EKF is not an optimal filter, due to the linearization process of the system. Furthermore, the matrices Φ_{k-1} and \mathbf{H}_k depend on the previous state estimation and the measurement noise. Therefore, the EKF may diverge if the consecutive linearizations are not a good approximation of the linear model in the whole domain.

4. SIMULATION AND RESULTS

The simulation of the ROV dynamics, the observer algorithm, and an LQR controller were implemented in Simulink®. The ROV dynamics was implemented as a continuous-time model, and the EKF runs in discrete time with a 0.5s fixed sample time. The implementation was done using four main functions, see Fig. 3:

- **ROV_Nonlinear_Discrete**: calculates the next state of the ROV described by (32) and (33).
- **ROVSaI_Nonlinear_Discrete**: calculates the output of the ROV according to the sensors.
- **ROV_linear_Discrete**: evaluates the Jacobian in each state estimation described by (37).
- **ROVSaI_linear_Discrete**: evaluates the output of the ROV given the Jacobian described by (41).

For the measurement matrix, it was considered that Visor3 has a MEMSENSE® IM05-0300C050A35 triaxial micro inertial measurement unit (μ IMU) that provides three linear accelerations and three angular velocities, with noise of 5.0 mg and 0.5 °/s. In this work, all measurements are assumed to be made in the body-fixed frame. The measurement matrix is given by

$$\mathbf{H}_k = [\mathbf{I}_{6 \times 6} \quad \mathbf{0}_{6 \times 6}]. \quad (42)$$

4.1 Visor3 simulation parameters

Visor3 parameters were obtained using CAD models (Solid-Edge® software) and CFD simulation (ANSYS® software). Table 1 contains all the model parameters used in the simulation to represent the dynamics of the vehicle.

To test the performance of the EKF algorithm and its implementation, several experiments were conducted. Visor3 has four controllable DOFs: surge, sway, heave and yaw. The task which consist in generating a particular command to be sent to each individual actuator according to the control law and thrusters configuration is called control allocation (Fossen, 2011). For this work, it is assumed that an individual actuator generates force in the direction of each controllable DOF.

Table 1. ROV Visor3 parameters for simulation

| Parameter | Value |
|-------------------|---|
| m | 64.5 kg |
| I_{xx} | 2.9 kg m ² |
| I_{yy} | 2.5 kg m ² |
| I_{zz} | 3.0 kg m ² |
| I_{xy} | -7.0×10^{-3} kg m ² |
| I_{xz} | -2.1×10^{-3} kg m ² |
| I_{yz} | -7.2×10^{-3} kg m ² |
| ∇ | 1.8×10^{-2} m ³ |
| $[x_g, y_g, z_g]$ | [0, 0, 0] m |
| $[x_b, y_b, z_b]$ | $[1.7, 1.8, 68] \times 10^{-3}$ m |
| $X_{\dot{u}}$ | 6.5 kg |
| $Y_{\dot{v}}$ | 59.8 kg |
| $Z_{\dot{w}}$ | 59.8 kg |
| $K_{\dot{p}}$ | 0 kg |
| $M_{\dot{q}}$ | 2.2 kg |
| $N_{\dot{r}}$ | 2.2 kg |
| $X_{u u }$ | -10.3 N s/m |
| $Y_{v v }$ | -100.8 N s/m |
| $Z_{w w }$ | -100.8 N s/m |
| $K_{p p }$ | -400.3 N s/m |
| $M_{q q }$ | -100.8 N s/m |
| $N_{r r }$ | -100.8 N s/m |

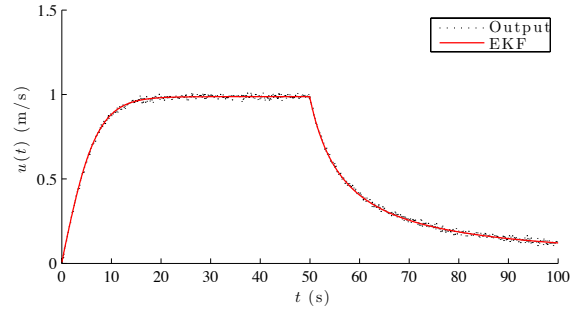


Fig. 4. Command velocity in surge motion.

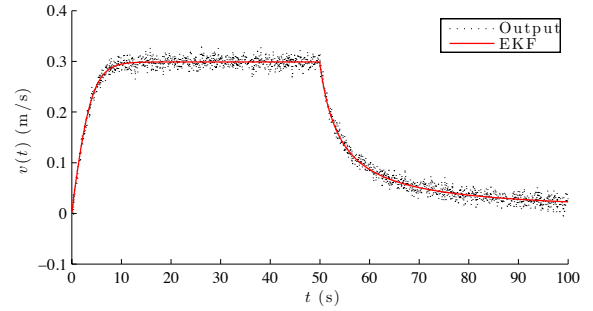


Fig. 5. Command velocity in sway motion.

Visor3 is maneuvered through a joystick that sends a velocity command to each thruster. The first experiment was performed by moving Visor3 in three dimensions (surge, sway and heave). Three different velocity references were commanded to the ROV: in the surge direction a reference of 1 m/s (see Fig. 4), in sway 0.3 m/s (see Fig. 5), and heave 0.5 m/s (see Fig. 6).

The second experiment was performed assuming that the vehicle is rotating (change in heading) with constant velocity of 0.5 rad/s (see Fig. 7).

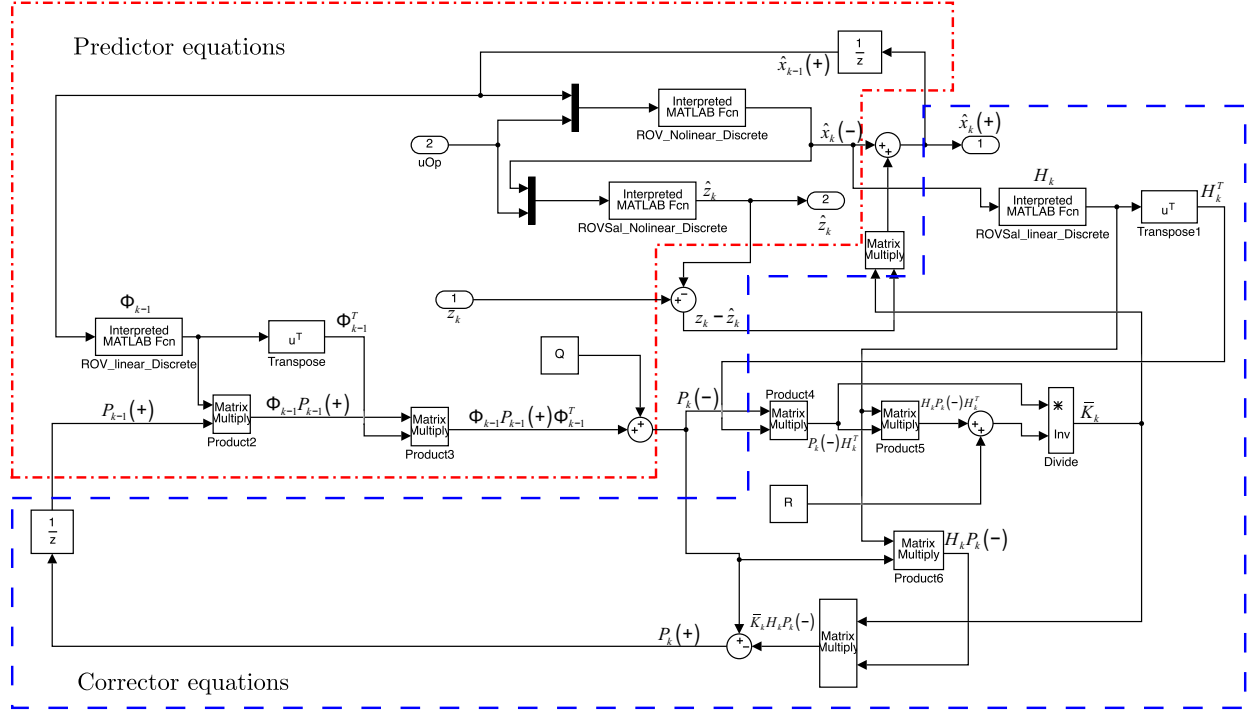


Fig. 3. EKF Simulink® implementation.

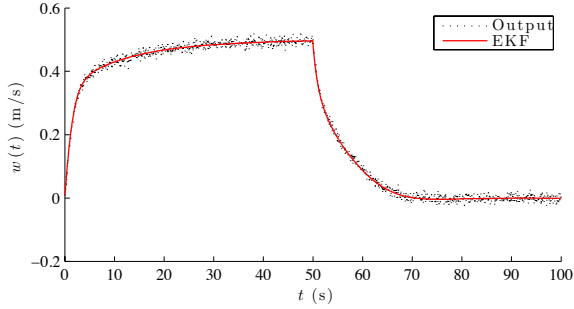


Fig. 6. Command velocity in heave motion.

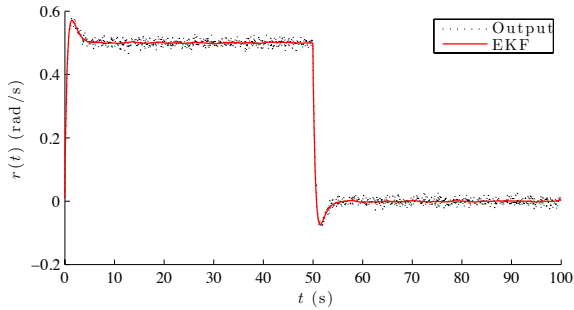


Fig. 7. Command velocity in yaw motion.

As it can be seen from Figures 4, 5, 6, and 7, the navigation systems provides a good estimation of the vehicle's velocities in its four DOF controllable directions. This will be a helpful tool for Visor3's operators since the pilot does not have feedback of such variables in the surface control station.

5. CONCLUSIONS

The dynamic model of the underwater remotely operated vehicle Visor3 has been presented. This model considers forces and moments generated by the movement of the vehicle within the fluid, damping, and the restoring forces. The model was defined using body-fixed and Earth-fixed coordinate systems, and Visor3's parameters were obtained using CAD models and CFD simulations.

The full ROV system and the EKF were simulated to compare the performance of the navigation system with the use of an LQR control algorithm that depends on a good estimation of the state. It is important to state that the estimation in large periods of time, can divergence due to the integration of the noise acceleration measurements to obtain the velocity of the vehicle in the body-fixed frame. More sensors (such a USBL) can be used in Visor3 to overcome such problem.

As it was shown, the EKF-based navigation system is capable to filter the noise in the measurement and accurately estimate the state of the vehicle, which is important since a noisy signal that enters into the feedback system, can cause greater efforts in the thrusters and more energy consumption.

Implementing the proposed navigation system in Visor3's digital system requires the knowledge of the dynamic response of the vehicle and appropriate selection of the sample time since it affects the EKF algorithm's convergence. Moreover, many operations are in matrix form and with floating-point format, so the implementation of such navigation system requires a high computation capacity of the on-board processor.

REFERENCES

- Blain, M., Lemieux, S., and Houde, R. (2003). Implementation of a ROV navigation system using acoustic/Doppler sensors and Kalman filtering. In *Proceedings of the OCEANS 2003*, volume 3, 1255–1260 Vol.3. doi: 10.1109/OCEANS.2003.178033.
- Caccia, M., Casalino, G., Cristi, R., and Veruggio, G. (1998). Acoustic motion estimation and control for an unmanned underwater vehicle in a structured environment. *Control Engineering Practice*, 6(5), 661 – 670. doi:10.1016/S0967-0661(98)00057-4.
- Caccia, M. and Veruggio, G. (2000). Guidance and control of a reconfigurable unmanned underwater vehicle. *Control Engineering Practice*, 8(1), 21 – 37. doi: 10.1016/S0967-0661(99)00125-2.
- Chyba, M., Haberkorn, T., Smith, R., and Choi, S. (2008). Design and implementation of time efficient trajectories for autonomous underwater vehicles. *Ocean Engineering*, 35(1), 63 – 76. doi:10.1016/j.oceaneng.2007.07.007.
- Drolet, L., Michaud, F., and Cote, J. (2000). Adaptable sensor fusion using multiple Kalman filters. In *Proceedings of the International Conference on Intelligent Robots and Systems, 2000.*, volume 2, 1434–1439 vol.2. doi:10.1109/IROS.2000.893222.
- Dukan, F. (2014). *ROV Motion Control Systems*. Ph.D. thesis, Norwegian University of Science and Technology (NTNU).
- Fossen, T.I. (1994). *Guidance and Control of Ocean Vehicles*. John Wiley and Sons.
- Fossen, T.I. (2011). *Handbook of marine craft hydrodynamics and motion control*. John Wiley & Sons, West Sussex, United Kingdom.
- Geng, Y. and Sousa, J. (2010). Hybrid derivative-free EKF for USBL/INS tightly-coupled integration in AUV. In *Proceedings of the 2010 International Conference on Autonomous and Intelligent Systems (AIS)*, 1–6. doi: 10.1109/AIS.2010.5547035.
- Grewal, M.S. and Andrews, A.P. (2001). *Kalman Filtering Theory and Practice using MATLAB*. Wiley, 2 edition.
- Gutiérrez, L.B., Zuluaga, C.A., Ramírez, J.A., Vásquez, R.E., Flórez, D.A., Taborda, E.A., and Valencia, R.A. (2010). Development of an underwater remotely operated vehicle (ROV) for surveillance and inspection of port facilities. In *Proceedings of the ASME IMECE2010*. doi:10.1115/IMECE2010-38217.
- Kinsey, J.C., Eustice, R.M., and Whitcomb, L.L. (2006). A survey of underwater vehicle navigation: Recent advances and new challenges. In *IFAC Conference of Manoeuvring and Control of Marine Craft*.
- Lee, P.M. and Jun, B.H. (2007). Pseudo long base line navigation algorithm for underwater vehicles with inertial sensors and two acoustic range measurements. *Ocean Engineering*, 34(3-4), 416 – 425. doi: 10.1016/j.oceaneng.2006.03.011.
- Li, J.H., Jun, B.H., Lee, P.M., and Hong, S.W. (2005). A hierarchical real-time control architecture for a semi-autonomous underwater vehicle. *Ocean Engineering*, 32(13), 1631 – 1641. doi: 10.1016/j.oceaneng.2004.12.003.
- Loebis, D., Sutton, R., Chudley, J., and Naeem, W. (2004). Adaptive tuning of a Kalman filter via fuzzy logic for an intelligent AUV navigation system. *Control Engineering Practice*, 12(12), 1531 – 1539. doi: 10.1016/j.conengprac.2003.11.008.
- Ramírez, J.A., Vásquez, R.E., Gutiérrez, L.B., and Flórez, D.A. (2007). Mechanical/naval design of an underwater remotely operated vehicle (ROV) for surveillance and inspection of port facilities. In *Proceedings of the ASME IMECE2007*. doi:10.1115/IMECE2007-41706.
- Roberts, G. (2008). Trends in marine control systems. *Annual Reviews in Control*, 32(2), 263 – 269. doi: 10.1016/j.arcontrol.2008.08.002.
- Tan, H.P., Diamant, R., Seah, W.K., and Waldmeyer, M. (2011). A survey of techniques and challenges in underwater localization. *Ocean Engineering*, 38(14-15), 1663 – 1676. doi:10.1016/j.oceaneng.2011.07.017.
- Watanabe, Y., Ochi, H., Shimura, T., and Hattori, T. (2009). A tracking of AUV with integration of SSBL acoustic positioning and transmitted INS data. In *OCEANS 2009 - EUROPE*, 1–6. doi: 10.1109/OCEANSE.2009.5278145.
- Xu, F., Zou, Z.J., Yin, J.C., and Cao, J. (2013). Identification modeling of underwater vehicles’ nonlinear dynamics based on support vector machines. *Ocean Engineering*, 67(0), 68 – 76. doi: http://dx.doi.org/10.1016/j.oceaneng.2013.02.006.

B. MASTER THESIS PROPOSAL

**SIMULATION OF THE CONTROL SYSTEM FOR A REMOTELY
OPERATED UNDERWATER VEHICLE
(SIMULACIÓN DEL SISTEMA DE CONTROL PARA UN VEHÍCULO
SUBACUÁTICO OPERADO REMOTAMENTE)**

SANTIAGO RÚA PÉREZ

**UNIVERSIDAD PONTIFICIA BOLIVARIANA
ESCUELA DE INGENIERÍAS
MAESTRÍA EN INGENIERÍA
MEDELLÍN**

2014

**SIMULATION OF THE CONTROL SYSTEM FOR A REMOTELY
OPERATED UNDERWATER VEHICLE
(SIMULACIÓN DEL SISTEMA DE CONTROL PARA UN VEHÍCULO
SUBACUÁTICO OPERADO REMOTAMENTE)**

SANTIAGO RÚA PÉREZ

Master thesis proposal

**Advisor
Rafael Esteban Vásquez Moncayo
Doctor of Philosophy**

**UNIVERSIDAD PONTIFICIA BOLIVARIANA
ESCUELA DE INGENIERÍAS
MAESTRÍA EN INGENIERÍA
MEDELLÍN
2014**

TABLE OF CONTENTS

| | Pág. |
|---|------|
| 1. PARTICIPANTS | 7 |
| 1.1. Student | 7 |
| 1.2. Advisor | 7 |
| 2. THESIS TYPE | 7 |
| 3. PROJECT TOPICS | 8 |
| 4. DEDICATION | 8 |
| 5. INTRODUCTION AND PROBLEM STATEMENT | 9 |
| 6. STATE OF THE ART | 10 |
| 6.1. Control System for ROV | 11 |
| 6.1.1. Mission Planning | 11 |
| 6.1.2. Planning trajectories | 13 |
| 6.1.3. Navigation System | 17 |
| 6.1.4. Control System | 19 |
| 6.1.5. Mathematical Model | 20 |
| 6.1.6. Hardware and software | 21 |
| 7. OBJECTIVES | 21 |
| 7.1. General objective | 21 |
| 7.2. Specific objectives | 21 |

| | | |
|------|---|----|
| 8. | METHODOLOGY | 22 |
| 8.1. | Mathematical model of the ROV | 22 |
| 8.2. | Navigation system | 23 |
| 8.3. | Control system | 23 |
| 8.4. | Simulation | 24 |
| 9. | JUSTIFICATION AND BENEFITS | 25 |
| 10. | SCOPE | 25 |
| 11. | BUDGET AND RESOURCES | 26 |
| 12. | SCHEDULE | 27 |
| | REFERENCES | 28 |

GLOSSARY

AUV: an Autonomous Underwater Vehicle is a robotic device that is driven through the water by a propulsion system, controlled and piloted by an on-board computer, and maneuverable in three dimensions. This type of vehicle works under most environmental conditions, and they use to follow precise preprogrammed trajectories wherever and whenever required [1].

EKF: an Extended Kalman Filter implements a Kalman filter for a system dynamics that results from the linearization of the original non-linear filter dynamics around the previous state estimates [2].

GNC: Guidance, Navigation and Control.

KF: Kalman Filter is an estimator for the linear quadratic problem. The problem of estimating the instantaneous “state” of a linear dynamic system perturbed with white noise, by using measurements linearly related to the state but corrupted by white noise [3].

PID: it is a control algorithm, based on a proportional, integral and derivative actions. It is the most commonly used controller in industry.

ROV: Remotely Operated Vehicle. The motion of the vehicle can be via autonomous logic direction or remote operator control depending upon the vehicle’s capability and the operator’s ability [4].

UKF: the Unscented Kalman Filter belongs to a bigger class of filters called Sigma-Point Kalman Filters or Linear Regression Kalman Filters, which use the statistical linearization technique. This technique is used to linearize a nonlinear function of a random variable through a linear regression between n points drawn from the prior distribution of the random variable. The technique tends to be more accurate than Taylor series linearization [5].

UUV: Unmanned Underwater Vehicle is defined as a self-propelled submersible whose operation is either fully autonomous (preprogrammed or real-time adaptive mission

control) or under minimal supervisory control and is untethered except, possibly, for data links such as a fiber-optic cable [\[4\]](#).

1. PARTICIPANTS

1.1. STUDENT

Santiago Rúa Pérez

Document: 1.152.436.700

Telephone: (+574) 421 8808

Id: 000121318

E-mail: santiago.ruape@alfa.upb.edu.co

Degree: Master of Science

1.2. ADVISOR

Rafael E. Vásquez, Ph.D.

Document: 71.791.914

Telephone: (+574) 448 8388 Ext. 14165

Id: 000008718

E-mail: rafael.vasquez@upb.edu.co

Company: Universidad Pontificia Bolivariana

2. THESIS TYPE

This thesis is done in the research assistance modality.

3. PROJECT TOPICS

This thesis is being developed with the funding of the Fondo Nacional de Financiamiento para la Ciencia, la Tecnología y la Innovación, Francisco José de Caldas; the Colombian petroleum company, ECOPETROL; the Universidad Pontificia Bolivariana – Medellín, UPB; the Universidad Nacional de Colombia – Sede Medellín, UNALMED; through the Strategic Program for the Development of Robotic Technology for Offshore Exploration of the Colombian Sea Bottoms, project 1210-531-30550, contract 0265 – 2013.

4. DEDICATION

Table 1 shows the percentages of dedication to the project.

Table 1. Project dedication

| Type | % |
|-------------|----|
| Research | 60 |
| Development | 30 |
| Writing | 10 |

Table 2 shows the areas associated with the project and the percentages of dedication associated with each one.

Table 2. Areas of work

| Area | % |
|----------------|----|
| Control theory | 70 |
| Simulation | 30 |

5. INTRODUCTION AND PROBLEM STATEMENT

Due to the growing interest around the world to explore the sea bottom, several researchers have focused their interests on the construction of underwater vehicles that allows one to explore the ocean from a surface station. Underwater vehicles are designed to fulfill different tasks such as observation, sampling, handling objects, among others. Regardless, if they are operated by cable (ROVs) or autonomous (AUVs), it is necessary to develop control strategies to achieve the desired movements [6, 7].

The design of some controllers is based in the mathematical model of the system. Having accurate models for prediction and control is desirable, however, this is not a simple task due to the highly non-linear behavior that appears in the fluid-vehicle interaction [8].

The Automation and Design (A+D) Group from the Universidad Pontificia Bolivariana has developed a ROV called Visor3; used for surveillance and maintenance of ship shells and underwater structures of Colombian port facilities and oceanographic research. The mechanical/naval design was performed through an iterative process by using computational tools CAD/CAE/CFD. The hardware architecture was divided in three layers: instrumentation, communications and control [9]. Although the ROV Visor3 has such a hardware infrastructure, a closed-loop control system has not been developed yet.

The goal of this work is to simulate the motion control system of the Visor3 underwater vehicle. This control system will be a first approach to manipulate the behavior of the ROV under certain scenarios. The low level control system comprises a state observer to estimate the state of the vehicle and a low level control strategy. The verification of the low level control system will be done through simulation for different operation modes.

6. STATE OF THE ART

Underwater vehicles are divided into two categories: manned underwater vehicles and unmanned underwater vehicles (UUVs). The UUVs are all kinds of underwater vehicles that are able to operate without a human inside of them. UUVs are designed to accomplish different tasks such as observation, exploration and mapping of the sea bottom [10]; sampling; object manipulation [11]; monitoring and maintenance of structures and pipelines; and other underwater engineering operations [12].

There are two kinds of UUVs (see Figure 1.): remotely operated underwater vehicles (ROVs), which are remotely controlled from a surface vessel and by a human operator; therefore, there is a physical connection (data and power) between the vehicle and the surface [4]; and the autonomous underwater vehicles (AUVs), which are self-propelled vehicles that are typically deployed from a surface vessel, and can operate independently for periods that vary from a few hours to several days [12].

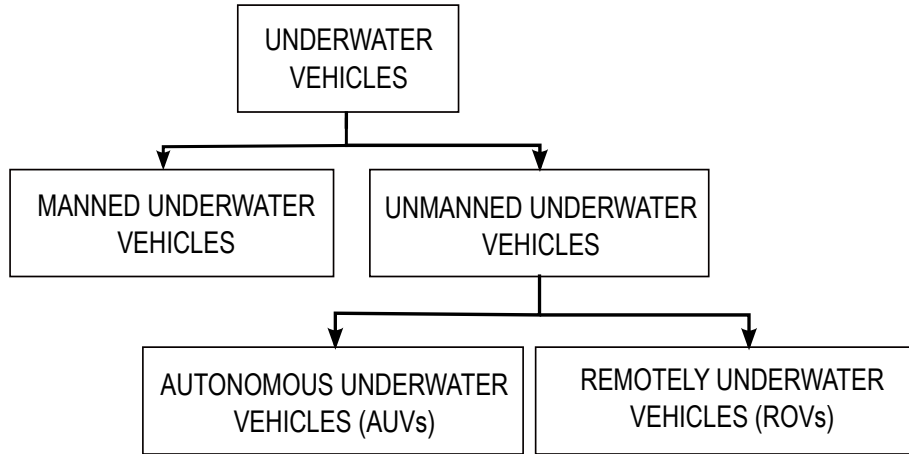


Figure 1. Underwater vehicles categories

UUVs mobility is defined by the number of independent movements they can perform (degrees of freedom), and it is directly associated with the thrusters that are present in the propulsion system. These thrusters can be controlled directly by the operator by using a joystick and an appropriate system to translate signals from the joystick to the the thrusters.

When precise control is needed to follow a certain path, commands provided by a human operator are not enough. When a vehicle is moving under the water, it is affected by viscous hydrodynamics and inertial forces [13, 14]. Whether they are operated by cable (ROVs) or autonomous (AUVs), it is necessary to develop strategies to control the desired motion [7, 6].

Control decisions are affected by several factors: mission type, energy cost [15], obstacle avoidance, among others. Such factors impose constraints that allow one to select appropriate algorithms for the UUVs' control system.

6.1. CONTROL SYSTEM FOR ROV

The guidance, navigation, and control (GNC) system for an underwater vehicle can have different degrees of sophistication, depending on the type of operation that is to be performed, and the autonomy levels that need to be achieved [7, 6]. One of the important vehicle design parameters, is the number of degrees of freedom needed to perform the planned operations, because they represent the number of independent movements that the vehicle can achieve in the three-dimensional space. Additionally, the tasks that are to be performed, determine the instrumentation (sensors, actuators, complementary systems, among others) required to control the vehicle. The desired level of autonomy, will determine what kind of algorithms are necessary to control the variables of interest, which are normally given by the position, attitude (orientation) and vehicle speed with respect to an inertial reference system located at the surface [16]. Figure 2 shows a three-level hierarchical GNC structure for a underwater vehicle; this kind of structure is useful to control and stabilize the vehicle [17].

6.1.1. Mission Planning

The highest level of the control structure contains the missions which are required for the vehicle's operation, according to its application. A mission may be: going from one point to another and then return to the initial point; search and classification [18]; or when the energy storage drops below certain level in the journey, stop and go up to the

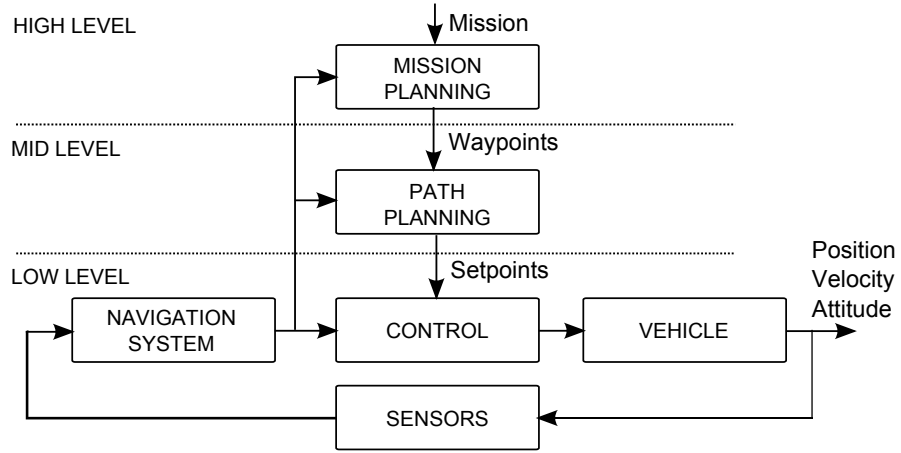


Figure 2. Control structure for an underwater vehicle.

surface [19]. This part of the control scheme is regularly executed in the surface control station.

According to Oliveira et al. [20] there are three important characteristics of the mission control system:

- Enable an operator to define the vehicle’s mission using a high level language, and translate it into a mission plan.
- Provide adequate tools to convert a mission plan into a mission program that can be formally verified and executed in real-time.
- Endow an operator with the capability to follow the progress of the mission program as it is executed, and modify it if required.

Martin et al. [21] reported that many authors have focused their attention on developing mission controllers to be easily programmable and prioritize the vehicle performance, security, and responsiveness. A big part of tasks done by an underwater vehicle are specified point to point, however in some mission planners the vehicle must not only go from one point to another, but stay in a boundary region, or avoid obstacles located in a known region [22]. A good example of a mission control system was presented by Bian et al. [23], who developed a hierarchical structure for the mission control of an autonomous underwater vehicle (AUV) based on Petri nets.

Eichhorn et al. [24] presented a mission planning system for an autonomous underwater

vehicle in time-varying ocean currents. The mission planner collects oceanic data during the exploration and in conjunction with numerical ocean models, makes decisions in order to avoid regions of adverse currents that can affect the vehicle's performance, see Figure 3.

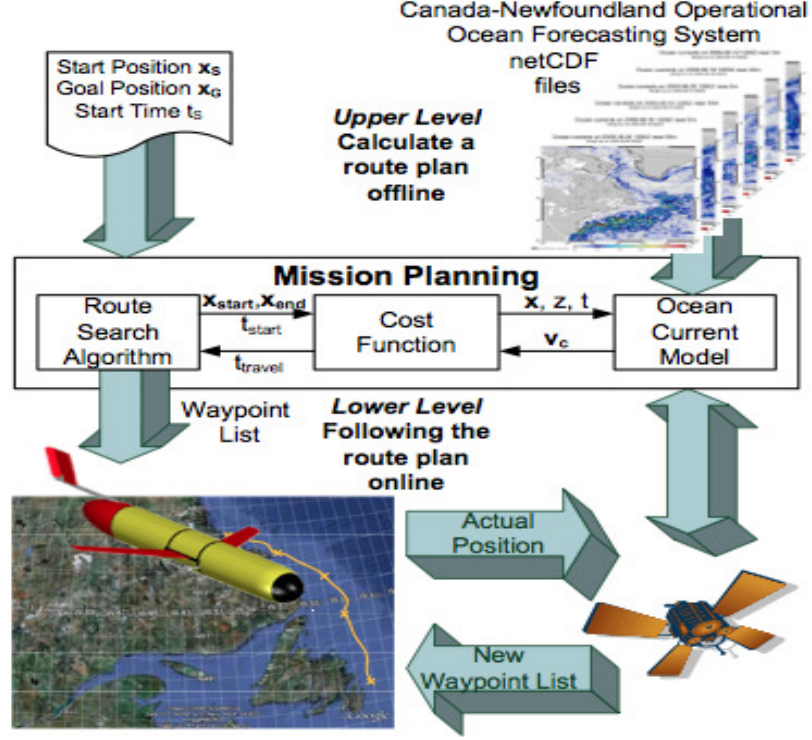


Figure 3. Control structure for an underwater vehicle presented in [24].

A good mission control system must include a failure manager for situations such as the presence of obstacles in the trajectory, environmental limitations, vehicle malfunction, among others. The system must classify the failures by the level of criticality, in order to take actions in case they happen [25].

6.1.2. Planning trajectories

The mid level of the control structure includes a motion planning system that uses the outputs of the mission planner as inputs. Motion planning refers to the determination of points and guidelines under which the vehicle must be, and the time characteristics that must be achieved by the low-level controllers [26]. The trajectory generation is

important in the operation of underwater vehicles, because it is necessary to generate commands for the vehicles to move from a starting point to an end point with a set of constraints [27, 28, 29, 30, 31]. For example, Maki et al. [32] presented a map-based path-planning system for inspection of artificial structures. The algorithm generates a set of waypoints for the AUV to follow the surface of the platform at a constant distance, based on the pre-given information of the platform. Such waypoints are generated by a set of ellipses that draw an initial route around each structural element, Figure 4. The performance of the method was verified through tank experiments using the AUV Tri-Dog 1 [33].

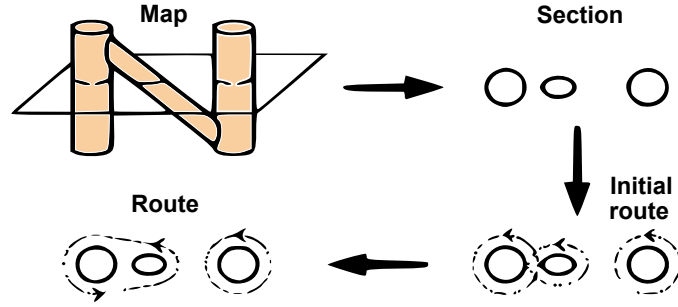


Figure 4. Path-planning procedure described by Maki et al. [32].

It is also important that the path planning algorithm is able to perform route changes if obstacles or disturbances are present during the motion of the vehicle [34, 35].

There are several methodologies for the generation of trajectories, including efficient algorithms that calculate trajectories based on geometric vehicle control [7], methodologies based on evolutionary computation [30], fuzzy logic [36], neural networks [37], reinforcement learning [38], homotopy classes [39], B-spline curves [40, 41], Rapidly-exploring Random Trees (RRT) [42], among others.

The three most common evolutionary techniques for path planning are: genetic algorithms (GA) [43, 44], particle swarm optimization (PSO) [45, 46], and ant colony optimization. GAs were invented by John Holland and his students at the University of Michigan in the 1960s [47]. The idea was to study the phenomenon of adaptation that occurs in nature. This GA tried to imitate natural processes such as crossover, mutation, survival of the fittest, etc. Zhang [48] proposed a hierarchical global path

planning approach based on GAs. This approach consist of successive decomposition of the workspace and searching for a path at each level of decomposition. The path planning processes described in [48] include the following tasks:

1. To initialize the AUV workspace.
2. To define the starting and ending points.
3. To construct a channel connecting the source and the goal among the empty cells and mixed cells at the leaf level of the current octree by using the genetic algorithm.
4. If there are mixed cells in the channel, go to 5. Otherwise, a path that only contains empty cells is found, go to 6.
5. To divide and label all the cells in the channel, go to 2.
6. A safe path from the source to the goal is obtained by connecting all the centers of the cells in the channel.

Figure 5 shows the performance of the algorithm reported in [48].

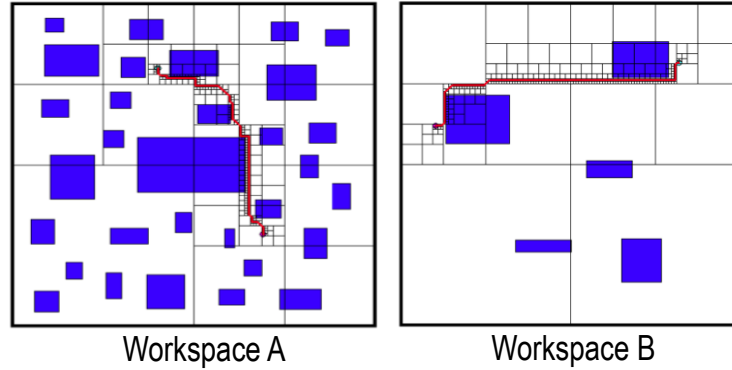


Figure 5. Results for path planning based on genetic algorithms [48].

Particle swarm optimization (PSO) is a technique based on swarm intelligence. The idea came from the research on the behavior of birds or fish swarms looking for food. Every particle follows the two best positions in the swarm in each iteration, so it converges very fast, but may fall in a local minimum [49]. Yang and Zhang [45] proposed an adapted inertia-weight particle swarm optimal (AIPSO) for path planning of an AUV in a sea environment. The approach use the model of the sea environment presented in [50]. The algorithm use a self-adapted inertia-weight (ω) update strategy to accelerate the path planning, where every particle has his own ω , which change according to the evolution of the swarm. The PSO algorithm steps are:

1. To initialize a population, in which each individual correspond to a candidate solution path and the population is a group of such potential solution.
2. To evaluate the desired optimization fitness function for each particle.
3. To compare the evaluation of each particle with the best position of its history (pid). If the current value is better than pid, then set the current location as the pid location. Also, if it is better than the best position of global (pgd), then reset the pgd with this current value.
4. To compute the variance of the swarm, the performance function of each particle, and the inertia weight.
5. To change the velocity and location of each particle.
6. Loop to step 2 until a stop criterion is achieved.

The AIPSO algorithm was tested in a grid of 50×50 cells. The distances between grid points are 20 km for a total system of 1000 km. A stationary current is randomly generated. Table 3 presents a comparative analysis for the performance of the PSO and the AIPSO.

Table 3. Comparative analysis of PSO and AIPSO [45]

| No. | Algorithm | Distance (km) | Energy cost |
|-----|-----------|---------------|-------------|
| 1 | PSO | 65.183 | 3002.26442 |
| 2 | AIPSO | 75.790 | 1770.66017 |

Finally, the ant colony optimization is characterized by the behavior of ants using pseudo-random proportional rule to select the next position [51]. The ant colony can not guarantee a safe path or maintain a safe distance, for this reason the introduction of the concept of penalty factor or other techniques is necessary. Wang et al. [52] presented a hybrid adaptive ant colony algorithm for an AUV to improve deficiencies such as slow converge rate, and falls to local minima. They tested the algorithm through simulation and the results show that the proposed method was effective.

The previously described techniques try to solve the problem in a two dimensional space, but it is important to consider that the vehicle is moving inside a 3D environment. Guanglei and Heming [53] presented a 3D path planning using an improved ant colony optimization technique. The 3D environment was built through octree model and the algorithm of ant colony optimization is adopted for it. The core of the model consist in abstract a rectangular space into nodes, each node has eight child nodes or none and

the volume of child nodes are equal to the parent nodes. The ant colony algorithm is improved to maintain a safe distance. The method can guarantee the security of the planned path and improve the efficiency of large-size local path planning.

6.1.3. *Navigation System*

One of the main elements located on the lower level of the control structure is the navigation system. It allows one to estimate the position, velocity, and attitude of the vehicle with respect to an inertial system located in the surface control station, from measurements made with different sensors (IMU, magnetometer, depth, DVL, USBL, among others). Given the characteristics of water, the development of underwater localization systems is not trivial and presents a number of challenges [54]. Therefore, for certain operating depths, knowing the vehicle's position is not a simple issue, and this should be taken into account from the design stage in order to achieve a synchronized operation between the surface station (usually located on a ship) and the underwater vehicle. The need to implement location systems for ROVs was born in 1963, with the loss and difficulty to find the USS Thresher submarine, which sank to 2560 m deep, and with the loss of an atomic bomb at the coast of Spain in 1966 [4]. Important information about determining the location of underwater vehicles can be found in [54, 55, 56, 57, 58].

The Kalman Filter is an estimator, statistically optimal with respect to a quadratic error function, which allows one to determine the state of the vehicle [3]. Armstrong et al. [59] presented an Extended Kalman Filter (EKF) used for navigation of an AUV. The AUV contains a magnetic compass and angular velocity sensor which exhibit disturbances and drift. To solve this problem, the EKF algorithm fuses the information from sensors in order to produce a more accurate estimate of heading and learns a heading bias. This heading bias can correct a poorly calibrated magnetic heading sensor, and the angular velocity improves heading estimation. The test for the approach was a simulation of an artificial compass bias (see Figure 6). A permanent magnet was placed to create magnetic field disturbances for compass, causing a deflection of 3-5 degrees. Several Kalman Filter based navigation systems have been developed for years, see for reference [60, 61, 62, 63, 64, 65, 66, 67, 68].

When the observation model is highly nonlinear, the Extended Kalman Filter can show

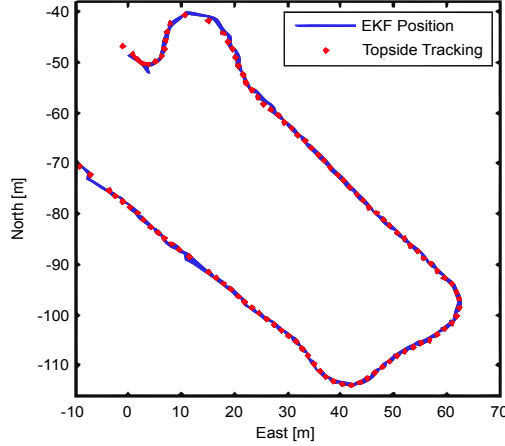


Figure 6. Simulation results of the approach in [59].

poor performance, then the Unscented Kalman Filter (UKF) can be used. The UKF uses a probabilistic sample technique called sigma points. Each sigma point is propagated through the nonlinearity yielding at the end, a cloud of transformed points. The new estimated mean and covariance are then computed based on their statistics. This process is called unscented transformation [5]. Karimi et al. [69] presented an approach to estimate the position of an AUV using EKF and UKF, using the fusion of data from two sensors: Doppler Velocity Log (DVL) and Inertial Navigation System (INS). The EKF is based on the linealization of a nonlinear system around a point on the trajectory, and the use of the linear Kalman Filter to estimate the state. The UKF estimates the state of the system through an unscented transformation. This transformation is based in two principles: first, performing a nonlinear transformation on a single point; and second, finding a set of individual points in the state space whose sample probability density function (PDF) approximates the true PDF of the state vector.

Another method commonly used when the system is highly nonlinear and there are uncertainties in the model, is the H_∞ filtering algorithm. Different from the EKF, the design criteria for the H_∞ filter is an uniformly small estimation error for any kind of noise. H_∞ filtering has strong robustness, so it can ensure navigation accuracy, improve the system reliability, and prevent filtering divergence [70]. Batista et al. [71] presented a set of optimal filtering results for a class of kinematic systems with particular application to the estimation of linear quantities in Integrated Navigation Systems for mobile platforms. The design was based on the Kalman or H_∞ filtering

steady state solutions for an equivalent LTI system and allows one to use frequency weights to achieve disturbance rejection and attenuation of noise from sensors on the state estimates.

6.1.4. *Control System*

The control system is another component of the lowest level of the control structure. It contains a set of algorithms that stabilize the state of the vehicle, so it can follow the commands generated at the path planning system. The control of an underwater vehicle is complex because there are highly nonlinear hydrodynamic effects resulting from the interaction with the environment that can not be quantified [72]. Cohan [73] states that the development of control systems for ROVs is a current and promising topic for future developments; this can be verified with the number of papers that can be found in literature.

Caccia and Veruggio [61] implemented and tested a guidance and control system for underwater vehicles using programmed controllers to regulate speed at the lowest level in a hierarchical three-level structure. Do et al. [74] developed a robust adaptive control strategy to ensure that a six-degree-of-freedom vehicle follows a prescribed path using four actuators. Van de Ven et al. [75] presented a qualitative assessment of the performance of control strategies using neural networks, indicating the advantages, disadvantages and application recommendations. Hoang and Kreuzer [76] designed an adaptive PD controller for dynamic positioning of ROVs when the mission is executed in places near submerged structures and requires great execution precision. Bessa et al. [77] used sliding mode controllers, combined with fuzzy adaptive algorithms for controlling depth in ROVs. Alvarez et al. [78] developed a robust PID controller for controlling an AUV used in oceanographic sampling work. Subudhi et al. [79] presented the design of a feedback controller for tracking paths in vertical planes. Ishaque et al. [80] presented a simplification of the conventional fuzzy controller for an underwater vehicle. Herman [81] presented a decoupled PD set-point controller which is expressed in terms of quasi-velocities for underwater vehicles. Petrich and Stilwell [82] presented a robust control for an autonomous underwater vehicle that suppresses pitch and yaw coupling.

6.1.5. Mathematical Model

The development of GNC systems for underwater vehicles is usually based on the equations of motion in the three-dimensional space. This mathematical model that represents the dynamic behavior is highly dependent on the hydrodynamic parameters caused by interaction with the environment in which the vehicle travels [83]. These parameters are important for the design of the control system, and it is possible to find in the literature several works that show different methodologies for the determination and identification of the mathematical model. Chin et al. [84] developed a computational toolbox for the analysis and design of an ROV which can simulate the behavior of the vehicle and the control system. Tiano et al. [85] used a Kalman Filter based method for the experimental evaluation of the dynamic behavior of an AUV. Chen [86] developed a system to identify ROVs parameters using a vision system for measurements, which is useful when there is no access to data for experimental modelling. Avila and Adamowski [87] developed an experimental identification system of hydrodynamic coefficients using the onboard sensors and signals from the thrusters of an ROV .

In order to improve the performance of the mathematical model, several works consider the dynamics and the configuration of thrusters. Akmal et al. [88] presented a model of forces and moments produced by four x-shape arranged thrusters over an ROV (see Figure 7), which allows the vehicle to move in three DOFs (surge, sway and yaw), see Figure 7.

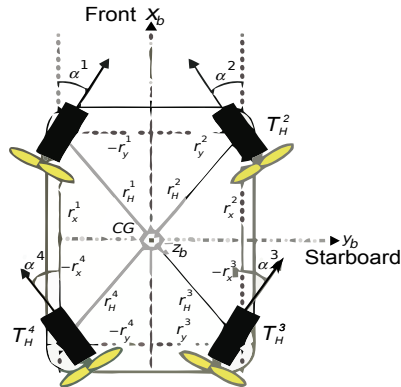


Figure 7. Thrusters allocation presented in [88].

6.1.6. *Hardware and software*

The following characteristics are considered for the processing system in the design of the ROV: cost, architecture, power consumption, communication protocols, operating systems, software programming, accessibility, memory, flexibility, reconfiguration capability, among others. The hardware must also have interfaces to ensure connections to sensors, actuators, and communication with the surface station.

The development of software architectures for ROVs is a difficult labor [89] . The software has several tasks, and according to Gutiérrez et al. [9] some of them are: reading data from sensors, running the navigation system, updating commands from the trajectory generator, executing control algorithms, commanding propellers, contacting the surface station, among others. The ROV should be monitored from the surface station using a human-machine interface, whose development depends on the variables of interest and the tasks that are executed in the ROV.

7. OBJECTIVES

7.1. GENERAL OBJECTIVE

To simulate the low level control system for a remotely operated vehicle used for observation tasks in underwater environments.

7.2. SPECIFIC OBJECTIVES

- To obtain a mathematical model that represents the dynamic behavior of the remotely operated vehicle, in order to show its response to different inputs.
- To design the navigation system using an observer to integrate data from sensors

and estimate the state of the vehicle.

- To select a control technique that stabilizes the state and allows the vehicle to follow prescribed commands for different operation modes.
- To simulate the behavior of the low level control system, including the vehicle's mathematical model, the control technique, and the navigation system.

8. METHODOLOGY

This thesis seeks the development of a simulator for the low level control system of an underwater remotely operated vehicle (ROV). The ROV that will be used for this thesis is Visor3 (See Figure 8), an ROV developed at the Universidad Pontificia Bolivariana by the Automation and Design (A+D) Group. Visor3 has four degrees of freedom: surge, sway, heave, and yaw. The pitch and roll degrees of freedom were made naturally stable by locating the center of mass below the center of buoyancy [9, 90]. To successfully complete this work, the next methodology will be followed:

8.1. MATHEMATICAL MODEL OF THE ROV

The ROV's mathematical model will be studied through a literature review that will be done using databases, books, among others; a state of the art is expected at the end of this phase. To build the mathematical model of the Visor3, some considerations have to be taken into account: degrees of freedom, environmental considerations, fluid-vehicle interaction, among others. Some parameters that appear in the vehicle-structure interaction will be determined through experimentation and simulation, within a work that is being developed by a person in the Jóvenes Investigadores program.

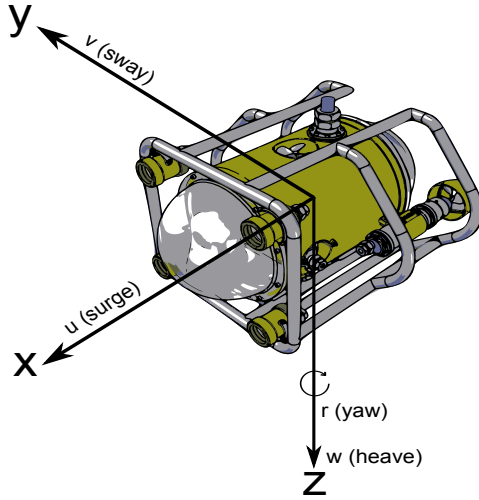


Figure 8. Visor3 computer aided design (CAD) model.

8.2. NAVIGATION SYSTEM

The ROV's navigation system will be studied through a literature review that will be done using databases, books, among others; a state of the art is expected at the end of this phase. To develop the navigation system, sensor dynamics, time response, and noise characteristics will be studied. Then, the state of the vehicle will be defined, by using variables such as position and attitude, velocity, among others. The goal of the navigation system is to provide an estimation of the estate of the vehicle, through measurements made with different sensors (IMU, magnetometer, depth, DVL, USBL, etc.). To select the appropriate navigation system performance, accuracy of the state prediction, and execution time will be considered. Finally, it will be implemented in Matlab[®].

8.3. CONTROL SYSTEM

Control techniques for ROVs will be studied through a literature review that will be done using databases, books, among others; a state of the art is expected at the end of

this phase. Controllers for underwater vehicles are traditionally based on the equations of motion derived by applying the Newtonian and Lagrangian formalism [91]. Several approaches such as classical control, adaptive control, intelligent control, robust control, among others, will be considered. Two operation modes will be defined: planar motion control, which consist in maintaining depth while the ROV is moving within the horizontal plane; and depth control which is the opposite, while the ROV goes down and up in the water, the system must maintain the same position in x-y (see Figure 9). Algorithm's performance, execution time, and complexity will be considered. Finally, the simulation will be implemented using Matlab[®].

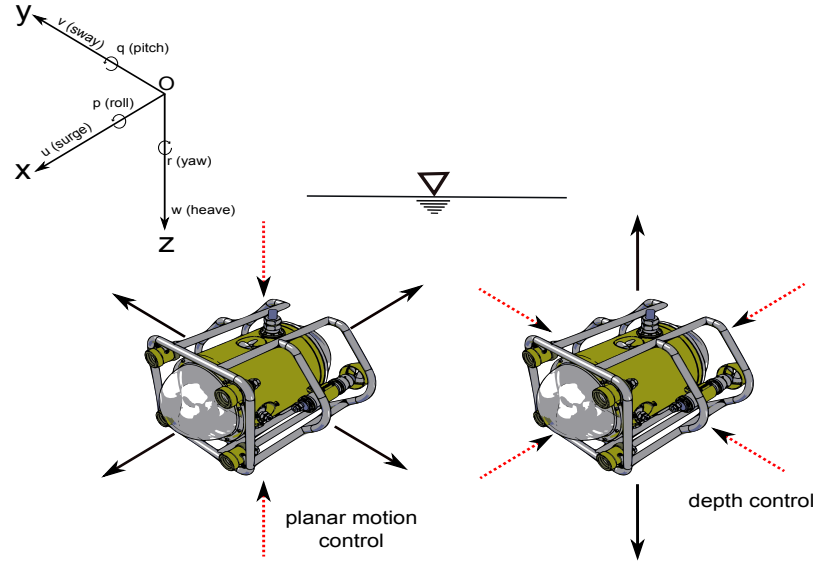


Figure 9. Low level planar motion control and depth control.

8.4. SIMULATION

To simulate the behavior of the control system, a software platform will be implemented using Matlab[®]. The system will be tested in different scenarios, where different disturbances such as oceans currents will be simulated. The simulator will allow one to give commands to the ROV, such as movements in the plane, go down or up, or a combination of both.

9. JUSTIFICATION AND BENEFITS

Due to the high cost of the implementation and the time consumption to construct a ROV, it is necessary to have a mathematical model that represents the dynamics of the system. Having a mathematical model, allows one to predict the behavior of the vehicle in different situations. With the mathematical model of the vehicle, several controllers can be designed and tested, in order to verify the performance in different operation modes such as stabilization, regulation or tracking.

The simulation platform will allow the user to test the performance of controllers and observers for different scenarios, including disturbance and noise rejection. It can provide the basis for the manipulation performance analysis and support for control system design [92].

10. SCOPE

At the end of this thesis, a simulation platform that includes Visor3's mathematical model, the navigation and control systems, will be obtained. This platform will be implemented in Matlab[®], and will allow the users to change parameters in order to evaluate the vehicle's performance. The simulation will allow one to know variables such as power requirements of the thrusters, behavior of the vehicle under the water, among others.

The products expected at the end are:

- Master's thesis document.
- A registered software.
- A paper to be submitted to a peer reviewed journal.

11. BUDGET AND RESOURCES

Table 4 shows the budget and resources for the master thesis.

Table 4. Budget and Resources

| Resources | Participation (thousand pesos) | | | Disbursement | |
|-----------------------------------|--------------------------------|------------------|-----------------|------------------|------------------|
| | Student | UPB | Donation | Yes (New) | No (Existent) |
| Bibliography | 120,00 | 600,00 | - | - | 720,00 |
| Stationery | 50,00 | - | - | 50,00 | - |
| Equipment | 2.000,00 | 3.000,00 | - | - | 5.000,00 |
| Transport | 100,00 | - | - | 100,00 | - |
| Student work 600h @30.000 \$/h | - | 18.000,00 | - | 18.000,00 | - |
| Advisor work 50h @75.000 \$/h | - | - | 3.750,00 | - | 3.750,00 |
| Matlab [®] license | - | 200,00 | - | - | 200,00 |
| Academic degree | 600,00 | - | - | 600,00 | - |
| SUBTOTAL | 2.870,00 | 21.800,00 | 3.750,00 | 18.750,00 | 9.670,00 |
| Unforeseen events (10%) | 287,00 | 2.180,00 | 375,00 | 1.875,00 | 967,00 |
| TOTAL | 3.157,00 | 23.980,00 | 4.125,00 | 20.625,00 | 10.637,00 |

12. SCHEDULE

Table 5 shows the timeline for the master thesis work.

Table 5. Master thesis time-line

| Activity \ Month | Jun | Jul | Aug | Sep | Oct | Nov |
|------------------------|-----|-----|-----|-----|-----|-----|
| Kinematic analysis ROV | ■ | | | | | |
| Equation of motion | | ■ | | | | |
| Model simulation | | ■ | | | | |
| Observer design | | ■ | ■ | | | |
| Control strategy | | | ■ | ■ | ■ | |
| Full system simulation | | | ■ | ■ | ■ | ■ |
| Master thesis writing | | ■ | ■ | ■ | ■ | ■ |
| Master thesis defense | | | | | | ■ |

REFERENCES

- [1] S. Vijay, “Autonomous underwater vehicles,” internet, 2010.
- [2] M. I. Ribeiro, “Kalman and extended kalman filters: Concept, derivation and properties,” Instituto Superior Técnico, February 2004.
- [3] M. S. Grewal and A. P. Andrews, *Kalman Filtering Theory and Practice using MATLAB*, 2nd ed. Wiley, 2001.
- [4] R. D. Christ and R. L. W. Sr, *The ROV Manual, a user guide for Remotely Operated Vehicles*. Oxford: Butterworth-Heinemann, 2014.
- [5] G. A. Terejanu, “Unscented kalman filter tutorial,” *Department of Computer Science and Engineering, University of Buffalo, Buffalo, NY14260*, vol. 1, pp. 1–6, 2011.
- [6] G. Roberts, “Trends in marine control systems,” *Annual Reviews in Control*, vol. 32, no. 2, pp. 263 – 269, 2008. [Online]. Available: <http://dx.doi.org/10.1016/j.arcontrol.2008.08.002>
- [7] M. Chyba, T. Haberkorn, R. Smith, and S. Choi, “Design and implementation of time efficient trajectories for autonomous underwater vehicles,” *Ocean Engineering*, vol. 35, no. 1, pp. 63 – 76, 2008. [Online]. Available: <http://dx.doi.org/10.1016/j.oceaneng.2007.07.007>
- [8] F. Xu, Z.-J. Zou, J.-C. Yin, and J. Cao, “Identification modeling of underwater vehicles’ nonlinear dynamics based on support vector machines,” *Ocean Engineering*, vol. 67, no. 0, pp. 68 – 76, 2013. [Online]. Available: <http://www.sciencedirect.com/science/article/pii/S0029801813000863>
- [9] L. B. Gutiérrez, C. A. Zuluaga, J. A. Ramírez, R. E. Vásquez, D. A. Flórez, E. A. Taborda, and R. A. Valencia, “Development of an underwater remotely operated vehicle (ROV) for surveillance and inspection of port facilities,” in *Proceedings of the ASME IMECE2010*, 2010.

- [10] L. Whitcomb, M. Jakuba, J. Kinsey, S. Martin, S. Webster, J. Howland, C. Taylor, D. Gomez-Ibanez., and D. Yoerger, "Navigation and control of the nereus hybrid underwater vehicle for global ocean science to 10,903 m depth: Preliminary results," in *Robotics and Automation (ICRA), 2010 IEEE International Conference on*, 2010, pp. 594–600. [Online]. Available: <http://dx.doi.org/10.1109/ROBOT.2010.5509265>
- [11] H. Shim, B.-H. Jun, P.-M. Lee, H. Baek, and J. Lee, "Workspace control system of underwater tele-operated manipulators on an ROV," *Ocean Engineering*, vol. 37, no. 11-12, pp. 1036 – 1047, 2010. [Online]. Available: <http://dx.doi.org/10.1016/j.oceaneng.2010.03.017>
- [12] R. B. Wynn, V. A. Huvenne, T. P. L. Bas, B. J. Murton, D. P. Connelly, B. J. Bett, H. A. Ruhl, K. J. Morris, J. Peakall, D. R. Parsons, E. J. Sumner, S. E. Darby, R. M. Dorrell, and J. E. Hunt, "Autonomous underwater vehicles (AUVs): their past, present and future contributions to the advancement of marine geoscience," *Marine Geology*, no. 0, pp. –, 2014. [Online]. Available: <http://dx.doi.org/10.1016/j.margeo.2014.03.012>
- [13] S. bo FAN, L. LIAN, P. REN, and G. liang HUANG, "Oblique towing test and maneuver simulation at low speed and large drift angle for deep sea open-framed remotely operated vehicle," *Journal of Hydrodynamics, Ser. B*, vol. 24, no. 2, pp. 280 – 286, 2012. [Online]. Available: [http://dx.doi.org/10.1016/S1001-6058\(11\)60245-X](http://dx.doi.org/10.1016/S1001-6058(11)60245-X)
- [14] J. Luo, Z. Tang, Y. Peng, S. Xie, T. Cheng, and H. Li, "Anti-disturbance control for an underwater vehicle in shallow wavy water," *Procedia Engineering*, vol. 15, no. 0, pp. 915 – 921, 2011. [Online]. Available: <http://dx.doi.org/10.1016/j.proeng.2011.08.169>
- [15] X. Wang, J. Shang, Z. Luo, L. Tang, X. Zhang, and J. Li, "Reviews of power systems and environmental energy conversion for unmanned underwater vehicles," *Renewable and Sustainable Energy Reviews*, vol. 16, no. 4, pp. 1958 – 1970, 2012. [Online]. Available: <http://dx.doi.org/10.1016/j.rser.2011.12.016>
- [16] T. I. Fossen, *Guidance and Control of Ocean Vehicles*. John Wiley and Sons, 1994.

- [17] J.-H. Li, B.-H. Jun, P.-M. Lee, and S.-W. Hong, “A hierarchical real-time control architecture for a semi-autonomous underwater vehicle,” *Ocean Engineering*, vol. 32, no. 13, pp. 1631 – 1641, 2005. [Online]. Available: <http://dx.doi.org/10.1016/j.oceaneng.2004.12.003>
- [18] A. Caiti, D. Martini, V. Morellato, and G. Vettori, “A Monte Carlo simulator for evaluation of AUV configuration in object search and classification missions,” in *Oceans 2005 - Europe*, vol. 2, June 2005, pp. 1024–1027 Vol. 2. [Online]. Available: <http://dx.doi.org/10.1109/OCEANSE.2005.1513198>
- [19] M. Kao, G. Weitzel, X. Zheng, and M. Black, “A simple approach to planning and executing complex AUV missions,” in *Autonomous Underwater Vehicle Technology, 1992. AUV '92., Proceedings of the 1992 Symposium on*, Jun 1992, pp. 95–102. [Online]. Available: <http://dx.doi.org/10.1109/AUV.1992.225188>
- [20] P. Oliveira, A. Pascoal, V. Silva, and C. Silvestre, “Design, development, and testing at sea of the mission control system for the marius autonomous underwater vehicle,” in *OCEANS '96. MTS/IEEE. Prospects for the 21st Century. Conference Proceedings*, vol. 1, Sep 1996, pp. 401–406 vol.1. [Online]. Available: <http://dx.doi.org/10.1109/OCEANS.1996.572781>
- [21] S. Martin, L. Whitcomb, D. Yoerger, and H. Singh, “A mission controller for high level control of autonomous and semi-autonomous underwater vehicles,” in *OCEANS 2006*, 2006, pp. 1–6. [Online]. Available: <http://dx.doi.org/10.1109/OCEANS.2006.306809>
- [22] Z. H. Ismail and M. W. Dunnigan, “A region boundary-based control scheme for an autonomous underwater vehicle,” *Ocean Engineering*, vol. 38, no. 18, pp. 2270 – 2280, 2011. [Online]. Available: <http://dx.doi.org/10.1016/j.oceaneng.2011.10.002>
- [23] X. Bian, Z. Yan, T. Chen, D. Yu, and Y. Zhao, “Mission management and control of BSA-AUV for ocean survey,” *Ocean Engineering*, vol. 55, no. 0, pp. 161 – 174, 2012. [Online]. Available: <http://dx.doi.org/10.1016/j.oceaneng.2012.06.022>
- [24] M. Eichhorn, C. Williams, R. Bachmayer, and B. de Young, “A mission planning system for the AUV glider; for the Newfoundland and labrador shelf,”

- in *OCEANS 2010 IEEE - Sydney*, May 2010, pp. 1–9. [Online]. Available: <http://dx.doi.org/10.1109/OCEANSSYD.2010.5603919>
- [25] L. Nana, L. Marce, J. Opderbecke, M. Pettier, and V. Rigaud, “Investigation of safety mechanisms for oceanographic AUV missions programming,” in *Oceans 2005 - Europe*, vol. 2, June 2005, pp. 906–913 Vol. 2. [Online]. Available: <http://dx.doi.org/10.1109/OCEANSE.2005.1513177>
- [26] R. P. Kumar, A. Dasgupta, and C. Kumar, “Real-time optimal motion planning for autonomous underwater vehicles,” *Ocean Engineering*, vol. 32, no. 11-12, pp. 1431 – 1447, 2005. [Online]. Available: <http://dx.doi.org/10.1016/j.oceaneng.2004.11.010>
- [27] K. Carroll, S. McClaran, E. Nelson, D. Barnett, D. Friesen, and G. William, “AUV path planning: an A* approach to path planning with consideration of variable vehicle speeds and multiple, overlapping, time-dependent exclusion zones,” in *Autonomous Underwater Vehicle Technology, 1992. AUV '92., Proceedings of the 1992 Symposium on*, Jun 1992, pp. 79–84. [Online]. Available: <http://dx.doi.org/10.1109/AUV.1992.225191>
- [28] D. Kruger, R. Stolkin, A. Blum, and J. Briganti, “Optimal AUV path planning for extended missions in complex, fast-flowing estuarine environments,” in *Robotics and Automation, 2007 IEEE International Conference on*, April 2007, pp. 4265–4270. [Online]. Available: <http://dx.doi.org/10.1109/ROBOT.2007.364135>
- [29] B. He and X. Zhou, “Path planning and tracking for AUV in large-scale environment,” in *Informatics in Control, Automation and Robotics (CAR), 2010 2nd International Asia Conference on*, vol. 1, March 2010, pp. 318–321. [Online]. Available: <http://dx.doi.org/10.1109/CAR.2010.5456835>
- [30] M. P. Aghababa, “3D path planning for underwater vehicles using five evolutionary optimization algorithms avoiding static and energetic obstacles,” *Applied Ocean Research*, vol. 38, no. 0, pp. 48 – 62, 2012. [Online]. Available: <http://dx.doi.org/10.1016/j.apor.2012.06.002>
- [31] Y. J. Heo and W. K. Chung, “RRT-based path planning with kinematic constraints of AUV in underwater structured environment,” in *Ubiquitous Robots*

- and Ambient Intelligence (URAI), 2013 10th International Conference on*, Oct 2013, pp. 523–525. [Online]. Available: <http://dx.doi.org/10.1109/URAI.2013.6677328>
- [32] T. Maki, T. Ura, and T. Sakamaki, “Map based path-planning and guidance scheme of an AUV for inspection of artificial structures,” in *OCEANS 2009, MTS/IEEE Biloxi - Marine Technology for Our Future: Global and Local Challenges*, Oct 2009, pp. 1–7.
 - [33] T. Maki, H. Mizushima, H. Kondo, T. Ura, T. Sakamaki, and M. Yanagisawa, “Real time path-planning of an AUV based on characteristics of passive acoustic landmarks for visual mapping of shallow vent fields,” in *OCEANS 2007*, Sept 2007, pp. 1–8. [Online]. Available: <http://dx.doi.org/10.1109/OCEANS.2007.4449321>
 - [34] A. Kume, T. Maki, T. Sakamaki, and T. Ura, “Path re-planning method for an AUV to image rough terrain by on-site quality evaluation,” in *OCEANS, 2012 - Yeosu*, May 2012, pp. 1–9. [Online]. Available: <http://dx.doi.org/10.1109/OCEANS-Yeosu.2012.6263618>
 - [35] Y. Sato, T. Maki, A. Kume, T. Matsuda, T. Sakamaki, and T. Ura, “Field experimental results of path re-planning method for an AUV to visualize complicated surface in 3D,” in *Underwater Technology Symposium (UT), 2013 IEEE International*, March 2013, pp. 1–7. [Online]. Available: <http://dx.doi.org/10.1109/UT.2013.6519892>
 - [36] S. Liu, Y. Wei, and Y. Gao, “3D path planning for AUV using fuzzy logic,” in *Computer Science and Information Processing (CSIP), 2012 International Conference on*, Aug 2012, pp. 599–603. [Online]. Available: <http://dx.doi.org/10.1109/CSIP.2012.6308925>
 - [37] S. Li and Y. Guo, “Neural-network based AUV path planning in estuary environments,” in *Intelligent Control and Automation (WCICA), 2012 10th World Congress on*, July 2012, pp. 3724–3730. [Online]. Available: <http://dx.doi.org/10.1109/WCICA.2012.6359093>
 - [38] B. Liu and Z. Lu, “AUV path planning under ocean current based on reinforcement learning in electronic chart,” in *Computational and Information*

- Sciences (ICCIS), 2013 Fifth International Conference on*, June 2013, pp. 1939–1942. [Online]. Available: <http://dx.doi.org/10.1109/ICCIS.2013.507>
- [39] E. Hernandez, M. Carreras, J. Antich, P. Ridao, and A. Ortiz, “A topologically guided path planner for an AUV using homotopy classes,” in *Robotics and Automation (ICRA), 2011 IEEE International Conference on*, May 2011, pp. 2337–2343. [Online]. Available: <http://dx.doi.org/10.1109/ICRA.2011.5980108>
- [40] T. Maekawa, T. Noda, S. Tamura, T. Ozaki, and K. ichiro Machida, “Curvature continuous path generation for autonomous vehicle using B-spline curves,” *Computer-Aided Design*, vol. 42, no. 4, pp. 350 – 359, 2010. [Online]. Available: <http://dx.doi.org/10.1016/j.cad.2009.12.007>
- [41] C.-W. Chen, J.-S. Kouh, and J.-F. Tsai, “Modeling and Simulation of an AUV simulator with guidance system,” *Oceanic Engineering, IEEE Journal of*, vol. 38, no. 2, pp. 211–225, April 2013. [Online]. Available: <http://dx.doi.org/10.1109/JOE.2012.2220236>
- [42] J. Poppinga, A. Birk, K. Pathak, and N. Vaskevicius, “Fast 6-DOF path planning for autonomous underwater vehicles (AUV) based on 3D plane mapping,” in *Safety, Security, and Rescue Robotics (SSRR), 2011 IEEE International Symposium on*, Nov 2011, pp. 345–350. [Online]. Available: <http://dx.doi.org/10.1109/SSRR.2011.6106771>
- [43] W. Hong-jian, B. Xin-qian, Z. Jie, D. Fu-guang, and X. Guo-qing, “A GA path planner based on domain knowledge for AUV,” in *OCEANS '04. MTTs/IEEE TECHNO-OCEAN '04*, vol. 3, Nov 2004, pp. 1570–1573 Vol.3. [Online]. Available: <http://dx.doi.org/10.1109/OCEANS.2004.1406356>
- [44] Z. hu Chang, Z. dong Tang, H. gao Cai, X. cheng Shi, and X. qian Bian, “GA path planning for AUV to avoid moving obstacles based on forward looking sonar,” in *Machine Learning and Cybernetics, 2005. Proceedings of 2005 International Conference on*, vol. 3, Aug 2005, pp. 1498–1502 Vol. 3. [Online]. Available: <http://dx.doi.org/10.1109/ICMLC.2005.1527181>
- [45] G. Yang and R. Zhang, “Path planning of AUV in turbulent ocean environments used adapted Inertia-Weight PSO,” in *Natural Computation, 2009. ICNC '09*.

- Fifth International Conference on*, vol. 3, Aug 2009, pp. 299–302. [Online]. Available: <http://dx.doi.org/10.1109/ICNC.2009.355>
- [46] D. Zhu, Y. Yang, and M. Yan, “Path planning algorithm for AUV based on a Fuzzy-PSO in dynamic environments,” in *Fuzzy Systems and Knowledge Discovery (FSKD), 2011 Eighth International Conference on*, vol. 1, July 2011, pp. 525–530. [Online]. Available: <http://dx.doi.org/10.1109/FSKD.2011.6019479>
 - [47] M. Mitchell, *An Introduction to genetic algorithms*, MIT, Ed. MIT Press, 1999.
 - [48] Q. Zhang, “A hierarchical global path planning approach for AUV based on genetic algorithm,” in *Mechatronics and Automation, Proceedings of the 2006 IEEE International Conference on*, June 2006, pp. 1745–1750. [Online]. Available: <http://dx.doi.org/10.1109/ICMA.2006.257478>
 - [49] D. Chaojun and Q. Zulian, “Particle Swarm Optimization Algorithm Based on The Idea of Simulated Annealing,” *IJCSNS International Journal of Computer Science and Network Security*, vol. 6, no. 10, pp. 152–157, October 2006.
 - [50] A. Alvarez, A. Caiti, and R. Onken, “Evolutionary path planning for autonomous underwater vehicles in a variable ocean,” *Oceanic Engineering, IEEE Journal of*, vol. 29, no. 2, pp. 418–429, April 2004. [Online]. Available: <http://dx.doi.org/10.1109/JOE.2004.827837>
 - [51] Z. Guang-lei and J. He-Ming, “Global path planning of AUV based on improved ant colony optimization algorithm,” in *Automation and Logistics (ICAL), 2012 IEEE International Conference on*, Aug 2012, pp. 606–610. [Online]. Available: <http://dx.doi.org/10.1109/ICAL.2012.6308150>
 - [52] P. Wang, P. Meng, and T. Ning, “Path planning based on hybrid adaptive ant colony algorithm for AUV,” in *Distributed Computing and Applications to Business, Engineering Science (DCABES), 2012 11th International Symposium on*, Oct 2012, pp. 157–160. [Online]. Available: <http://dx.doi.org/10.1109/DCABES.2012.64>
 - [53] Z. Guanglei and J. Heming, “3D path planning of AUV based on improved ant colony optimization,” in *Control Conference (CCC), 2013 32nd Chinese*, July

2013, pp. 5017–5022.

- [54] H.-P. Tan, R. Diamant, W. K. Seah, and M. Waldmeyer, “A survey of techniques and challenges in underwater localization,” *Ocean Engineering*, vol. 38, no. 14-15, pp. 1663 – 1676, 2011. [Online]. Available: <http://dx.doi.org/10.1016/j.oceaneng.2011.07.017>
- [55] J. C. Kinsey and L. L. Whitcomb, “Preliminary field experience with the DVLNAV integrated navigation system for oceanographic submersibles,” *Control Engineering Practice*, vol. 12, no. 12, pp. 1541 – 1549, 2004. [Online]. Available: <http://dx.doi.org/10.1016/j.conengprac.2003.12.010>
- [56] A. Alcocer, P. Oliveira, and A. Pascoal, “Study and implementation of an EKF GIB-based underwater positioning system,” *Control Engineering Practice*, vol. 15, no. 6, pp. 689 – 701, 2007. [Online]. Available: <http://dx.doi.org/10.1016/j.conengprac.2006.04.001>
- [57] H.-H. Chen, “In-situ alignment calibration of attitude and ultra short baseline sensors for precision underwater positioning,” *Ocean Engineering*, vol. 35, no. 15, pp. 1448 – 1462, 2008. [Online]. Available: <http://dx.doi.org/10.1016/j.oceaneng.2008.06.013>
- [58] X. Bian, J. Zhou, Z. Yan, H. Jia, and S. Peng, “Simulation research of H_∞ filter for the pitch control of AUV,” in *Control and Decision Conference (CCDC), 2010 Chinese*, May 2010, pp. 1788–1792. [Online]. Available: <http://dx.doi.org/10.1109/CCDC.2010.5498556>
- [59] B. Armstrong, E. Wolbrecht, and D. Edwards, “AUV navigation in the presence of a magnetic disturbance with an extended Kalman filter,” in *OCEANS 2010 IEEE - Sydney*, May 2010, pp. 1–6. [Online]. Available: <http://dx.doi.org/10.1109/OCEANSSYD.2010.5603905>
- [60] M. Caccia, G. Casalino, R. Cristi, and G. Veruggio, “Acoustic motion estimation and control for an unmanned underwater vehicle in a structured environment,” *Control Engineering Practice*, vol. 6, no. 5, pp. 661 – 670, 1998. [Online]. Available: [http://dx.doi.org/10.1016/S0967-0661\(98\)00057-4](http://dx.doi.org/10.1016/S0967-0661(98)00057-4)

- [61] M. Caccia and G. Veruggio, "Guidance and control of a reconfigurable unmanned underwater vehicle," *Control Engineering Practice*, vol. 8, no. 1, pp. 21 – 37, 2000. [Online]. Available: [http://dx.doi.org/10.1016/S0967-0661\(99\)00125-2](http://dx.doi.org/10.1016/S0967-0661(99)00125-2)
- [62] L. Drolet, F. Michaud, and J. Cote, "Adaptable sensor fusion using multiple Kalman filters," in *Intelligent Robots and Systems, 2000. (IROS 2000). Proceedings. 2000 IEEE/RSJ International Conference on*, vol. 2, 2000, pp. 1434–1439 vol.2. [Online]. Available: <http://dx.doi.org/10.1109/IROS.2000.893222>
- [63] M. Blain, S. Lemieux, and R. Houde, "Implementation of a ROV navigation system using acoustic/Doppler sensors and Kalman filtering," in *OCEANS 2003. Proceedings*, vol. 3, 2003, pp. 1255–1260 Vol.3. [Online]. Available: <http://dx.doi.org/10.1109/OCEANS.2003.178033>
- [64] D. Loebis, R. Sutton, J. Chudley, and W. Naeem, "Adaptive tuning of a Kalman filter via fuzzy logic for an intelligent AUV navigation system," *Control Engineering Practice*, vol. 12, no. 12, pp. 1531 – 1539, 2004. [Online]. Available: <http://dx.doi.org/10.1016/j.conengprac.2003.11.008>
- [65] J. C. Kinsey, R. M. Eustice, and L. L. Whitcomb, "A survey of underwater vehicle navigation: Recent advances and new challenges," in *IFAC Conference of Manoeuvring and Control of Marine Craft*, 2006.
- [66] P.-M. Lee and B.-H. Jun, "Pseudo long base line navigation algorithm for underwater vehicles with inertial sensors and two acoustic range measurements," *Ocean Engineering*, vol. 34, no. 3-4, pp. 416 – 425, 2007. [Online]. Available: <http://dx.doi.org/10.1016/j.oceaneng.2006.03.011>
- [67] Y. Watanabe, H. Ochi, T. Shimura, and T. Hattori, "A tracking of AUV with integration of SSBL acoustic positioning and transmitted INS data," in *OCEANS 2009 - EUROPE*, May 2009, pp. 1–6. [Online]. Available: <http://dx.doi.org/10.1109/OCEANSE.2009.5278145>
- [68] Y. Geng and J. Sousa, "Hybrid derivative-free EKF for USBL/INS tightly-coupled integration in AUV," in *Autonomous and Intelligent Systems (AIS), 2010 International Conference on*, June 2010, pp. 1–6. [Online]. Available: <http://dx.doi.org/10.1109/AIS.2010.5547035>

- [69] M. Karimi, M. Bozorg, and A. Khayatian, “A comparison of DVL/INS fusion by UKF and EKF to localize an autonomous underwater vehicle,” in *Robotics and Mechatronics (ICRoM), 2013 First RSI/ISM International Conference on*, Feb 2013, pp. 62–67. [Online]. Available: <http://dx.doi.org/10.1109/ICRoM.2013.6510082>
- [70] L. Ning and D. Wei, “Model-Aided Strapdown Inertial Navigation Integrated Method for AUV Based on H_∞ Filtering,” in *Computational and Information Sciences (ICCIS), 2013 Fifth International Conference on*, June 2013, pp. 1088–1092. [Online]. Available: <http://dx.doi.org/10.1109/ICCIS.2013.289>
- [71] P. Batista, C. Silvestre, and P. J. Oliveira, “Kalman and H Infinity Optimal Filtering for a Class of Kinematic Systems,” in *Proceedings of the 17th IFAC World Congress*, vol. 17, no. 1, 2008, pp. 12 528–12 533. [Online]. Available: <http://dx.doi.org/10.3182/20080706-5-KR-1001.02120>
- [72] F. Azis, M. M. Aras, M. Rashid, M. Othman, and S. Abdullah, “Problem identification for underwater remotely operated vehicle (ROV): A case study,” *Procedia Engineering*, vol. 41, no. 0, pp. 554 – 560, 2012. [Online]. Available: <http://dx.doi.org/10.1016/j.proeng.2012.07.211>
- [73] S. Cohan, “Trends in ROV development,” *Marine Technology Society Journal*, vol. 42, no. 1, pp. 38–43, 2008. [Online]. Available: <http://dx.doi.org/doi:10.4031/002533208786861335>
- [74] K. Do, J. Pan, and Z. Jiang, “Robust and adaptive path following for underactuated autonomous underwater vehicles,” *Ocean Engineering*, vol. 31, no. 16, pp. 1967 – 1997, 2004. [Online]. Available: <http://dx.doi.org/10.1016/j.oceaneng.2004.04.006>
- [75] P. W. van de Ven, C. Flanagan, and D. Toal, “Neural network control of underwater vehicles,” *Engineering Applications of Artificial Intelligence*, vol. 18, no. 5, pp. 533 – 547, 2005. [Online]. Available: <http://dx.doi.org/10.1016/j.engappai.2004.12.004>
- [76] N. Q. Hoang and E. Kreuzer, “Adaptive PD-controller for positioning of a remotely operated vehicle close to an underwater structure: Theory and

- experiments,” *Control Engineering Practice*, vol. 15, no. 4, pp. 411 – 419, 2007. [Online]. Available: <http://dx.doi.org/10.1016/j.conengprac.2006.08.002>
- [77] W. M. Bessa, M. S. Dutra, and E. Kreuzer, “Depth control of remotely operated underwater vehicles using an adaptive fuzzy sliding mode controller,” *Robotics and Autonomous Systems*, vol. 56, no. 8, pp. 670 – 677, 2008. [Online]. Available: <http://dx.doi.org/10.1016/j.robot.2007.11.004>
- [78] A. Alvarez, A. Caffaz, A. Caiti, G. Casalino, L. Gualdesi, A. Turetta, and R. Viviani, “Fòlaga: A low-cost autonomous underwater vehicle combining glider and AUV capabilities,” *Ocean Engineering*, vol. 36, no. 1, pp. 24 – 38, 2009. [Online]. Available: <http://dx.doi.org/10.1016/j.oceaneng.2008.08.014>
- [79] B. Subudhi, K. Mukherjee, and S. Ghosh, “A static output feedback control design for path following of autonomous underwater vehicle in vertical plane,” *Ocean Engineering*, vol. 63, no. 0, pp. 72 – 76, 2013. [Online]. Available: <http://dx.doi.org/10.1016/j.oceaneng.2013.01.029>
- [80] K. Ishaque, S. Abdullah, S. Ayob, and Z. Salam, “A simplified approach to design fuzzy logic controller for an underwater vehicle,” *Ocean Engineering*, vol. 38, no. 1, pp. 271 – 284, 2011. [Online]. Available: <http://dx.doi.org/10.1016/j.oceaneng.2010.10.017>
- [81] P. Herman, “Decoupled PD set-point controller for underwater vehicles,” *Ocean Engineering*, vol. 36, no. 7, pp. 529 – 534, 2009. [Online]. Available: <http://dx.doi.org/10.1016/j.oceaneng.2009.02.003>
- [82] J. Petrich and D. J. Stilwell, “Robust control for an autonomous underwater vehicle that suppresses pitch and yaw coupling,” *Ocean Engineering*, vol. 38, no. 1, pp. 197 – 204, 2011. [Online]. Available: <http://dx.doi.org/10.1016/j.oceaneng.2010.10.007>
- [83] J. P. Avila, D. C. Donha, and J. C. Adamowski, “Experimental model identification of open-frame underwater vehicles,” *Ocean Engineering*, vol. 60, no. 0, pp. 81 – 94, 2013. [Online]. Available: <http://dx.doi.org/10.1016/j.oceaneng.2012.10.007>

- [84] C. Chin, M. Lau, E. Low, and G. Seet, “Software for modelling and simulation of a remotely-operated vehicle (ROV),” *International Journal of Simulation Modeling*, vol. 5, no. 3, pp. 114–125, 2006.
- [85] A. Tiano, R. Sutton, A. Lozowicki, and W. Naeem, “Observer Kalman filter identification of an autonomous underwater vehicle,” *Control Engineering Practice*, vol. 15, no. 6, pp. 727 – 739, 2007. [Online]. Available: <http://dx.doi.org/10.1016/j.conengprac.2006.08.004>
- [86] H.-H. Chen, “Vision-based tracking with projective mapping for parameter identification of remotely operated vehicles,” *Ocean Engineering*, vol. 35, no. 10, pp. 983 – 994, 2008. [Online]. Available: <http://dx.doi.org/10.1016/j.oceaneng.2008.03.001>
- [87] J. P. J. Avila and J. C. Adamowski, “Experimental evaluation of the hydrodynamic coefficients of a ROV through morison’s equation,” *Ocean Engineering*, vol. 38, no. 17-18, pp. 2162 – 2170, 2011. [Online]. Available: <http://dx.doi.org/10.1016/j.oceaneng.2011.09.032>
- [88] M. Akmal, M. Yusoff, and M. Arshad, “Active fault tolerant control of a remotely operated vehicle propulsion system,” *Procedia Engineering*, vol. 41, no. 0, pp. 622 – 628, 2012. [Online]. Available: <http://dx.doi.org/10.1016/j.proeng.2012.07.221>
- [89] F. de Assis, F. Takase, N. Maruyama, and P. Miyagi, “Developing an ROV software control architecture: A formal specification approach,” in *IECON 2012 - 38th Annual Conference on IEEE Industrial Electronics Society*, 2012, pp. 3107–3112.
- [90] J. A. Ramírez, R. E. Vásquez, L. B. Gutiérrez, and D. A. Flórez, “Mechanical/naval design of an underwater remotely operated vehicle (ROV) for surveillance and inspection of port facilities,” in *Proceedings of the ASME IMECE2007*, 2007.
- [91] P. Herman, “Transformed equations of motion for underwater vehicles,” *Ocean Engineering*, vol. 36, no. 4, pp. 306 – 312, 2009. [Online]. Available: <http://dx.doi.org/10.1016/j.oceaneng.2008.11.009>

- [92] L. Ye, S. Qinglei, Y. Mulan, and F. Lin, “Nonlinear dynamics performance prediction of large AUV,” in *Control Conference (CCC), 2013 32nd Chinese*, July 2013, pp. 5802–5807.

C. INTELLECTUAL PROPERTY

| | | |
|---|---|---|
|  Universidad Pontificia Bolivariana | ACTA DE PROPIEDAD INTELLECTUAL TRABAJOS DE GRADO | VICERRECTORÍA ACADÉMICA FO-IP-009 |
|---|---|---|

FECHA: 25 de Junio de 2014

1. NOMBRE DEL PROYECTO: Simulación del sistema de control para un vehículo subacuático operado remotamente.

2. PARTICIPANTES

2.1 ESTUDIANTES

Nombre: Santiago Rúa Pérez

No. c.c.: 1.152.436.700

Dedicación al proyecto: 600 horas

Función dentro del proyecto de grado: desarrollo de la plataforma de simulación para el control de un vehículo subacuático.

Facultad en la cual se encuentra matriculado: Maestría en Ingeniería, énfasis en Automática.

2.2 DIRECTOR

Nombre: Rafael E. Vásquez, Ph.D.

No. c.c.: 71.791.914

Dedicación al proyecto: 50 horas

Función dentro del proyecto: dirigir al estudiante.

3. FUENTES DE FINANCIACIÓN

| Fuentes de financiación | Aporte en efectivo | Aporte en especie | Total |
|--------------------------------|---------------------------|--------------------------|--------------|
| Estudiantes | 750.000 | 2.120.000 | 2.870.000 |
| UPB | 18.000.000* | 3.800.000 | 21.800.000 |
| Total | 18.750.000 | 5.920.000 | 24.670.000 |

* Este aporte se da con la financiación del Fondo Nacional de Financiamiento para la Ciencia, la Tecnología y la Innovación, Francisco José de Caldas; la Empresa Colombiana de Petróleos, ECOPETROL; la Universidad Pontificia Bolivariana – Sede Medellín, UPB; y la Universidad Nacional de Colombia – Sede Medellín, UNALMED; a través del Programa Estratégico para el Desarrollo de Tecnología Robótica Orientada a la Exploración Petrolera de los Fondos Marinos Colombianos, proyecto 1210-531-30550, contrato 0265 – 2013.

4.PRODUCTOS

Los productos a entregar de este trabajo son:

- Documento escrito de la tesis de Maestría.
- Un software registrado.

- Un paper para ser sometido a una revista indexada.
- Copia a la Biblioteca Central de la UPB del documento en medio magnético, que soporta el trabajo de grado, una vez sea aprobado.

5. PROPIEDAD INTELECTUAL

5.1 DERECHOS MORALES

Los derechos morales de autor corresponden a los estudiantes, al director y a toda persona que a criterio de éstos, haga aportes originales intelectuales en los avances y en el resultado final del proyecto.

En cualquier tipo de divulgación se dará crédito a los autores y la Universidad Pontificia Bolivariana.

5.2 DERECHOS PATRIMONIALES

Pertenecen al estudiante los derechos morales y patrimoniales sobre la producción intelectual que realice personalmente o con la orientación de un asesor, en desarrollo de las actividades académicas. En cualquier otro caso se aplica el Estatuto de Propiedad Intelectual de la Universidad.

Cuando el director tenga una fuerte ingerencia en la realización de del trabajo y se hace responsable de los resultados en conjunto con los estudiantes, posee derechos patrimoniales sobre dichos resultados o productos.

Nota: cuando exista una fuente de financiación diferente a los estudiantes, se debe establecer en este numeral cual es su participación en los derechos patrimoniales, dependiendo del monto asignado al proyecto y cuanto representa sobre el costo total.

Los autores de este trabajo de grado autorizamos a la Universidad Pontificia Bolivariana a publicar los resultados en la página web de la institución.

6. EQUIPOS Y MATERIAL BIBLIOGRAFICO

Los estudiantes, director y asesor, se comprometen a devolver a la Universidad Pontificia Bolivariana todo el equipo y material bibliográfico, obtenido con recursos proporcionados por las dependencias académicas y administrativas de la Universidad, una vez termine el proyecto.

7. DURACION DEL PROYECTO

El proyecto tendrá una duración de 6 meses, contado a partir del 1 de Julio de 2014.

8. SOLUCION DE CONFLICTOS

En caso de controversia sobre la interpretación o aplicación de la presente acta, se agotarán en primera instancia los conductos regulares de la Universidad, y en caso de no llegar a ningún acuerdo, se dirimirá el conflicto mediante dos (2) amigables componedores designados por cada parte. La decisión será en equidad y tendrá fuerza vinculante para los intervinientes.

9. CONSTANCIA

Todos los partícipes declaran conocer el Estatuto de Propiedad Intelectual de la Universidad Pontificia Bolivariana.

En caso que algún participante se retire antes del 80% de ejecución del cronograma del proyecto, perderá todos los derechos sobre los resultados de la misma.

En caso de presentarse alguna circunstancia que altere los términos de la presente acta, deberá anexarse al presente documento la respectiva modificación aprobada por la respectiva facultad.

Para constancia se firma en Medellín, el día 25 de Junio de 2014.


Santiago Rúa Pérez
ESTUDIANTE MAESTRÍA


Rafael E. Vásquez Moncayo Ph.D.
DIRECTOR TESIS DE MAESTRÍA